TESE DE DOUTORADO Nº 200

A PERIFOCAL INTRAOCULAR LENS WITH EXTENDED DEPTH OF FOCUS

Felipe Tayer Amaral

DATA DA DEFESA: 25/05/2015

Universidade Federal de Minas Gerais
Escola de Engenharia
Programa de Pós-Graduação em Engenharia Elétrica

A PERIFOCAL INTRAOCULAR LENS WITH EXTENDED DEPTH OF FOCUS

Felipe Tayer Amaral

Tese de Doutorado submetida à Banca Examinadora designada pelo Colegiado do Programa de Pós-Graduação em Engenharia Elétrica da Escola de Engenharia da Universidade Federal de Minas Gerais, como requisito para obtenção do Título de Doutor em Engenharia Elétrica.

Orientador: Prof. Davies William de Lima Monteiro

Belo Horizonte – MG

Maio de 2015

"A Perifocal Intraocular Lens with Extended Depth of Focus"

Felipe Tayer Amaral

Tese de Doutorado submetida à Banca Examinadora designada pelo Colegiado do Programa de Pós-Graduação em Engenharia Elétrica da Escola de Engenharia da Universidade Federal de Minas Gerais, como requisito para obtenção do grau de Doutor em Engenharia Elétrica.

Aprovada em 25 de maio de 2015.

Por:

Prof. Dr. Davies William de Lima Monteiro
DEE (UFMG) - Orientador

Prof. Drª. Luciana Pedrosa Salles
DEE (UFMG)

Prof. Dr. Rodney Rezende Saldanha
DEE (UFMG)

Prof. Dr. Paulo Schor
Departamento de Oftalmologia (UNIFESP)

Prof. Dr. Marcos Roberto da Rocha Gesualdi
CECS (UFABC - Universidade Federal do ABC)

Dr. Otávio Gomes de Oliveira
Departamento de Pesquisa e Desenvolvimento (Mediphacos S.A.)

To my parents, for always believing in me, for dedicating themselves to me with so much love and for encouraging me to dream big to make a difference.

"Aos meus pais, por sempre acreditarem em mim, por se dedicarem a mim com tanto amor e por me encorajarem a sonhar grande para fazer a diferença."

ACKNOWLEDGEMENTS

I would like to acknowledge all my friends and family for the fondness and incentive whenever I needed. I thank all those who contributed directly and indirectly to this work.

I thank my parents Suzana and Carlos for being by my side in the darkest hours comforting me, advising me and giving me all the support and unconditional love to move on. I thank you for everything you taught me to be a better person: you are winners and my life example!

I thank Fernanda for being so lovely and for listening to my ideas and for encouraging me all the time. I am so grateful that you have calmed me and gave so much love and care especially when I was tense. By knowing that I could always count on you, I had the strength to carry on!

I thank my friends at OptMA Lab and UFMG for the technical discussions that contributed to enhance my knowledge on the subject of this work, especially to Bruno Trindade for the partnership in writing papers and for the discussions and contact with ophthalmology in our Thursday meetings.

I thank all my friends at Mediphacos Ltda for helping me to find effective solutions every time I was stuck in technical problems. Your support was essential!

Special thanks to Professor Davies, for the teachings, incentive, friendship and for the technical and emotional support. With your expertise, your patience, your perfectionism and encouragements you taught me that I must get the best of me to go further.

ABSTRACT

This work presents the design of a perifocal intraocular lens (IOL) with extended depth of focus for replacement of the human eye crystalline lens in cataract and presbyopia treatment, for example. By extending the depth of focus in IOLs, individuals can benefit from both near and far vision quality with a single IOL, which increases their comfort to perform daily activities that require a short focal length, such as using smartphones or tablets without the need of spectacles. The extended depth of focus can also reduce discomfort caused by IOL imbalance resulting from the monovision technique, favoring individuals adaptation. Besides its potential alternative use to monovision, the Perifocal IOL reduces the inconvenient experiences of halos, glare and loss of contrast when looking at near objects, which are inherent issues with the conventional multifocal (bifocal or trifocal) IOLs. The use of these lenses is not restricted to cataract and presbyopia, but could be extended to cameras, microscopes, endoscopes, binoculars and augmented-reality glasses. The Perifocal IOL, herein proposed, has four structures in the shape of lenticles that yield four additional foci off the main optical axis, hence its coined name. The design of the Perifocal IOL was carried out with the optical system design software Zemax®. The Perifocal IOL was optimized to yield extended depth of focus with no substantial loss of contrast. The optimization metric used was the MTF (modulation transfer function), which is related to the optical system contrast. Its optical performance was compared to four different commercial monofocal IOLs that comprise the most common types of implanted lenses currently. The simulations were performed in a computational human-eye model in order to make the results closer to an actual IOL implantation. The results show that the Perifocal IOL presents larger depth of focus and no significant loss of contrast related to the commercial IOLs, showing that the Perifocal IOL can be an alternative implant when the goal is to reach more comfort and spectacle independence.

Keywords: Intraocular lenses, depth of focus, contrast sensitivity, perifocal, optical aberration, optical performance.

RESUMO

Este trabalho apresenta o desenvolvimento de uma lente intraocular (LIO) perifocal com profundidade de foco estendida para a substituição da lente cristalina do olho humano, por exemplo, no tratamento de catarata e presbiopia. O aumento da profundidade de foco de LIOs permite que o usuário desfrute de qualidade de visão tanto de longe quanto de perto com uma mesma lente, aumentando seu conforto para realizar atividades cotidianas de foco próximo como utilizar smartphones ou tablets sem o uso de óculos. A profundidade de foco estendida também pode reduzir os incômodos causados pelo desequilíbrio das lentes utilizadas na técnica de monovisão, facilitando a adaptação dos indivíduos. Além do potencial uso alternativo à técnica de monovisão, a LIO Perifocal possibilita a visão de objetos próximos reduzindo a experiência inconveniente de auras, ofuscamento e perda de contraste, que são inerentes às lentes multifocais (bifocais ou trifocais) convencionais. O uso destas lentes não se restringe somente à catarata e presbiopia, podendo se estender para câmeras, microscópios, endoscópios, binóculos e óculos de realidade aumentada. Para aumentar a profundidade de foco, a LIO conta com quatro estruturas em forma de lentículas, que são responsáveis por criar quatro focos adicionais deslocados em relação ao eixo óptico principal da lente. O termo perifocal se refere ao deslocamento dos quatro focos para o entorno do eixo óptico central da lente. O desenvolvimento da LIO Perifocal foi feito com o auxílio do software de design de sistemas ópticos Zemax®. A LIO Perifocal foi otimizada para gerar a maior profundidade de foco sem perda substancial de contraste. A métrica utilizada para a otimização foi o MTF (função de transferência de modulação), que está relacionado ao contraste que um sistema óptico é capaz de atingir. O seu desempenho óptico foi comparado ao de quatro LIOs monofocais comerciais, que compreendem os tipos mais comuns de lentes implantadas atualmente. As simulações foram feitas em um modelo computacional do olho humano de modo a tornar os resultados mais próximos de uma situação em que a LIO estivesse realmente implantada. Os resultados mostram que a LIO Perifocal apresenta maior profundidade de foco e perda pouco significativa de contraste em relação às LIOs comerciais, mostrando que a lente perifocal possa ser uma alternativa de implante quando se deseja alcançar maior conforto e independência de óculos.

Palavras chave: Lentes intraoculares, profundidade de foco, sensibilidade ao contraste, perifocal, aberrações ópticas, desempenho óptico.

SUMMARY

LIST OF FIGURES 1
LIST OF TABLES 3
1. INTRODUCTION 4
1.1. INTRAOCULAR LENSES 4
1.2. CATARACT SURGERY AND PRESBYOPIA 4
1.3. IOL FEATURES 5
1.4. OBJECTIVE 7
2. CONCEPTS AND CONTEXT 8
2.1. WAVEFRONT 8
2.2. POINT SPREAD FUNCTION 8
2.3. IMAGE FORMATION 12
2.4. MODULATION TRANSFER FUNCTION 13
2.5. CONTRAST SENSITIVITY FUNCTION 16
2.6. DEPTH OF FOCUS 18
2.7. TOLERANCING 25
2.8. LUMINOSITY 26
3. TECHNICAL DEVELOPMENT 31
3.1. HOW IS DOF EXTENDED? 33
3.2. COMPUTATIONAL MODEL 36
4. RESULTS AND DISCUSSION 39
4.1. OPTIMIZATION INPUTS 39
4.2. OPTIMIZATION RESULTS 41
4.3. SIMULATION RESULTS 45
4.4. TOLERANCE ANALYSIS 60
5. CONCLUSIONS 66
6. PROPOSED NEXT STEPS 68
7. REFERENCES 69
APPENDIX 75

LIST OF FIGURES

Figure 2.1. Contrast of five images composed of one line pair decreasing from left (100%) to right (10%). 9
Figure 2.2. Cone cells sensitivity as a function of wavelength. 11
Figure 2.3. Convolution operation: The first situation shows a perfect version of a letter "F" being convoluted with a diffraction limited PSF yielding a slightly blurred letter "F". In the second situation the letter "F" is blurred, point by point by the PSF, to produce a simulation of the blurred image..... 12
Figure 2.4. The first situation shows the convolution of an object composed of four squares with a diffraction limited PSF yielding a slightly blurred image. In the second situation the object is blurred, point by point by the PSF and its shape resembles that of a single larger square..... 13
Figure 2.5. MTF curves and images formed by a $F_{\#}1.4$ and $F_{\#}2.0$ lenses. 15
Figure 2.6. Contrast sensitivity function of the human eye, CSF..... 17
Figure 2.7. Image blur and spot size variation as a function of the focal shift..... 18
Figure 2.8. Defocus and spherical aberration as a function of lens focal shift..... 19
Figure 2.9. Depth of focus for a given circle of confusion diameter c. 20
Figure 2.10. Depth of focus for an unaberrated $F_{\#}3.33$ lens. The DOF (D) is defined as the defocus range for which the MTF stays above 50% of its maximum value. 23
Figure 2.11. Depth of focus for a 4 different lenses. 24
Figure 2.12. Field of view schematic diagram. 26
Figure 2.13. Illustration of benchmark light sources and respective related luminances. 29
Figure 2.14. Pupil diameter as a function of the luminance, field diameter in degrees and age in years..... 30
Figure 3.1. Schematics of IOL anterior and posterior pieces. Light enters the anterior piece..... 32
Figure 3.2. Perifocal IOL: side view [left] perspective view [right]. 32
Figure 3.3. Schematic diagram of the optical system and the image of a single letter "F" formed by an optical system with only the four overlapping lenticles. 33
Figure 3.4. Image of a single letter "F" formed by an optical system with four lenticles and a standard lens in cascade where 90% of the system optical power is due to the standard lens and 10 percent due to the lenticles..... 34
Figure 3.5. Decreasing dioptric power relationship between lenticles and standard lens from left (10% lenticles and 90% standard lens) to right (0% lenticles and 100% standard lens)..... 34
Figure 3.6. Image of a single letter "F" formed by an optical system with four lenticles and a power dominant standard lens. 35
Figure 3.7. Schematic diagram showing the modified Liou & Brennan computational eye model with the IOL. 37
Figure 3.8. Chromatic dispersion of NOA73 and NOA68. 38
Figure 4.1. Pareto-front: Optimal solutions obtained by NSGA-II. 42
Figure 4.2. Schematic diagram of the lenticles center position and diameter. 43
Figure 4.3. Polychromatic MTF curves. From above: object at infinity (+0D), 6m (+0.17D), 2m (+0.5D), 1m (+1D) and 80cm (+1.25D), for 3.0mm [left] and 5.0mm [right] diameter pupils. 46

Figure 4.4. Polychromatic MTF through focus curves obtained for each IOL model for 3mm diameter pupil at spatial frequencies in lp/mm equal to 20 (A), 30 (B), 50 (C), 100 (D). 47
Figure 4.5. Polychromatic MTF through focus curves obtained for each IOL model for 5mm diameter pupil at spatial frequencies in lp/mm equal to 20 (A), 30 (B), 50 (C), 100 (D). 48
Figure 4.6. Perifocal IOL MTF through focus surface contour for 3mm [left] and 5mm [right] diameter pupils..... 49
Figure 4.7. Residual MTF through focus surface for 3mm [left] and 5mm [right] diameter pupils. Negative 51
Figure 4.8. Polychromatic focal range calculated for each IOL model for 3mm [up] and 5mm [down] pupils..... 53
Figure 4.9. Polychromatic MTF curves versus pupil diameter variation. From above: object at infinity (+0D), 6m (+0.17D), 2m (+0.5D), 1m (+1D) and 80cm (+1.25D), for 50lp/mm [left] and 100lp/mm [right]. 54
Figure 4.10. Image simulation result for 3mm diameter pupil: Pelli-Robson Contrast Sensitivity Chart..... 56
Figure 4.11. Image simulation result for 5mm diameter pupil: Pelli-Robson Contrast Sensitivity Chart..... 57
Figure 4.12. Image simulation result for 3mm diameter pupil: Mona Lisa..... 58
Figure 4.13. Image simulation result for 5mm diameter pupil: Mona Lisa..... 59
Figure 4.14. MTF variation caused by manufacturing errors for 3mm [up] and 5mm [down] diameter pupil with the object placed at infinity. The dotted and dashed curves represents 0.25D and 0.5D of myopia, respectively. 63
Figure 4.15. MTF variation caused manufacturing errors for 3mm [up] and 5mm [down] diameter pupil with the object placed at 80cm. The dotted and dashed curves represents 0.25D and 0.5D of hyperopia, respectively..... 64
Figure 4.16. Comparison between the areas under MTF curve for the tolerated lens for 3 and 5mm diameter pupil: object placed at infinity versus 0.25D and 0.5D of myopia [left] and object placed at 80cm [right] versus 0.25D and 0.5D of hyperopia..... 65
Figure 0.1. Schematic diagram of a thin lens. 75
Figure 0.2. Schematic diagram used to calculate d_{near}..... 77
Figure 0.3. Schematic diagram used to calculate d_{far}..... 78

LIST OF TABLES

Table 1.1. IOL types and their common derivation 7
Table 2.1. Typical manufacturing tolerances for a BK7 50mm diameter lens 25
Table 2.2. Luminance benchmark for different light sources. 28
Table 3.1. Optical design data for the modified Liou & Brennan eye model used in simulations. .. 36
Table 4.1. Design variables boundaries used for optimization. 39
Table 4.2. Perifocal IOL parameters obtained by NSGA II optimization. 42
Table 4.3. Lenticle center position obtained by NSGA II optimization and diameter. 43
Table 4.4. Optical design data of the tested IOLs. 44
Table 4.5. Manufacturing tolerances for 50mm and 6mm diameter lenses 61
Table 4.6. Perifocal IOL manufacturing parameter variation range 62

1. INTRODUCTION

1.1.*INTRAOCULAR LENSES*

An intraocular lens (IOL) is a surgically implantable lens indicated to replace the crystalline of the human eye mainly due to cataract. The choice of the correct IOL should take into account the physiological characteristics of the patient eye such as corneal refractive power, axial length and anterior chamber depth (ACD). These parameters are measured by commercial ophthalmic instruments before the surgery. Besides these physiological parameters, the IOL selection also depends on the patient's most frequent habits, e.g. driving at night, practicing outdoor activities, using a smartphone, working in front of a computer or reading a book.

This work proposes the development of an optimized IOL to increase the number of tasks to be performed with acceptable quality without the need of spectacle correction. The IOL is composed of a standard lens with four structures in the shape of lenticles within it. The center of each lenticle is shifted from the standard lens center, so the IOL presents five different optical axes: one for each lenticle and another for the standard lens. This assembly results in an IOL with five foci: a principal focus formed by the standard lens and four foci on its periphery formed by the lenticles. Because this IOL features four foci on periphery of the central optical axis, it has been here denominated Perifocal IOL, where the objective of each focus is to extend the depth of focus of the entire optical system, thus providing more comfort to individuals to perform daily activities without spectacles.

The perifocal technique is not restricted only to IOLs. It might be extended to any optical equipment such as cameras, endoscopes, telescopes, binoculars and microscopes. These equipments would benefit by lenses with extended depth of focus allowing them to provide images of objects located in a wider range of distances without experiencing significant loss of contrast. Perifocal lenses have greater potential of use in short focal length equipments like cameras and microscopes because these equipments feature narrow depth of focus requiring constant focus adjustment during their use. Augmented reality glasses have been developed and consist of optical devices that merge virtual reality with the real world [1,2]. The main problem with this technology regards the location of the display where virtual information is provided. The small screen is placed too close to the user, who is not able to see the real and the virtual world simultaneously because of the limited depth of focus of the human eye. Perifocal lenses are able to shorten the difference in dioptric power[1] needed to see the real world and interact with the virtual world through the display bringing more comfort to the user since it is capable of extending the depth of focus. In ophthalmology

1.2.*CATARACT SURGERY AND PRESBYOPIA*

Cataract surgery was first carried out in 1949 and today is the most common ophthalmic procedure performed worldwide. It consists of removing the clouded crystalline lens and replacing

[1] The optical power is commonly expressed in diopters which is the reciprocal of the focal length in meters.

it by an implantable artificial intraocular lens (IOL). Considered one of the safer and most successful surgeries, it is estimated that next to 20 million cataract surgeries were performed in 2011 [3]. The World Health Organization estimates that there should be approximately 32 million cataract extractions in the year 2020 [4]. Its growth is associated to improvements on surgery techniques which have currently become more sophisticated and safer, being now performed in a much earlier stage of the disease than it was in the past. The results of the modern surgery are much better than they were 20 years ago, due to the reduction of operative and postoperative complications and to significant improvements in visual outcome [5]. The latter have been so satisfactory that the patients have high expectations on the treatment success [6]. There are many issues that impact directly on the visual outcome of people undergoing cataract surgery: the surgeon ability concerning the IOL position and fixation in the eye, the size of the incision, the residual astigmatism or high-order aberrations induced by the surgery and finally the choice of the most adequate IOL for each patient.

Cataract surgery causes patients to lose the accommodation[2] that the phakic eye previously had, leading them to experience presbyopia. Presbyopia is an age-related visual impairment that results from the gradual decrease in accommodation. This visual condition starts approximately over the age of 40 years and is not incapacitating if corrected with reading glasses. If not corrected, it may result in an inability to perform some near tasks effortlessly without experiencing, for instance, visual blur [7].

1.3.*IOL FEATURES*

The loss of accommodation is not related to presbyopia only. Commonly, a monofocal IOL is used to replace the crystalline removed in cataract surgery. In general, people with any sort of dysfunctional crystalline could benefit from an IOL. These lenses provide only one focus allowing individuals to see objects clearly at a specific distance: far or near. If a monofocal IOL is designed to provide far vision, spectacles are required for near vision. On the other hand, if it is designed for near vision, spectacles are required to see far objects. Despite the use of additional spectacles, many strategies have been developed to reduce the visual impairment caused by the loss of accommodation related to aphakia[3] or presbyopia. Bifocal lenses have two foci, where one is generally designed for near tasks and the other for far vision. Intermediate vision may also be provided by already developed lenses with three foci [8]. The multiple foci are obtained by two different strategies: refractive and/or diffractive. Refractive multifocal lenses provide multiple foci by zones with different curvatures, where each zone is designed to have a specific focal length for either far, near or intermediate vision. Diffractive lenses are composed of grooves (or discontinuities) on their surfaces that cause interference of the incident light. By controlling the

[2] The generally accepted theory is that of von Helmholtz: ciliary muscle contraction causes zonules to relax, allowing the lens to become more curved and increasing its focusing power; presbyopia is therefore due to loss of lens elasticity with age [119].

[3] Aphakia is a term which encompasses all situations in which the crystalline lens is missing from the pupillary area by disease (e.g. removed during cataract surgery), trauma, or even congenital malformation in which the individual is born without the crystalline lens.

groove distribution and height along the lens surface, the induced light phase delay forms constructive interference on the desired position of either the far, the near or the intermediate focus. Hybrid lenses are a combination of refractive and diffractive surfaces.

The main disadvantage of using multifocal IOL are the losses of light and contrast caused by the multiple foci. Although these lenses allows individuals to read without spectacles, they may experience halos and glare caused by the lens which may compromise their vision quality [9,10]. Monofocal IOLs provide higher image contrast and do not present loss of light or halos and glare.

Pseudo-accommodative IOLs are lenses that attempt to mimic the eye's natural method of focusing. Usually the optical power is altered by moving elements in the IOL that respond to the action of the ciliary muscle on an accommodative demand [11]. Some designs regards to the changes in the lens surface curvature and others to the axial displacement of the IOL optics [11]. However, studies show that is difficult to measure the lens accommodation [12], and to predict if the ciliary muscle contraction causes significant changes on the lens axial position [11,13-17].

A viable option for presbyopia treatment is monovision. It consists of implanting one monofocal IOL in each eye: in one eye it is targeted for near and in the other it is targeted for far distance. Monovision with monofocal IOLs, currently accounts for as much as 50 per cent of cataract procedures in some practices [18]. It offers a less costly option than the premium bifocal IOLs to individuals who want to have reduced spectacle dependence. Although patients treated this way have approximately the same level of spectacle independence as those implanted with bifocal or trifocal IOLs, they lose a significant amount of stereoacuity[4] and it is not everyone that tolerate the imbalance between their eyes [19]. Usually, the imbalance between the near and the far IOLs is set to 1.25D in order to avoid asthenopia[5] and preserve contrast and stereoacuity [18,20].

The IOLs are classified according to their eccentricity: spherical or aspheric. In spherical IOLs the curvature is constant over the entire lens surface. Aspheric IOLs have their surface described by a conic function (hyperbola). The spherical IOLs present positive spherical aberration [21] which compromises the focal point quality because its surface differs from the ideal hyperbolic surface [22]. The aspheric IOLs can present null or negative spherical aberration. Eyes with null aspheric IOLs will have only the positive spherical aberration introduced by the cornea which can be entire or partially corrected by negative aspheric IOLs [23]. Despite the loss of contrast caused by spherical aberration, the depth of focus and consequently the depth of field are larger in spherical IOLs. Comparative studies show that individuals with aspheric IOL suffer fewer impacts of spherical aberration than patients with spherical IOLs having vision with better contrast [24]. However, individuals with spherical IOLs benefit from vision with larger depth of field than patients with aspheric IOLs [25,26].

Toric IOLs are lenses with at least one of the two surfaces (anterior or posterior) having maximum and minimum radii of curvature perpendicular to each other in order to compensate corneal astigmatism. Because astigmatism is not rotationally symmetrical [27], these lenses must be positioned in the eye in a very specific orientation [28] to avoid residual refractive errors [29].

---

[4] Stereoacuity is the smallest detectable depth difference that can be seen in binocular vision.

[5] Asthenopia is an ophthalmological term often used to describe a collection of symptoms such as pain in or around the eyes, blurred vision, headache and occasional double vision.

Toric IOLs are very effective in compensating corneal astigmatism [30-32]. However, the visual function after toric IOL implantation is significantly compromised by the post-operative lens tilt and rotation [33].

The IOLs can be made of polymers, silicone and acrylics. The first IOL was manufactured with PMMA, which is a thermo-plastic polymer with refractive index of 1.493. Although lenses made of PMMA are cost effective, they are rigid and require a larger incision, which may submit individuals to a higher risk during cataract surgery and a longer recovery time [34]. Silicone, hydrophilic and hydrophobic acrylics are soft materials and have been widely used in foldable IOLs. Silicone IOLs are slippery when inserted in aqueous medium complicating its manipulation during surgery [34]. Hydrophilic acrylics are polymers that swell up by absorbing water but do not dissolve therein. Lenses made of this material have a high content of water resulting in very soft lenses which resemble a living tissue. However, epithelial cells reaction on its anterior surface usually occurs and may cause IOL loss of transparency. Hydrophobic acrylic IOLs are similar to PMMA but foldable, and is the material of most implanted lenses in the United States. Although hydrophobic acrylics feature a higher refractive index resulting in thinner lenses, their manipulation is difficult because they are sticky [34]. IOLs may also be covered by a thin layer of specific materials serving as ultraviolet filter [35].

Table 1.1 shows IOLs characteristics and their most common derivation:

Table 1.1. IOL types and their common derivation				
IOL Type	Rigid or Foldable			
	With or without UV-Filter			
	Monovision or Standalone IOL			
	Toric		Non-Toric	
Monofocal	Spherical	Aspheric	Spherical	Aspheric
Multifocal (bifocal or trifocal)	Refractive	Refractive	Refractive	Refractive
	Diffractive	Diffractive	Diffractive	Diffractive
	Hybrid	Hybrid	Hybrid	Hybrid
Pseudo-Accommodative	Spherical	Aspheric	Spherical	Aspheric

1.4.*OBJECTIVE*

To develop a new concept of an IOL with extended depth of focus minimizing the loss of contrast and the sensitivity to defocus in comparison to commercial monofocal IOLs.

2. CONCEPTS AND CONTEXT

2.1.*WAVEFRONT*

A wavefront is a hypothetical surface defined as the locus of all points of a given wave featuring the same phase [36]. As the light is an electromagnetic radiation of any wavelength, its propagation follows the principles of wave theory [37]. In 1678 Huygens proposed that every point of a wavefront becomes a source of a secondary spherical wavelet. The sum of these wavelets determines the wave form in the subsequent instant [37]. The Huygens principle concluded that the wavefront propagates while maintaining its shape provided there are no obstacles and the surrounding media is homogeneous. The concept of wavefronts applies to the optical domain due to the wave nature of light [36].

The deviations between an arbitrary and an ideal or reference wavefont are defined as optical aberrations or wave aberrations. Usually plane wavefronts obtained by collimated beam profiles, in which the light rays are parallel are adopted as reference. The light emerged from a star can also be approximated to a plane wavefront. Considering the star as a single point source, and no disturbance in the propagating medium, the wavefront is in fact spherical, but as it propagates further from the source, its spherical radius increases and a segment of the surface wave approximates to a plane wave.

Aberrometry is the process used to assess the optical distortions and is based on wavefront analysis, which is widely used in adaptive optics and has become a very popular technique in optical engineering, astronomy and ophthalmology in recent years. The optical aberrations are divided in two main groups: monochromatic and chromatic. In ophthalmology, the most usual monochromatic aberrations are defocus (myopia and hyperopia), astigmatism, coma and spherical aberration. The most common form to represent the optical aberrations are the Zernike Polynomials which are a set of orthogonal basis functions defined within a unit circle with amplitude between -1 and 1 [36,38].

2.2.*POINT SPREAD FUNCTION*

The point spread function (PSF) is defined as the intensity profile of the image, formed by an optical system, of a point source. A PSF of any optical system will never represent exactly a single point, nor will it feature a perfectly uniform intensity distribution, even if it is perfectly manufactured and aberration free. Every optical system presents a finite-sized aperture which is responsible for sampling just a finite portion of the incoming light that will be diffracted. Consequently, the light diffraction degrades the image and limits any optical system resolution. Diffraction causes intensity oscillations of the PSF intensity profile and is mathematically described by a sinc^2 function [36].

An optical system with its resolution only limited by diffraction is defined as diffraction limited. The PSF of a diffraction limited system is defined as the Airy Disk, which is a small disk of light surrounded by light and dark concentric rings [27]. The angular resolution θ of an optical system, measured in radians and limited by the diffraction (Airy Disk) pattern, depends on the incident

light wavelength λ and the system aperture D (both given in the same unit), and is determined by the Rayleigh criterion: $\theta=1.22.\lambda/D$ [39]. Two points are distinguished if they are separated by an angle equal to or larger than θ. Because the PSF is described by a sinc² function which is infinite, its width can be arbitrated as the Airy Disk diameter, which depends on the wavelength λ and the F-number[6] ($F_{\#}$) and is given by $D_{Airy}=2.44.\lambda.F_{\#}$.

The smaller the pupil, the more diffraction degrades image quality limiting its resolution and causing loss of contrast. Contrast is one of the most important attribute for the visual quality of images. Considering an image composed of a series of alternating black and white lines, what differentiates them is the contrast. Distinguishing these lines becomes increasingly difficult if the black lines become progressively brighter and the white lines darker, until they reach the same gray level being impossible to differentiate them (no contrast). Resolution is commonly expressed by the number of line pairs (two adjacent lines of the same width, being one "black" and the other "white") that can be resolved. It is usually measured in line pairs per millimeter in the metric domain, and cycles per degree in the angular domain.

Considering one line pair, the contrast can be calculated as the difference between the overall intensity of the white and black lines. The Michelson formula is used to calculate contrast, where I_{max} and I_{min} are the maximum and minimum intensity values [40]:

$$\text{Contrast} = \frac{I_{max} - I_{min}}{I_{max} + I_{min}} \qquad 2.1$$

Contrast equal to 1 indicates a faithful representation of the contrast on the object plane, and values smaller than 1 represent loss of contrast.

An schematic example is shown in Figure 2.1 where one object was imaged by five different optical systems. The object consists of two adjacent rectangles of the same size. The rectangle on the left is totally white and the rectangle on the right is totally black (exactly equal to the left most image shown in Figure 2.1).

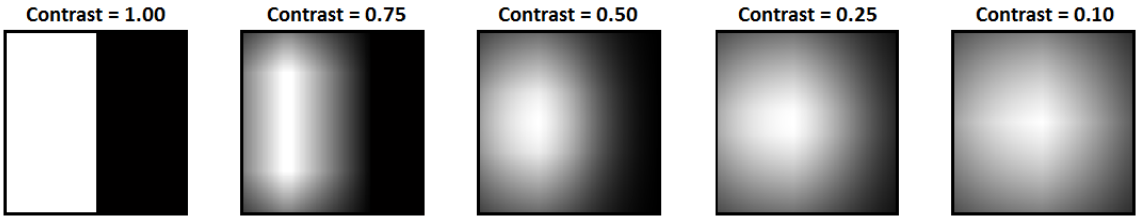

Figure 2.1. Contrast of five images composed of one line pair decreasing from left (100%) to right (10%).

The maximum and minimum intensities were obtained by the average of the pixel intensities on the white and black rectangle areas, respectively. The contrast is also related to the detection of edges. When the contrast is 1, the transition between black and white is abrupt and when the contrast decays, the transition is smooth as it is shown in Figure 2.1.

Contrast affects directly the ability of seeing details in any image: the higher the contrast the more details are perceived in the image. The contrast level of an optical system can be expressed by its

[6] $F_{\#}$ is defined as the ratio f/D, where f and D are respectively the focal length and the lens aperture diameter given in the same unit.

PSF width. Narrow PSFs yield small sized spots and consequently sharper images. By analyzing the angular resolution and the Airy Disk diameter calculations, it is concluded that an eye without optical aberrations obtains the best image at the largest pupil size because the larger the aperture, the narrower the PSF and the smaller the spot on the retina. Considered one of the most used image quality metric, the PSF is calculated by the Equation 2.2 [39]:

$$\mathrm{PSF}(x',y')=\left|\mathrm{FT2}\left\{p(x,y).e^{-2.j.\pi.\frac{w(x,y)}{\lambda}}\right\}\right|^2 \qquad 2.2$$

Where FT2 is the two dimensional Fourier Transform, $p(x,y)$ is the pupil function of the optical system. $w(x,y)$ is the wave aberration function and λ is the light wavelength, both given in the same unit. The wave aberration function is given by a weighted summation of Zernike terms [41]. These terms are basis functions, commonly deployed to describe surfaces in optics. Each term has a coefficient that relates to the amount of that particular aberration [39]. The Zernike polynomials are widely used to describe the optical aberrations mathematically in ophthalmology because they contain terms (shapes) with very convenient meanings like defocus, astigmatism, coma, and spherical aberration [42]. Purely hyperopic or myopic individuals present only defocus wave aberration which is given by $w_{defocus}=C_{def}.(-1+2.x^2+2.y^2)$, where C_{def} is the coefficient that defines the amplitude of the wave function $w_{defocus}$. This coefficient is related to the degree of hyperopia and myopia in human eyes. The sign of coefficient C indicates myopia (negative) and hyperopia (positive) [38]. An optical system with circular aperture will present pupil function equal to 1 if $x^2+y^2\leq r^2$, otherwise 0, with r being the circle radius. The two dimensional discrete Fourier Transform is numerically calculated according to Equation 2.3, where $f(x,y)$ is equal to $p(x,y).e^{-2.j.\pi.\frac{w(x,y)}{\lambda}}$ and N_1 and N_2 are $p(x,y)$ and $w(x,y)$ raster [43] height (x) and width (y) [44].

$$\mathrm{FT2}\{f(x,y)\}=F(x',y')=\sum_{x=0}^{N_2-1}\sum_{y=0}^{N_1-1} f(x,y).\,e^{2.j.\pi.\left[\frac{x.x'}{N_1}+\frac{y.y'}{N_2}\right]} \qquad 2.3$$

Although the PSF presented in Equation 2.2 is monochromatic, the intensity distribution that lands on the retina or on a camera sensor is typically polychromatic. A method to calculate the polychromatic PSF is proposed at [45]. This method consider the polychromatic PSF as the summation of each monochromatic PSF weighted by the intensity of each wavelength of the light source. The refractive index of any material is wavelength dependent. As single lens focal length varies with the refractive index, each color that composes the white light is focused on a different plane [27]. The difference between the focal lengths depending on the color of the incident light is defined as chromatic aberration that compromises image quality. Even if the optical system is free from monochromatic aberrations, it may present some chromatic aberration. This aberration should be corrected because color is one of the most important features for human image analysis due to the high sensitivity of the human visual system to small color changes [46]. There are three kinds of cells on the human retina which are sensitive to color: the red cones, the green cones and the blues cones. The cone cells sensitivity to color is shown in Figure 2.2, based on [47].

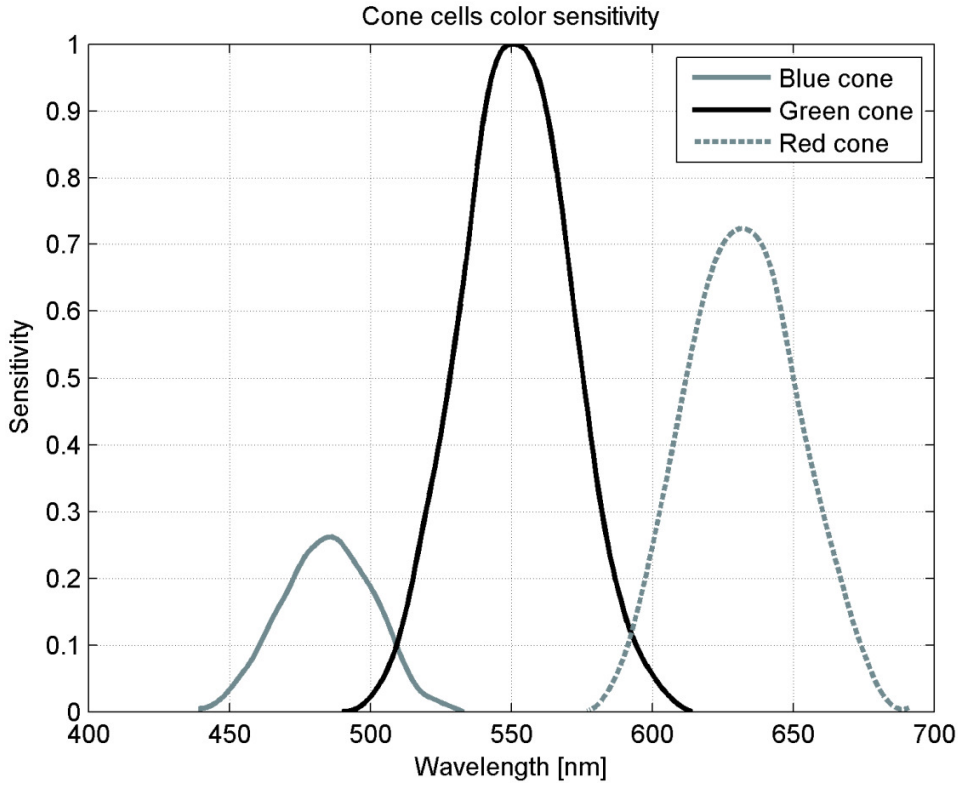

Figure 2.2. Cone cells sensitivity as a function of wavelength.

An optical system that compensates chromatic aberration is defined as an achromat which may be composed by a:

- combination of positive and negative lenses of different materials. Each material present a dispersion coefficient, which relates to the chromatic dependence of its refractive index.
- combination of refractive and diffractive lenses. While refractive elements focus the shorter wavelengths before the longer wavelengths, diffractive elements focus the shorter wavelengths further than the longer wavelengths.

Although defocus, astigmatism, coma and spherical aberration compromise the resulting vision quality after cataract surgery, chromatic dispersion is a relevant cause of image contrast degradation. Violet and red[7] light rays are focused in front and behind the retina respectively, if the lens has been designed for green light. The dispersion of white light into colored components can reach approximately 2 diopters of refractive error observed between violet and red [48]. A commonly used measure of any material dispersion is the Abbe Number Vd, which is given by $V_d=(n_d - 1)/(n_F - n_C)$, where n_F, n_d and n_C are the refractive indices of the material at three standard wavelengths: blue at 486.1nm, yellow at 587.6nm and red at 656.3nm, respectively [49]. Materials with higher chromatic dispersion present higher differences of refractive index between each standard wavelength. According to the expression, the smaller the V_d value, the higher the chromatic dispersion of the material.

[7] Violet and red consist of the lower and upper limits of the visible wavelength spectrum respectively [79].

Chromatic aberration is a significant limiting factor of visual contrast being the reason why some studies have proposed the development of achromats IOLs [50-52]. The manufacturer Hanita Lenses (http://www.hanitalenses.com) has been also developing an IOL [53] which is already being under clinical tests and achieving satisfactory results [54].

2.3.*IMAGE FORMATION*

Considering the Huygens principle [55], any object can be considered as an array of independent point sources. Regarded as the most fundamental optical object, each independent point source present in the array will produce its own PSF. Mathematically, this process is described by the convolution operation. Every image is formed by the convolution of the object with the optical system PSF. The concept of convolution in practice is to give each point source in the array the shape of the system PSF. An example of image formation by convolution operation (denoted by $\otimes$) is shown in Figure 2.3 where the first PSF is diffraction limited and the second with spherical aberration and coma. The first PSF is convoluted to the object (sharp letter "F") yielding a still sharp letter "F". Although there are no optical aberrations in this situation, it is visible that the image is slightly blurred due to diffraction. The second PSF with some aberrations yields a blurred letter "F" when convoluted to the object. It is noticed that the PSF with aberrations is larger than the diffraction limited PSF.

Figure 2.3. Convolution operation: The first situation shows a perfect version of a letter "F" being convoluted with a diffraction limited PSF yielding a slightly blurred letter "F". In the second situation the letter "F" is blurred, point by point by the PSF, to produce a simulation of the blurred image.

The convolution operation is performed by Equation 2.4, where $O(x', y')$ and $IMG(n_1,n_2)$ represent the object array, and the image formed by the optical system, respectively. N_1 and N_2 are $O(x',y')$ and $PSF(x',y')$ raster [43] height (x') and width (y'), and n_1 and n_2 indicate the position of the pixels on the image array.

$$O(x',y')\otimes PSF(x',y')=IMG(n_1,n_2)=\sum_{x'=0}^{N_2-1}\sum_{y'=0}^{N_1-1} O\,(x',y').\,PSF(n_1-x',n_2-y') \qquad 2.4$$

Another simulation of convolution is shown in Figure 2.4 where the object consists of four white squares on a black background. The first PSF is diffraction limited and the second with spherical aberration and coma, reproducing the situation shown in Figure 2.3.

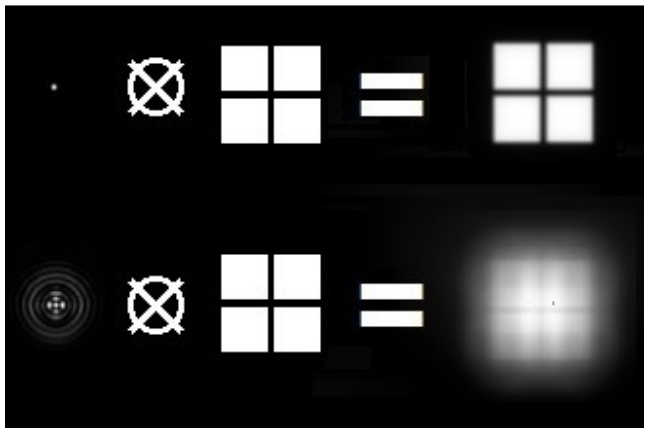

Figure 2.4. The first situation shows the convolution of an object composed of four squares with a diffraction limited PSF yielding a slightly blurred image. In the second situation the object is blurred, point by point by the PSF and its shape resembles that of a single larger square.

The quality of images obtained by cameras is determined by their optical and electronic parameters. These parameters regard the lens design including the correction of monochromatic and chromatic aberrations, the number of pixels on the image sensor and the chip fabrication process technology [56]. Unlike cameras in general, the image quality for the human eye is not well defined by just its optical and retinal properties, being still a mystery concerning how the human visual system translates the retinal image into a visual perception. Besides the optical properties of the eye, subjective characteristics must be considered when evaluating image quality perceived by patients undergoing cataract or presbyopia treatment.

2.4.*MODULATION TRANSFER FUNCTION*

The modulation transfer function (MTF) is defined as the spatial frequency response of an optical system. To calculate the MTF of an imaging system, it is necessary to calculate the Optical Transfer Function (OTF). The OTF is in general a complex function having both a magnitude and a phase terms, which are referred to as the MTF and the phase transfer function (PTF), respectively [57]. The OTF is defined as the two dimensional Fourier Transform of the PSF according to Equation 2.5 [58], where N_1 and N_2 are $\mathrm{PSF}(x',y')$ raster [43] height (x') and width (y'). If a polychromatic PSF is considered in Equation 2.5, then the resulting OTF and subsequently the MTF will also be polychromatic.

$$\mathrm{OTF}(\xi,\eta) = \mathrm{FT2}\{\mathrm{PSF}(x',y')\} = \sum_{x'=0}^{N_2-1}\sum_{y'=0}^{N_1-1} \mathrm{PSF}(x',y').\, e^{2.j.\pi.\left[\frac{x'.\xi}{N_1}+\frac{y'.\eta}{N_2}\right]} \qquad 2.5$$

The 2-dimensional OTF is a function of the spatial frequencies ξ and η. The spatial frequencies are usually given in cycles per degree (cpd), which is commonly used in ophthalmology or in line pairs per millimeter (lp/mm), which is more used in optical engineering and photography. Equation 2.6 is used to convert cpd to lp/mm, where f_{air} is the focal length of the optical system in air and ξ_{cpd} and $\xi_{lp/mm}$ are the spatial frequencies in cpd and lp/mm, respectively [59].

$$\xi_{cpd} = \xi_{lp/mm} \cdot \left[f_{air} \cdot \frac{\pi}{180} \right] \qquad 2.6$$

The MTF is defined as the normalized magnitude of the OTF. In practice, it is given by the complex modulus of the OTF divided by the maximum amplitude. The MTF is dimensionless and is commonly represented as a curve obtained by the central line/column of the 2-dimensional function. It represents the contrast of the image formed by an optical system along the spatial frequencies axis. The first value of the MTF curve is 1, when the frequency is 0. In diffraction limited systems, the higher the spatial frequency, the smaller the MTF until it reaches the value 0. The frequency where a diffraction limited system MTF reaches 0 is defined as the cutoff frequency which is an inherent characteristic of each optical system and is given in lp/mm by $\xi_{cutoff}=(\lambda.F_{\#})^{-1}$. A lens with a small focal length and a large aperture (small $F_{\#}$) will present large cutoff frequency. However, this lens have more spherical aberration than a lens with large $F_{\#}$, which compromises the MTF. If there were no aberrations, the first lens would form sharper images than the second lens, because the MTF would still remain high in a wider range of spatial frequencies before reaching the value 0. This analysis extends to the concept of the spot diameter: when receiving a collimated beam, small $F_{\#}$ lenses form smaller spots than large $F_{\#}$ lenses and as a consequence, those lenses feature more detailed images and greater contrast.

Figure 2.5 shows the MTF curve and the image formed by two diffraction limited lenses. These lenses present f-numbers ($F_{\#}$ equal to 1.4 and 2.0[8]) at 550nm wavelength. The $F_{\#}1.4$ lens have a larger cutoff frequency than the $F_{\#}2.0$ lens, resulting in a higher MTF curve yielding a sharper image. The spots diameters calculated for the $F_{\#}1.4$ and $F_{\#}2.0$ lenses used in this example are 1.88µm and 2.68µm, respectively.

[8] $F_{\#}1.4$ and $F_{\#}2.0$ are conventional values used in the field of optics. A $F_{\#}2.0$ lens has twice the amount of light passing through it than in a $F_{\#}1.4$ lens.

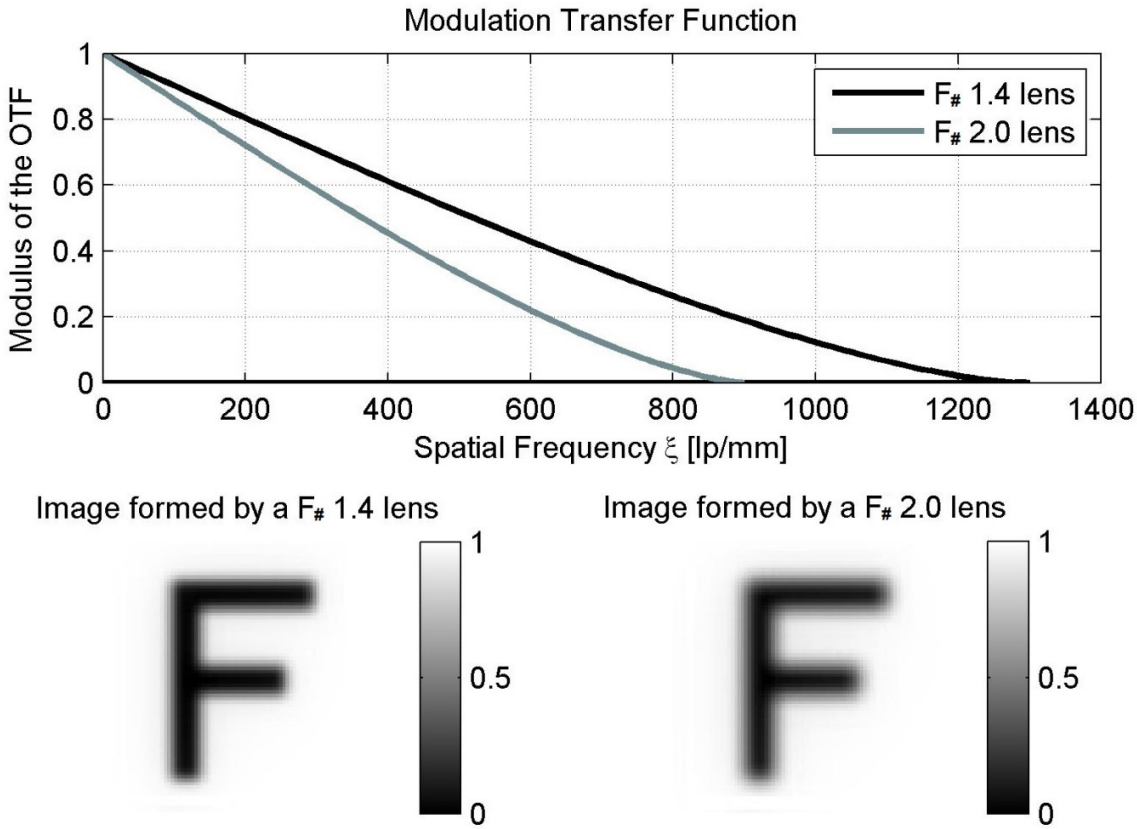

Figure 2.5. MTF curves and images formed by a $F_{\#}1.4$ and $F_{\#}2.0$ lenses.

Both monochromatic and chromatic aberrations are the factors that most influence the degradation of the MTF. If the optical system presents large amount of aberrations, the MTF curve will decay quickly reaching the value 0 in frequencies below the cutoff frequency, which depends on the aperture, the focal length and the wavelength considered. Beside the optics, the spatial resolution of the detector and the retina influence the cutoff frequency of cameras and of the eye, respectively. In conclusion, there are two factors that limit the cutoff frequencies of all optical systems: the optical and the detector resolution. Usually it is the lens system spatial resolution that determines the cutoff frequency of most cameras. The detectors may have a great density of pixels, being capable of capturing lots of details resulting in images with higher contrast. However, depending on the pixel size, the lens system may not be capable of forming a spot as small as one pixel [60]. If the spot that lands on the sensor is not as small as its pixels, then more than one pixel will be illuminated by the same spot. The human eye has cutoff frequency limited by both retina resolution and corneal aberrations. The retina resolution depends on the density of rods and cones and their respective pitch. There are average approximately 90 and 4.5 million rods and cone cells in the eye, respectively. The macula is a 3mm diameter region in the central retina with intense pigmentation [61]. The higher concentration of cones is in the fovea, which is a zone with less pigmentation located in the center of the macula, measuring approximately 1.2mm in diameter. The foveola which is the central 300µm of the fovea, is a region totally rods-free [62].

The density of cones varies from the center fovea to the periphery of the retina from approximately 160.000-180.000cones/mm² to 20.000-32.000cones/mm², showing that its higher concentration occurs in the foveola. Due to the highest density of cones, the foveola is the region where human vision achieves its highest spatial resolution [62,63]. The pitch of adjacent cones is crucial to contrast sensitivity: the higher the pitch, the lower the contrast sensitivity. On the foveola, the pitch of adjacent cones is approximately 2.53µm±0.29 [63]. The retina resolution ξ_{retina} is calculated by Equation 2.7 in lp/mm, where Δ_{cones} is the pitch of adjacent cones in millimeters [64].

$$\xi_{\text{retina}} = \frac{1}{2.\Delta_{\text{cones}}} \qquad 2.7$$

Considering Δ_{cones} equal to 2.53µm, the retina resolution on the foveola calculated by Equation 2.7 is approximately 197lp/mm. Retinal resolutions between 50 and 60cpd on the foveola are presented at [63,65,66]. The resolutions of 50 and 60cpd converted to lp/mm by Equation 2.6[9] result in 174 and 208lp/mm, respectively.

In 2013, Andrew B. Watson collected measurements of 200 eyes aberrations of 100 young and visual healthy subjects. Andrew proposed a formula to calculate eye MTF by the average data of the measured aberrations and the pupil size. The results obtained by Andrew's formula showed MTF curves reaching 0 when the spatial frequency was 60, 80, and 100cpd for pupil sizes of 2, 2.6 and 3-to-6mm, respectively [67]. It is concluded that both optical aberrations which impact considerably on the MTF and the retina resolution are limiting factors for the human visual acuity. The MTF of the human eye should consider both retina resolution limit and the optics MTF (which includes corneal and crystalline/IOL aberrations).

2.5.*CONTRAST SENSITIVITY FUNCTION*

The contrast of an image depends on the detector/retina and the optical system e.g. camera lens set or cornea and crystalline/IOL. However, after being finally projected on the retina, the image is subjected to physiological processes. As a result, the perceived contrast cannot be defined by just the detectors and optics characteristics, being necessary to introduce to the concept of the contrast sensitivity function (CSF). The CSF defines how sensitive humans are to different spatial frequencies stimuli. Mannos and Sakrison [68] have compared the impacts of distorted images in contrast perception, which were subjectively ranked by a group of observers. By comparing the observers judging results they have proposed a mathematical model for the CSF of the human eye. The CSF proposed by Mannos and Sakrison is used in this work and it is calculated by the Equation 2.8, where ξ is the spatial frequency in cpd.

$$\text{CSF}(\xi) = 2.6.(0.0192 + 0.114.\xi)e^{-(0.114.\xi)^{1.1}} \qquad 2.8$$

The graph on Figure 2.6 shows the plot of the CSF function where the spatial frequencies ξ are given in line pairs per millimeters. Equation 2.6 was used to convert the spatial frequencies from cpd to line pairs per millimeter with f_{air} equal to 16.5mm. The function increases from 0 to

[9] The focal length used for the conversion is 16.5mm which corresponds approximately to the focal length of the human eye unaccommodated [105,121].

approximately 1.0 which is its peak when the spatial frequency is approximately 30lp/mm and is close to 0 for frequencies above 200lp/mm indicating that the human eye is more sensitive to contrast at intermediate frequencies around 30lp/mm. The contrast sensitivity is small for very low and high frequencies.

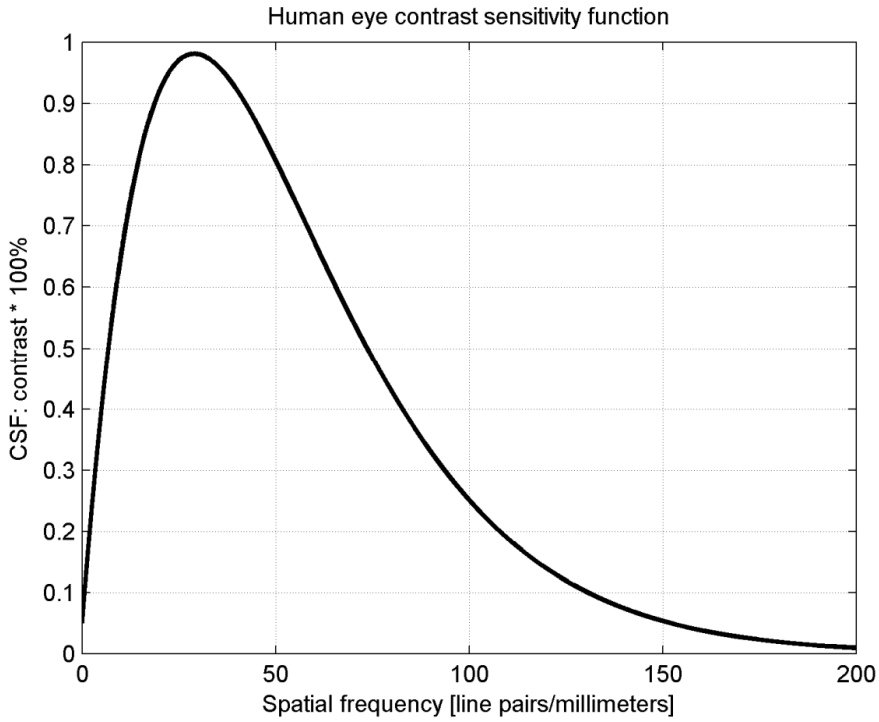

Figure 2.6. Contrast sensitivity function of the human eye, CSF.

The contrast perceived depends on three components: the retina, the eye optics and the subjectivity given by the brain interpretation of the stimuli. Considering individuals who have been submitted to cataract extraction the optics MTF is given by the corneal and IOL MTF. The optics MTF has been less impacted by aberrations because of the design of modern aspheric and toric IOLs to compensate for both the corneal spherical aberration and astigmatism, respectively. IOL designers should be concerned not only with the optics MTF, given by the IOL and the cornea, but with the set eye/optics MTF, which comprises the final contrast sensitivity perceived by the individual after having IOL implant. The eye MTF would be then calculated by Equation 2.9, where the MTF cornea/IOL is the resulting MTF of the optical system[10] formed by the cornea and the IOL and CSF is the contrast sensitivity function of the human eye.

$$\mathrm{MTF_{eye}} = \mathrm{CSF}.\,\mathrm{MTF_{Cornea/IOL}} \qquad 2.9$$

[10] If both cornea and IOL are aberration-free, the resulting MTF of the cornea/IOL system is obtained by the product of the individual MTFs of the cornea and the IOL. However, the resulting MTF obtained by direct multiplication is incorrect and lower if the IOL is intentionally designed to compensate for aberrations of the cornea. In this case, both the IOL and the cornea feature conjugated aberrations and their multiplied MTFs do not correspond to the higher and correct MTF of the combined system where aberrations are compensated.

2.6.*DEPTH OF FOCUS*

The depth of focus (DOF) is defined as the distance that the image plane can move longitudinally along the lens optical axis while maintaining the sharpness of the observed object. It is assumed that for a given optical system there exists blur due to defocusing. If it is sufficiently small, it will not adversely affect the performance of the system [69]. Figure 2.7 shows focal shifts of -100, -50, 0, 50 and 100µm of an aberration-free $F_{\#}$3.33 lens.

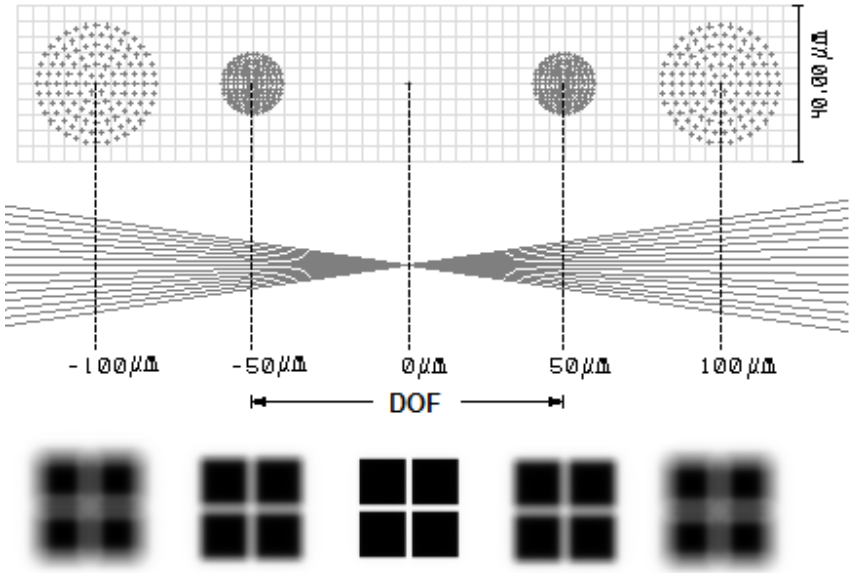

Figure 2.7. Image blur and spot size variation as a function of the focal shift.

The five dashed lines represent the location where each image is being formed, respectively (image planes). The focal plane is the plane where the best focus is obtained, which corresponds to the location of the smallest spot that the optical system can yield. The position of the focal and image planes may not coincide (e.g. when the object approaches or moves away from the optical system) and consequently yield image blur as it is shown in Figure 2.7. When the focal shift is equal to 0, the image plane and the focal plane are exactly located in the same position and as it is shown in Figure 2.7, it is the situation where the spot size is the smallest the lens can yield. As the displacement between the image and focal planes increases, the spot diameter starts to increase, leading to blurred images. By Figure 2.7 analysis it is concluded that the smaller the focal shift, the smaller the spot diameter and the sharper the image. The DOF is the maximum image plane displacement that results in acceptable image blur. The image blur is caused mainly by defocus which is an aberration related to images out of focus [70]. Spherical aberration also affects DOF [71] because its Zernike mathematical function carries the defocus aberration term with an additional higher order component [72]. The controlled use of spherical aberration to expand individuals DOF has been currently achieving satisfactory results [73-75].

Figure 2.8 shows the results of defocus and spherical aberration as a function of ±0.5mm focal shift for an aberration-free $F_{\#}$3.33 lens.

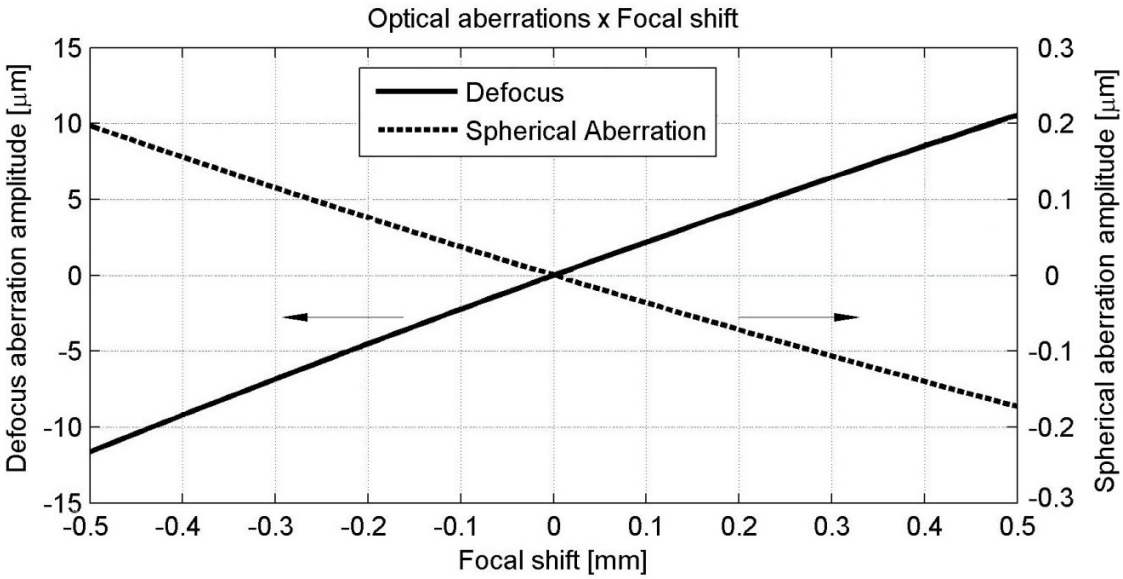

Figure 2.8. Defocus and spherical aberration as a function of lens focal shift.

Figure 2.8 shows that when the focal shift is 0, the image plane is in focus and as the lens is aberration-free, all of the aberrations amplitude are null. Spherical aberration is less sensitive to focal variation while it is critical for defocus.

As the image sharpness is degraded by the increase in the spot diameter, there will be a circle yielded by a cone of light rays intercepting a plane that is not coincident to the focal plane. This circle is defined as the circle of confusion (COC) also known as the largest blur circle that will still be perceived by the human eye as a point before being perceived as a circle [76]. The value of the COC is somewhat arbitrated and may vary between individuals. An estimation of the circle of confusion diameter (c) for the human eye which is also used in 35mm photography is given by the Equation 2.10 [77,78]:

$$c = \frac{1\text{inch}}{1000} = 1\text{mil} = 0.0254\text{mm} \qquad 2.10$$

According to Castrejón-Pita et al [77], a circle or dot with diameter equal or smaller than c will be seen as a point by the human eye at a comfort reading distance (250 mm). If each point that composes an object is imaged as a circle with diameter less or equal to 0.0254mm, than the image of the entire object is seeing by the human eye as if it was in perfect sharpness. Otherwise it will appear to be blurred.

The DOF of a thick lens[11] is illustrated in Figure 2.9 where F^* is the focal point, n' and n'' are the refractive index of the anterior and posterior media, respectively, n_L is the lens refractive index, s_o

[11] Real lenses have some non-zero central thickness which are considered null on the equation set for thin lenses. However the central thickness is not negligible when designing IOLs because these lenses feature short focal length (small curvature radius) resulting in large central thickness that if disregarded will affect significantly the determination of its dioptric power. Because this work regards to IOL design, all of the analysis will be focused on thick lenses.

is the distance between lens and object, P and P* are the anterior and posterior principal planes[12] and t is the lens thickness:

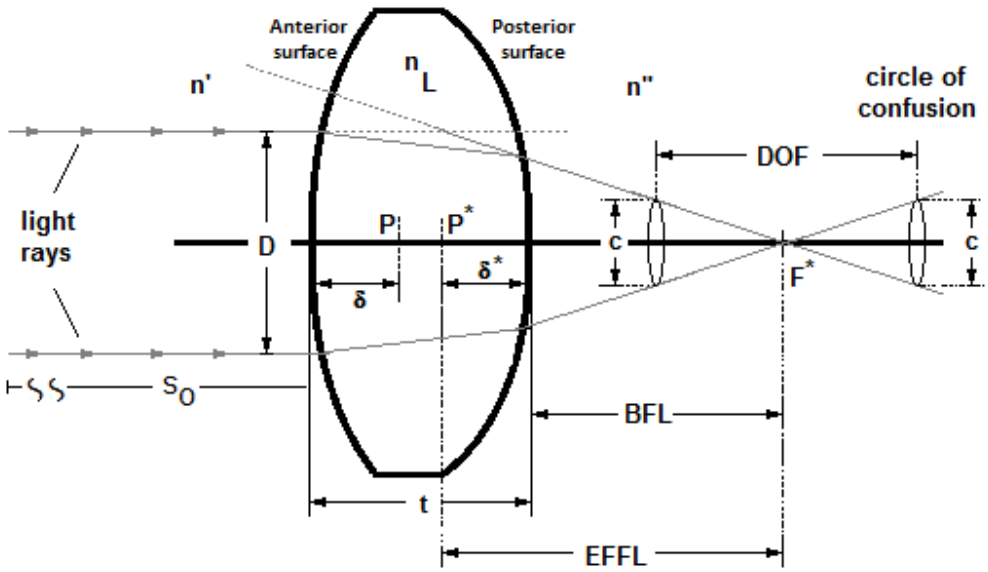

Figure 2.9. Depth of focus for a given circle of confusion diameter c.

The DOF is calculated by Equation 2.11 based on similar triangles (RSU and VXU) as shown in Figure 2.9,

$$\frac{\mathrm{DOF}}{2.\mathrm{c}} = \frac{\mathrm{EFFL}}{\mathrm{D}} \xrightarrow{\text{yields}} \mathrm{DOF} = \frac{2.\mathrm{c}.\mathrm{EFFL}}{\mathrm{D}} = 2.\mathrm{c}.\mathrm{F\#} \qquad 2.11$$

where EFFL is equal to the lens effective focal length, D is the pupil aperture and c the circle of confusion diameter. However, Equation 2.11 should be used only when the object is located at infinity (s_o=∞) yielding a null transversal magnification. Considering any object location, the DOF is calculated by Equation 2.12, which is demonstrated on the Appendix section of this work,

$$\mathrm{DOF} = 2.\mathrm{c}.\mathrm{F\#}.\left(1 + \frac{\mathrm{s_i}}{\mathrm{s_o}}\right) \qquad 2.12$$

where the ratio of image distance s_i and the distance between lens and object s_o is defined as the transversal magnification, which is dimensionless, so s_i and s_o must be given in the same unit. The image distance s_i for a thick lens is given in millimeters by the Equation 2.13 which is demonstrated on the Appendix section of this work,

$$\mathrm{s_i} = \left[\frac{1000 - \delta.\mathrm{OBJ_{verg}}}{\Phi_{\mathrm{lens}} + \mathrm{OBJ_{verg}} - 0.001\delta.\Phi_{\mathrm{lens}}.\mathrm{OBJ_{verg}}}\right] + \delta^* \qquad 2.13$$

where Φ_{lens} and $\mathrm{OBJ_{verg}}$ are respectively the thick lens total power and the object vergence, both given in diopters (m^{-1}). δ and δ*are the principal planes distance to the lens anterior and posterior

[12] The effective focal length of a thick lens is measured to a reference point associated with the lens principal planes position [79].

surfaces given in millimeters. Φ_{lens} and OBJ_{verg} are calculated by the Equations 2.14[13] [79], and 2.15 [80], where Φ_A and Φ_P are respectively the anterior and posterior lens power given in diopters and t is the lens thickness. Both t and s_o are given in millimeters.

$$\Phi_{lens} = \Phi_A + \Phi_P - \Phi_A.\Phi_P.\frac{0.001.t}{n_L} \qquad 2.14$$

$$OBJ_{verg} = \frac{-1000}{s_o} \qquad 2.15$$

Φ_A and Φ_P are calculated by the Equation 2.16, where R_A and R_P are the anterior and posterior lens curvature radii in millimeters:

$$\Phi_A = \frac{n_L - n'}{0.001.R_A}\ ;\ \Phi_P = \frac{n'' - n_L}{0.001.R_P} \qquad 2.16$$

The location of the anterior and the posterior principal planes is obtained by calculating δ and δ^* which are based on known lens parameters. δ is the distance between the lens front surface and the anterior principal plane P and δ^* is the distance between the lens rear surface and the posterior principal plane P^* as shown in Figure 2.9 and are calculated in millimeters by the Equation 2.17:

$$\delta = \frac{t.\Phi_P.n'}{\Phi_{lens}.n_L}\ ;\ \delta^* = -\frac{t.\Phi_A.n''}{\Phi_{lens}.n_L} \qquad 2.17$$

Considering a thick lens with R_A and R_P equal to +9mm and -7mm respectively, a central thickness of 2mm and refractive index of 1.55 surrounded by water (n'= n''=1.33), Equation 2.16 yields 24.44D and 31.43D for Φ_A and Φ_P respectively. Equation 2.14 yields Φ_{lens} equal to 54.88D. The principal planes location are calculated by Equation 2.17 which results in 0.983mm and -0.764mm for δ and δ^*, respectively. The effective focal length is the inverse of the optical power and is given in millimeters by 1000/ Φ_{lens} resulting in 18.220mm. According to Figure 2.9, the back focal length (BFL) is equal to EFFL-$|\delta^*|$resulting in 17.456mm. An important condition occurs when the object is at infinity which results in the image distance s_i exactly equal to BFL. If the object is located at a known distance s_o, than s_i must be calculated by Equation 2.13. If the lens in this example was considered thin (t=0), than the optical power Φ_{lens} would be 55.87D and δ and δ^* would be null. The absolute difference found when considering this lens thick or thin (54.88D and 55.87D) is approximately 1D which is not negligible.

The depth of field is defined as the distance that the object can move longitudinally along the optical axis while its image appears to be in focus [79]. The depth of field and the depth of focus are analogous concepts concerning maximum acceptable blur: the DOF is associated to image plane shifts while the object is fixed at the same position and the depth of field regards to object displacement while maintaining the image plane at a fixed location. Besides being analogous concepts, the depth of field and the DOF are proportional: a lens with extended DOF will also

[13] The optical power is commonly expressed in diopters which is the inverse of the focal length in meters and the lens parameters such as radii of curvature and central thickness are commonly expressed in millimeters. The conversion coefficients of 1000 and 0.001 were incorporated to the equations to unify the units used: millimeters to the lens parameters and diopters for optical power in order to facilitate the calculation in practice.

feature an extended depth of field, so objects located at different distances will appear to be in focus. The depth of field of a thick lens is calculated by Equation 2.18, which is demonstrated on the Appendix section of this work:

$$\text{Depth of field} = \begin{cases} d_{far} \text{ to } d_{near}, & \text{if } d_{far} > 0 \text{ and } s_o \neq \infty \\ \infty \text{ to } d_{near}, & \text{if } d_{far} < 0 \text{ or } s_o = \infty \end{cases} \qquad 2.18$$

Where d_{near} and d_{far} are the smaller and the largest distances between object and lens, respectively. If the object is located at infinity ($s_o = \infty$) or d_{far} results in a negative value, than d_{far} will be equal to infinity and the depth of field will extend from infinity to d_{near}, otherwise the depth of field extends from d_{far} to d_{near}. d_{near} and d_{far} are calculated in millimeters by Equations 2.19 and 2.20, where s_i was defined in Equation 2.13:

$$d_{near} = 1000.\left[\frac{(D.s_i - D.\delta^* + c.\delta^*).(0.001.\Phi_{lens}.\delta - 1) - \delta.(D - c)}{1000.(D - c) - (D.s_i - D.\delta^* + c.\delta^*).\Phi_{lens}}\right] \qquad 2.19$$

$$d_{far} = 1000.\left[\frac{(D.s_i - D.\delta^* - c.\delta^*).(0.001.\Phi_{lens}.\delta - 1) - \delta.(D + c)}{1000.(D + c) - (D.s_i - D.\delta^* - c.\delta^*).\Phi_{lens}}\right] \qquad 2.20$$

The lens power Φ_{lens} is given in diopters and s_i (image distance) D (diameter of the pupil), c (circle of confusion diameter), δ and δ^* are given in millimeters. An important condition occurs when the far point d_{far} extends to infinity. In this case, by moving to infinity an object that is focused at a distance to the lens will result in a spot diameter equal or smaller than the COC. The highest depth of field occurs when the focused object is moved to infinity and the spot diameter equals the COC. This is the situation where the optical system is focused at the hyperfocal distance (H). When focusing at the hyperfocal distance, the depth of field extends from infinity to approximately H/2, which is demonstrated on the Appendix section of this work. The hyperfocal distance is calculated in millimeters by the Equation 2.21, which is demonstrated on the Appendix section of this work:

$$H = 1000.\left[\frac{1000.(D + c) + \Phi_{lens}.c.(\delta^* - \delta - 0.001.\delta.\delta^*.\Phi_{lens})}{\Phi_{lens}.c.(1000 + \delta^*.\Phi_{lens})}\right] \qquad 2.21$$

The lens power Φ_{lens} is given in diopters and s_i (image distance), D (diameter of the pupil), c (circle of confusion diameter), δ and δ^* are given in millimeters.

The DOF can be determined graphically by calculating the MTF at a pre-established spatial frequency while the image plane moves along the optical axis. The curve obtained contains sufficient information to determine the DOF, and is defined as the MTF through focus curve. Usually the focal shift is expressed as defocus in diopters instead of millimeters yielding a DOF measured in diopters. A MTF through focus curve is shown in Figure 2.10 for an aberration-free $F_{\#}3.33$ lens at 50 and 100 lp/mm and 550nm wavelength:

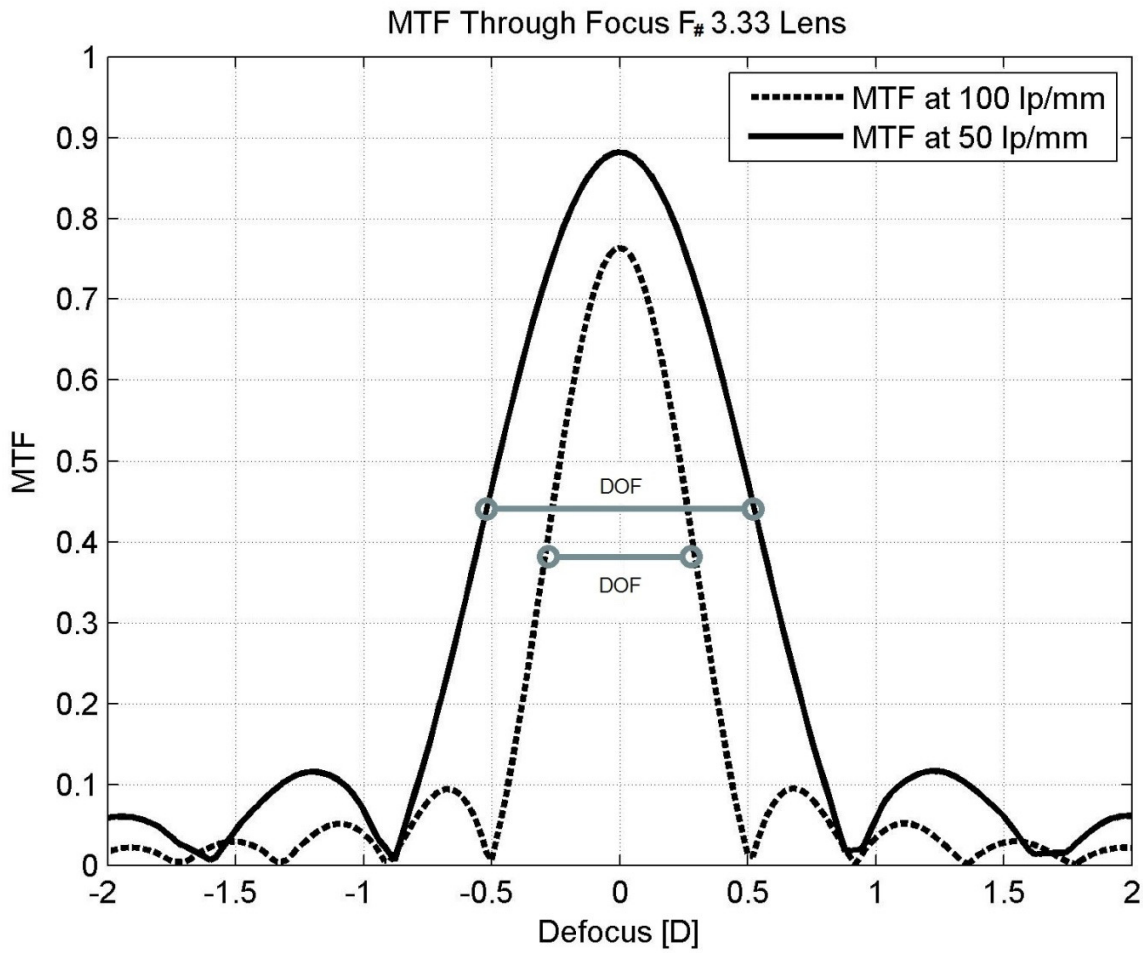

Figure 2.10. Depth of focus for an unaberrated $F_{\#}$3.33 lens. The DOF (D) is defined as the defocus range for which the MTF stays above 50% of its maximum value.

The DOF of the lens at 100 and 50lp/mm are approximately 0.5 and 1D, respectively. It is possible to conclude that the lower the spatial frequency, the larger the DOF. The spatial frequency considered to calculate the MTF through focus curve and the COC diameter are parameters that impact directly on the amplitude of the DOF obtained graphically and mathematically, respectively. The DOF is also related to the area under the MTF through focus curve: the higher the area under curve, the higher the DOF. However, the area under curve do not carry enough information to determine the DOF quantitatively.

Parameters such as the focal length, the pupil aperture and the COC diameter are critical to the DOF. Lenses with small apertures and large focal length yielding large $F_{\#}$, will provide long DOF. Figure 2.11 shows the DOF of 4 different aberration-free lenses at 550nm wavelength:

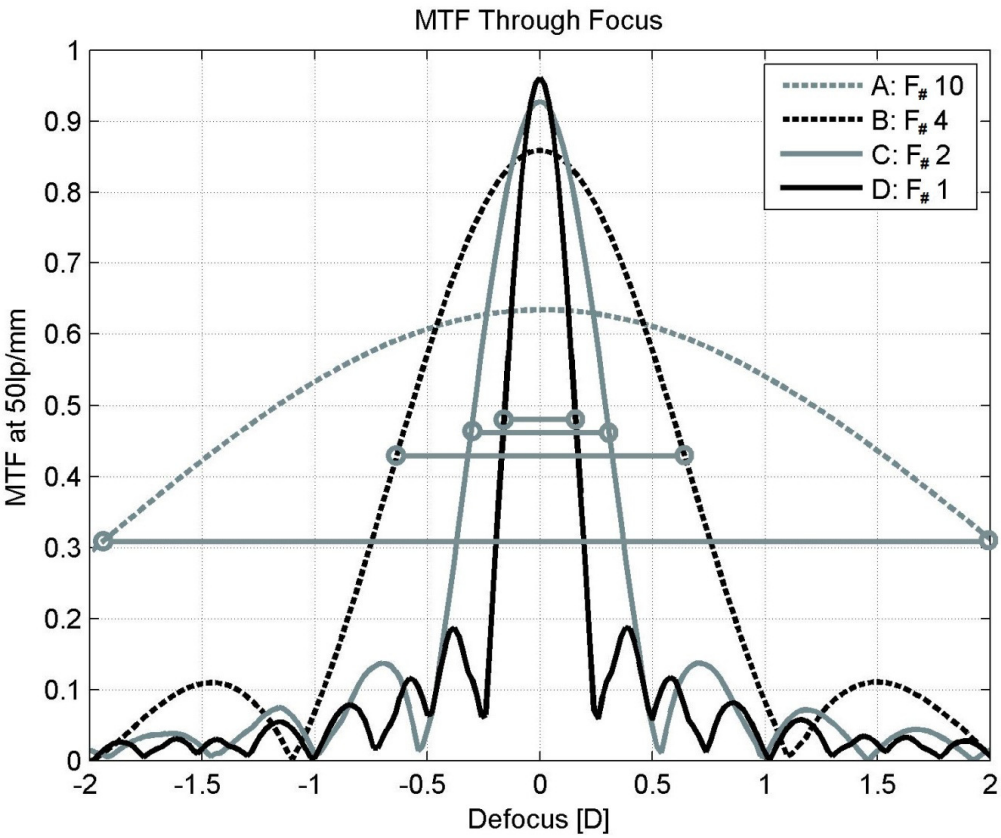

Figure 2.11. Depth of focus for a 4 different lenses.

Figure 2.11 shows that the lenses A and D present the longest and the shortest DOF, respectively. In agreement to the DOF, the area under the curves for lenses A and D are also the largest and smallest, respectively. On the other hand, the central peak for the lens D is the highest showing that this lens provides the highest contrast because it yields the smallest spot diameter[14]. Considering a COC of 0.0254mm, Equation 2.12 provides the DOF values of: 0.508, 0.2032, 0.1016 and 0.0508mm respectively for lens A, B, C and D, showing that the results obtained by Equation 2.12 are according to the results shown on the graph of Figure 2.11.

Focal length increase and reduction on the pupil size will provide long DOF of an IOL. However, the IOL focal length is determined by biometric parameters such as the axial length of the eye and the corneal dioptric power. This means that for a given corneal dioptric power Φ_{cornea} and an eye with axial length AL, there will be one IOL with specific power Φ_{IOL} capable of focusing rays coming from far objects on the retina properly. Furthermore it is impossible to intentionally decrease the pupil size without causing loss of incoming light. Patients vision at night would be compromised by the reduced light entrance. Besides varying the focal length and the aperture, the DOF is affected by aberrations, especially spherical aberration as shown in the study [71]. This study concluded that although contrast sensitivity is higher for aspheric in comparison to spherical lenses, the DOF is

[14] The spot diameter was calculated for the four lenses resulting in 13.42µm, 5.37µm, 2.68µm and 1.34µm for lens A, B, C and D, respectively.

shorter. Bifocal and trifocal lenses also provide extended DOF by using refractive, diffractive or both strategies. The refractive strategy consists of dividing the IOL optical zone into many annular zones where each zone yields a different optical power. Diffractive strategies are implemented by adding zonal discontinuities as steps with determined height to provide controlled interference and light distribution efficiency along the optical axis. Diffractive masks [81] are also used to control and extend the DOF. It consists of pupil function modification by adding diffractive grooves with different depths along the lens surface. The diffractive masks may be optimized to provide a lens PSF the most invariant to defocus as possible [82]. Hybrid strategies are combinations of refractive and diffractive solutions. The main disadvantage of extending the DOF is the loss of contrast. Both diffractive and refractive DOF extension strategies feature loss of contrast and may present wavelength dependence. The lens system behavior may be beneficial for a specific wavelength and detrimental for the others.

2.7.*TOLERANCING*

The main goal when designing an optical system is to achieve the best optical performance which is based on metrics such as maximum MTF response, minimum spot radius or minimum RMS wavefront error. Optimization algorithms have been widely used to improve the optical system performance by directing it towards a very specific optimal solution called theoretical design. Although the performance analysis of this particular solution is important, it does not take into account manufacturing errors, which may alter and degrade the optical performance of the theoretical design. Tolerance analysis allows the understanding of how variations in the product theoretical design parameters due to manufacturing errors affect its final performance. Considerations of manufacturing tolerances become increasingly important as the complexity of optical designs increases, like the aspheric profiles that may include up to eighth-order terms. There is a high likelihood that a designed optical component cannot be built because the fabrication tolerances are beyond the capability of optical manufacturing technology. Determining appropriate tolerances is one of the most important steps of an optical project because it allows the evaluation of the final produced component performance. Table 2.1 presents a reasonable starting point for typical manufacturing tolerances for lens radius of curvature, center thickness aspheric profile and wedges considering three different classes of precision: commercial, high quality and manufacturing limits [83]. Typical tolerance values determined for a 50mm diameter lens are shown in Table 2.1. The tolerances are not absolute and may vary depending on component size, shape or material [83].

Table 2.1. Typical manufacturing tolerances for a BK7 50mm diameter lens

Parameter	Commercial quality	Precision quality	Manufacturing limits
Radius of curvature [%]	±0.2	±0.1	±0.05
Diameter [mm]	±0.1	±0.025	±0.001
Wedge lens[1] [mm]	0.05	0.01	0.005
Aspheric profile[2] [μm]	±25	±1	±0.5

[1]Wedge is related to the absoulute lens edge thickness difference.
[2]Aspheric profile regards to the maximum deviation between the ideal aspheric profile and the manufactured.

The tolerance range is narrower as the precision enhances and as a general rule, price increases around 50% going from commercial to precision quality. Tolerancing is closely related to optimization: the basic tolerance computation is to calculate how much a performance metric changes for a small change in a construction parameter [84]. Every parameter is independently and randomly perturbed according to its assigned tolerance. This procedure creates random lenses on the computer, based on each parameter set of tolerances.

2.8.*LUMINOSITY*

The term luminosity may be associated to two different measures: luminance and illuminance. The luminance measures the quantity of light emanating from the image area of a light source or reflecting surface into the aperture area of a camera sensor, or the retina. The illuminance measures the incoming light flux striking a surface. The difference between these two terms is that the illuminance measures the amount of incoming light and the luminance the quantity of light measured off of the surface that has light hitting it. The SI units for luminance and illuminance are respectively candelas per squared meters ($cd.m^{-2}$) and lux: lumens per square meters ($lm.m^{-2}$). The retinal illuminance is measured in Trolands, which is the luminance in $cd.m^{-2}$ multiplied by the pupil area in mm^2.

Individuals pupil diameter is quickly and involuntary resized by the iris according to the environment lighting condition. Pupil size adapts to changes in luminance in order to control the light portion that strikes the retina. The brighter the environment, the smaller the pupil, so considering a sunny day on a beach, it is expected that individuals will feature small sized pupils. On the other hand, at night or within a place with dim lighting, individuals will present large sized pupils. The retina illuminance is proportional to the area of the entrance pupil, which also have a direct effect on DOF. Several studies have investigated the effect of luminance on the pupil size [85-89]. Besides luminance, variables such as the field of view size [90,91], individuals age [92] were also related to the causes of changes on the pupil size. The field of view of an optical system is often expressed as the maximum angular size of the object as seen from the system pupil [93]. The system pupil (D) defines the cones of light entering the optical system from any object point as shown in Figure 2.12, where f is the optical system focal length and α is the angular field of view.

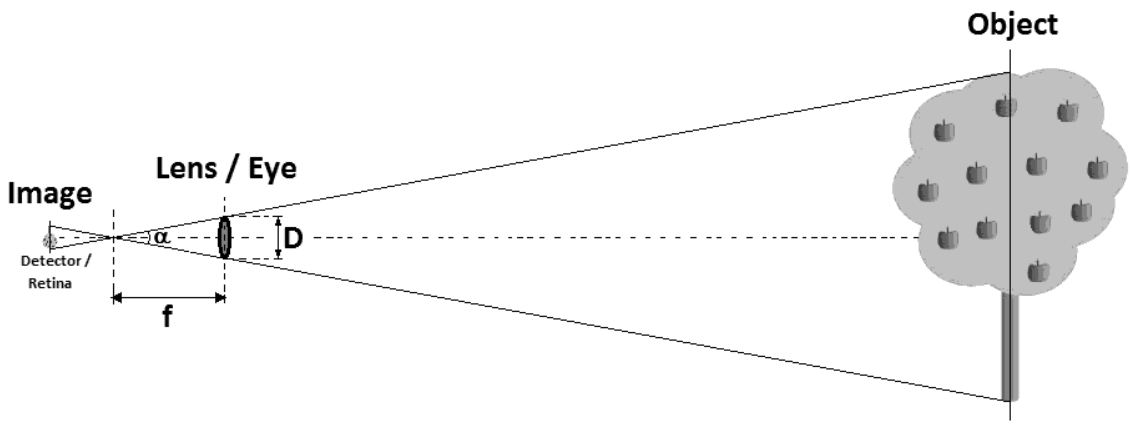

Figure 2.12. Field of view schematic diagram.

In fact, the field of view is limited by either the detector size if it is smaller than the image or by the system pupil. The system pupil may be determined by an aperture (e.g. diaphragm) assembled to the lens or by the lens diameter, which is the case shown in Figure 2.12. Considering the condition shown in Figure 2.12, the field of view can be calculated in degrees by Equation 2.22, where f and D are the optical system focal length and pupil, both given in the same unit. From Equation 2.22 it is concluded that lenses with smaller $F_{\#}$ feature larger field of view.

$$\alpha = 2.\tan^{-1}\left(\frac{D}{f}\right) = 2.\tan^{-1}\left(\frac{1}{F_{\#}}\right) \qquad 2.22$$

The pupil size also varies from monocular to binocular vision [94]. Watson and Yellott have proposed an unified formula to calculate the pupil diameter based on the published data provided by previous studies which that takes into account the luminance, field size, age and monocular/binocular effects [95].

Common activities such as driving at day and night, working in an office, reading a book, practicing outdoor activities, using the cell phone or tablet are performed under different light conditions. Table 2.2 shows the luminance benchmarks associated to different light sources [96,97]. Figure 2.13 shows an illustration of the benchmark light sources shown in Table 2.2 and their respective relative luminances with the photopic, mesopic and scotopic light boundaries.

Table 2.2. Luminance benchmark for different light sources.			
Light source	Luminance cd.m^{-2}	Light source	Luminance cd.m^{-2}
Lightning flash	$7.0*10^{10}$	LCD Monitor	$3.5*10^{2}$
Sun (zenith)	$3.2*10^{9}$	White paper under surgical light	$2.8*10^{2}$
Photoflash	$1.0*10^{8}$	Tablet white 50% Brightness	$1.7*10^{2}$
Carbon arc lamp	$1.6*10^{7}$	White color plasma television	$1.7*10^{2}$
Upper photopic limit	$1.0*10^{7}$	Overcast sky	$1.3*10^{2}$
Eye damage: brief exposure	$4.0*10^{6}$	White paper under office light	$1.3*10^{2}$
Sun (horizon)	$4.3*10^{5}$	White of computer monitor	$1.0*10^{2}$
Eye damage: long exposure	$3.2*10^{5}$	Wax candle flame	$1.0*10^{2}$
60W incandescent light	$1.2*10^{5}$	White paper under reading light	$8.4*10^{1}$
White paper in daylight shade	$3.0*10^{4}$	Upper mesopic limit	$1.4*10^{1}$
Clear sky (horizon)	$1.3*10^{4}$	LED light	$5.0*10^{0}$
T8 fluorescent light	$1.1*10^{4}$	Lower photopic limit	$3.3*10^{0}$
Cumulus cloud 90° from the sun	$1.0*10^{4}$	Clear sky twilight (zenith)	$1.0*10^{0}$
Low beam car headlights	$7.0*10^{3}$	Brightest star (Sirius)	$2.4*10^{-1}$
Average sky	$6.0*10^{3}$	White paper under full moon	$6.0*10^{-2}$
Full moon (zenith)	$4.2*10^{3}$	Upper scotopic limit	$3.9*10^{-3}$
White paper in daylight shade	$3.6*10^{3}$	Fairly bright moon	$3.0*10^{-3}$
Clear sky (zenith)	$2.5*10^{3}$	Lower mesopic limit	$6.9*10^{-3}$
Cloudy sky (zenith)	$2.0*10^{3}$	White paper under star light	$3.2*10^{-4}$
White paper in dark cloudy day	$2.0*10^{3}$	Starless night sky	$4.0*10^{-4}$
Full moon (horizon)	$5.6*10^{2}$	Lower scotopic limit	$8.3*10^{-7}$
Tablet white 100% brightness	$4.0*10^{2}$		

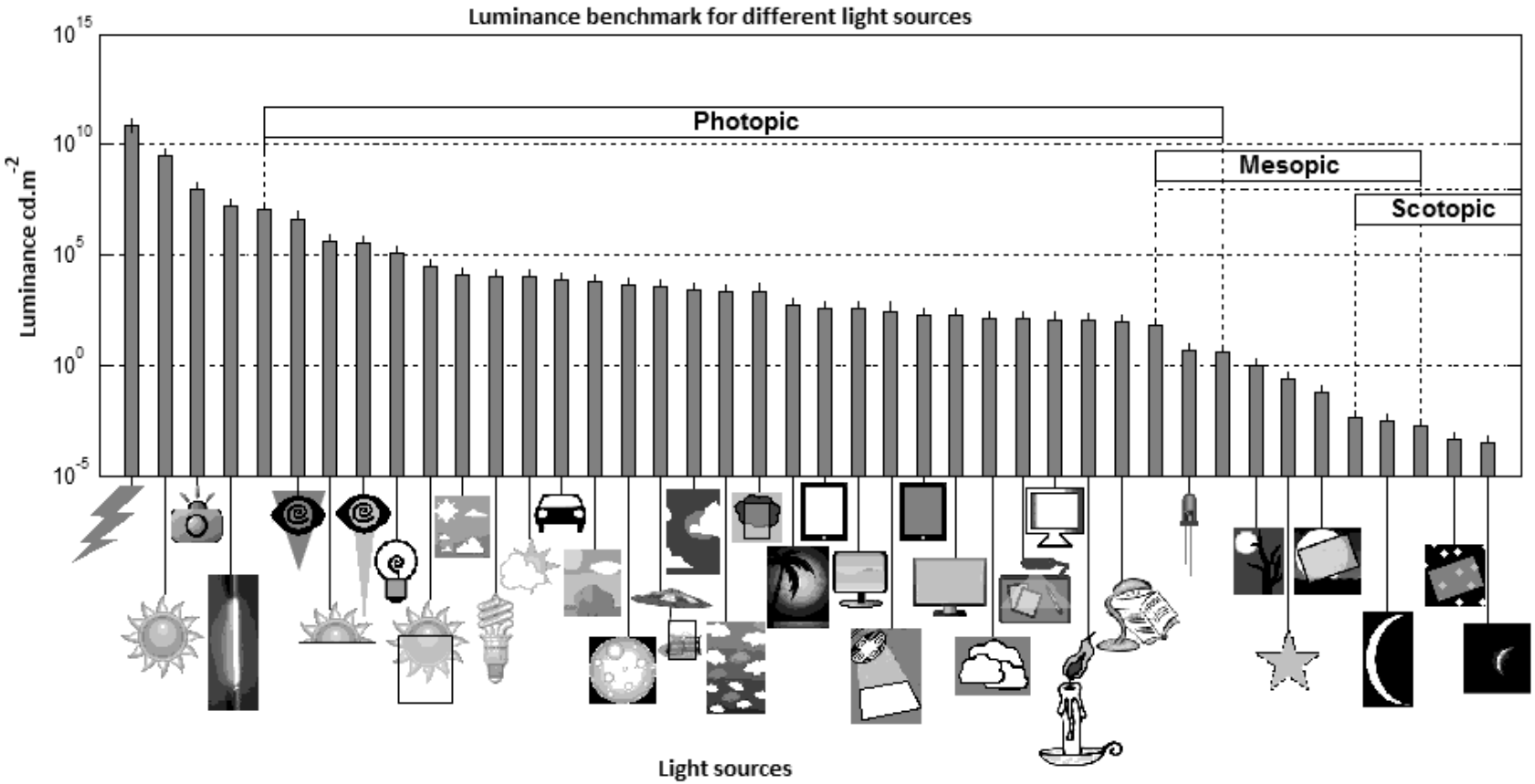

Figure 2.13. Illustration of benchmark light sources and respective related luminance values.

The unified formula provided by Watson and Yellott was used to calculate the pupil size for different values of luminance ranging from 10^{-4} to 10^{10} cd.m^{-2} considering field diameters of 0.4° and 25.4°, ages of 45 and 65 years and binocular vision. The values chosen for field diameter are the lower and upper field boundaries used in Stanley and Davies study [90] which represents one of the basis used in Watson and Yellott unified formula. The relation between the pupil diameter and luminance is shown in Figure 2.14 considering these field diameters and these ages.

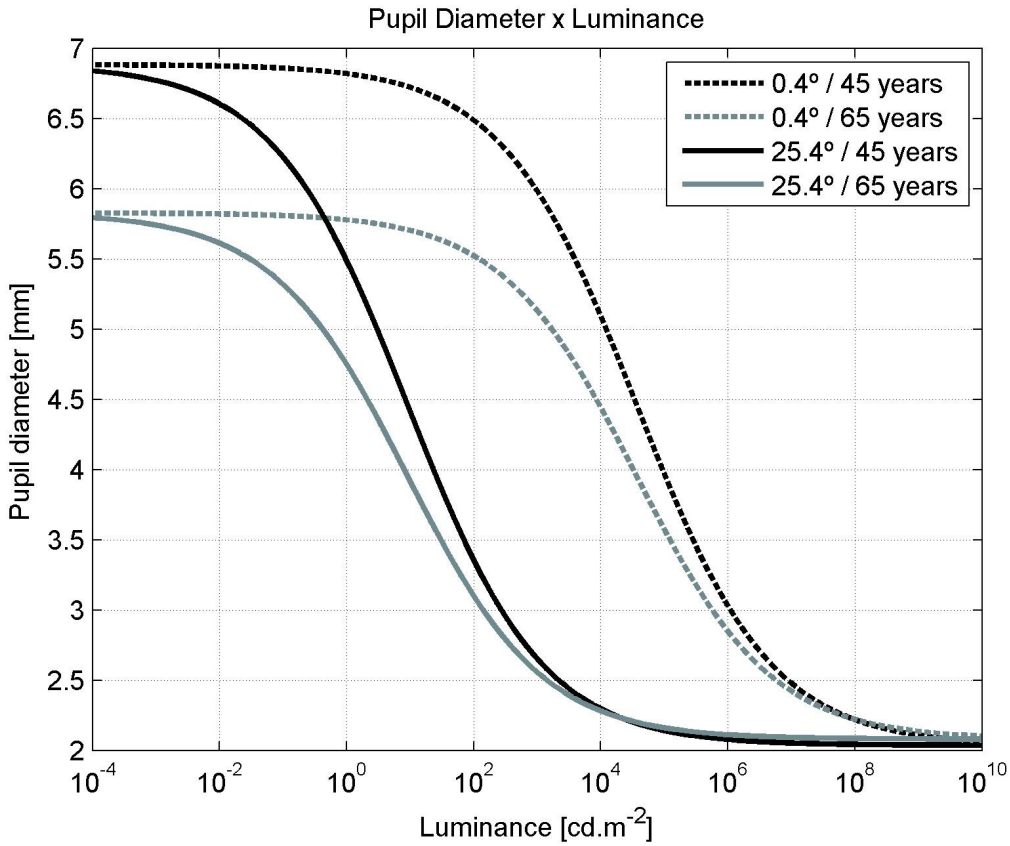

Figure 2.14. Pupil diameter as a function of the luminance, field diameter in degrees and age in years.

Figure 2.14 shows that the pupil diameter is highly influenced by the luminance, the field diameter and the individuals age. The smaller the field, the larger the pupil diameter at fixed luminance and age. The age represents a vertical offset of the pupil diameter: the older the individual the smaller the pupil diameter at small luminance~~s~~. The knowledge of the individual pupil size according to each light condition consists of a helpful information for designing an optimal and personalized IOL featuring extended DOF in order to maximize visual performance observing the patient age and privileging his or her daily habits.

3. TECHNICAL DEVELOPMENT

This work proposes the development of an IOL with extended depth of focus being less sensitive to defocus when compared to four different commercial monofocal IOLs, where three are aspheric and one is spherical. Aspheric IOLs minimize the spherical aberration component providing higher contrast, but compromise the DOF and consequently the depth of field. Furthermore, they are more sensitive to the effects of chromatic aberration by having short DOF associated with different wavelengths. Spherical IOLs have higher DOF in comparison to aspheric, but the spherical aberration compromises contrast sensitivity. Although contrast is somewhat reduced with an IOL with extended depth of focus, the development such IOL is beneficial to provide near vision improving cataract surgery outcome. Cataract surgery success depends on several factors, such as surgeon ability, lens power calculation, biometry precision and uncertainty regarding IOL final position within the eye. Due to these factors, and considering the current state of the art, an individual undergoing cataract surgery should expect to have refractive errors of ±0.5D [98,99], and by extending IOL depth of focus, it becomes less sensitive to variations in its final position within the eye.

The proposed lens is composed of two pieces (anterior and posterior) made each one, for instance, with different and flexible optical adhesive. In this particular case the convex depressions are filled by the adhesive that composes the anterior piece, that fit in and is bonded on the posterior piece. The other side of the posterior piece consists of a convex aspheric surface. The anterior piece consists of a plano-convex aspheric surface with four convex structures on the flat side. The extern surfaces of the anterior and posterior pieces are similar to standard lenses. A schematic diagram of the Perifocal IOL is presented in Figure 3.1. The four convex structures are lenticles which overlap about the center of the anterior surface. The overlap is intentional and beneficial in order to avoid the presence of edges and gaps between edges that would enhance detrimental effect of diffraction.

The number of lenticles was restricted to four because it is the smallest number of elements which provides bi-directional symmetry with minimum interface edge diffraction, allowing that incoming light energy is distributed equally over the X and Y axis. By using just one lenticle, it will only be axially symmetric, if it is centered on the principal standard lens optical axis, which is the case of conventional bifocal refractive lenses. Two lenticles favor only the axis that they have symmetry. Three lenticles have symmetry affected by IOL rotation within the eye, favoring a specific axis depending on the rotation amplitude. Four lenticles provide symmetry and regardless of IOL rotation, all the light energy is equally distributed over the X and Y axis. Other numbers greater than four lenticles would provide axial symmetry too, but in such cases there would be more boundaries causing more diffraction, which compromises the IOL optical performance.

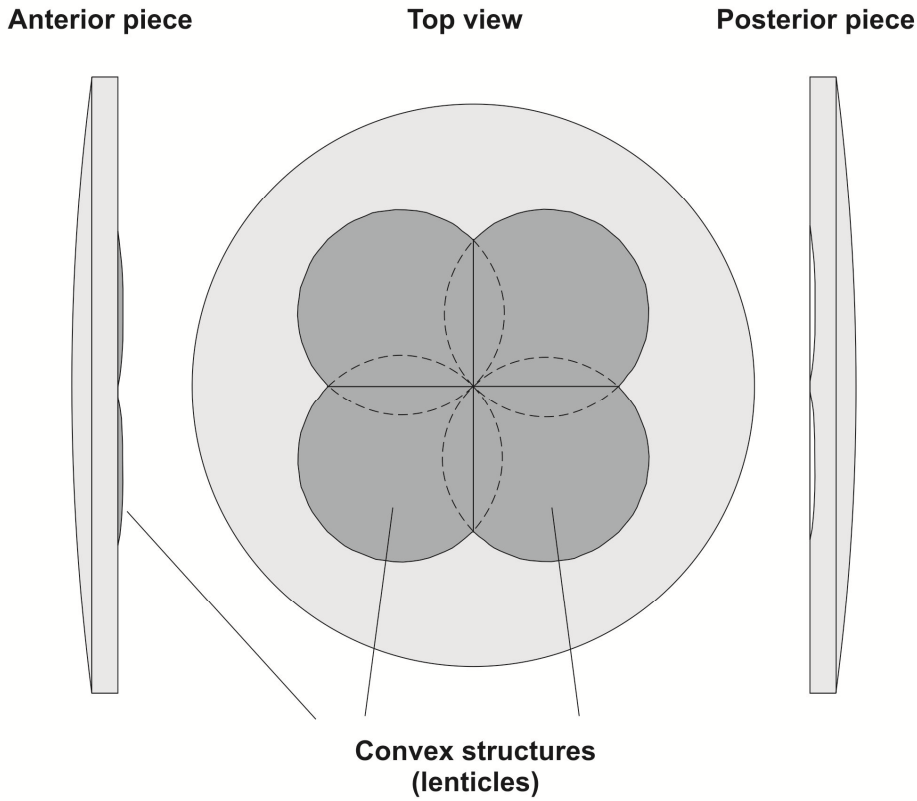

Figure 3.1. Schematics of IOL anterior and posterior pieces. Light enters the anterior piece.

An image of the IOL proposed (Perifocal IOL) is shown in Figure 3.2 where the side view and the perspective view are highlighted.

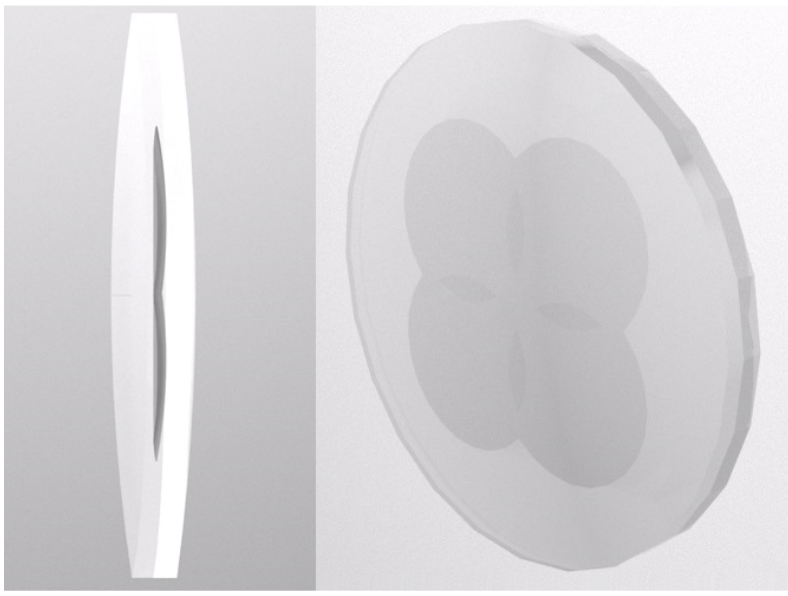

Figure 3.2. Perifocal IOL: side view [left] perspective view [right].

3.1.*HOW IS DOF EXTENDED?*

Conventional refractive multifocal lenses are composed of few surfaces with different dioptric powers along the lens optical zone. The refractive surfaces are centered at the same point, indicating that the focal points lie on the same optical axis. Unlike these lenses, the four lenticles are decentered from the main lens center, so each one has a different optical axis. As the lenticles are decentered, their respective focal points are shifted off axis, the reason why the proposed lens will be denominated Perifocal lens. The lenticles separately will form four overlapped and independent images, each one aligned with the respective lenticle optical axis. An image of a single letter "F" obtained by an optical system composed by only four shifted lens is shown in Figure 3.3, which also shows an schematic diagram of the optical system used in this simulation. The object was located at infinity and the image plane was optimized for the best focus position.

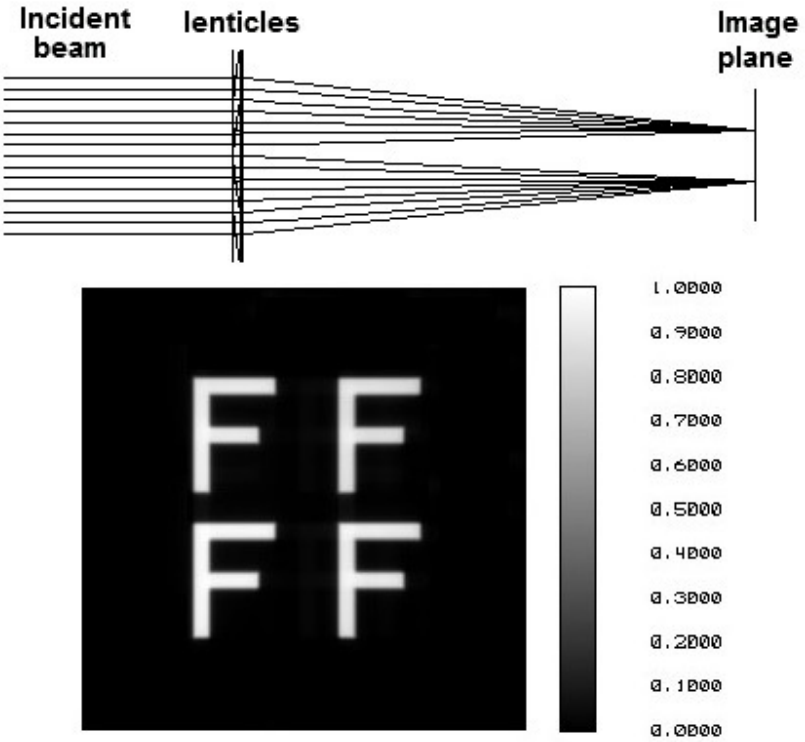

Figure 3.3. Schematic diagram of the optical system and the image of a single letter "F" formed by an optical system with only the four overlapping lenticles.

The single letter "F" is imaged four times by the optical system. Each letter was imaged by a different lenticle resulting in four letters because their optical axes are not coincident. The effect of adding a standard lens in cascade to the lenticles is observed in Figure 3.4. The lens is employed to superimpose the four images by shifting them to the center. The center of the standard lens must be coincident to the intersection of the four lenticles to guarantee that its optical axis traverses that point. The standard lens and the lenticles are responsible to 90 and 10 percent of the optical system total dioptric power, respectively. The object was located at infinity and the image plane was optimized for the best focus position. An schematic diagram of the optical system used in this simulation is also shown in Figure 3.4.

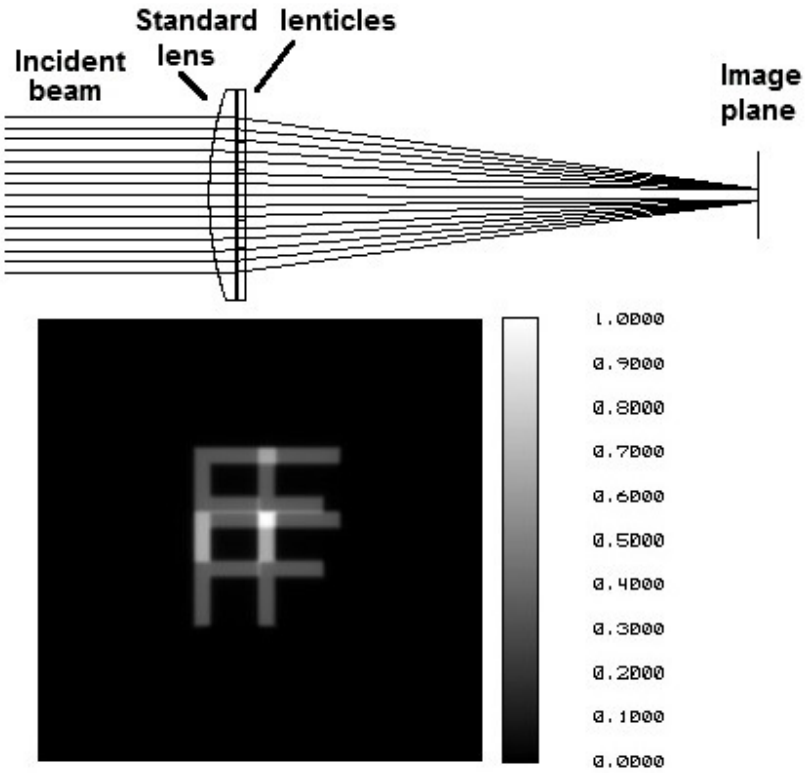

Figure 3.4. Image of a single letter "F" formed by an optical system with four lenticles and a standard lens in cascade where 90% of the system optical power is due to the standard lens and 10 percent due to the lenticles.

The brighter parts of the image indicate overlapping spots. The intensities are higher because more light is focused on these places. An IOL with these characteristics would be impractical because individuals would not be able to recognize any object with those superimposed images. To reduce the overlapping effect, the dioptric power relationship between the lenticles and the standard lens must change by increasing the power portion provided by the standard lens. Figure 3.5 shows images obtained by optical systems with different power relationship between the standard lens and the lenticles:

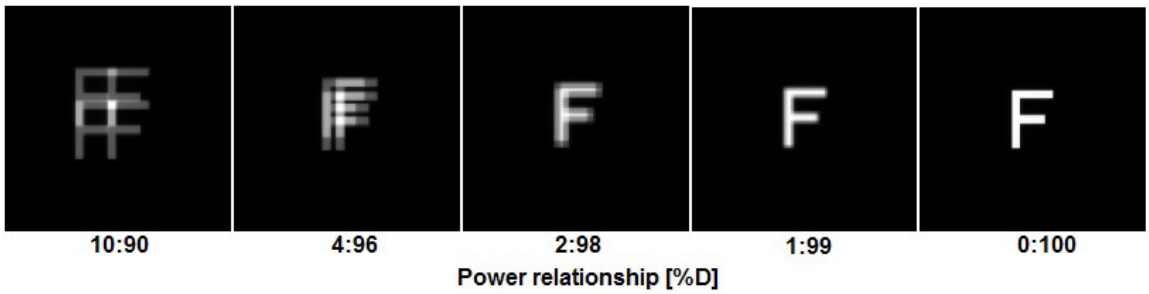

Figure 3.5. Decreasing dioptric power relationship between lenticles and standard lens from left (10% lenticles and 90% standard lens) to right (0% lenticles and 100% standard lens).

The higher the dioptric power of the standard lens compared to the lenticles, the smaller the displacement of images, as it is shown in Figure 3.5. If most of the optical power of the system is provided by the standard lens, then the displacement between the images will be decreased, otherwise the displacement will be increased. Although the pupil size is the same, the intensity of the images increases when the power dominance of the standard lens is higher because more incoming light is focused on coincident spots. Figure 3.6 shows an enlarged image evidencing the displacement and detailing the points of higher intensity (brighter).

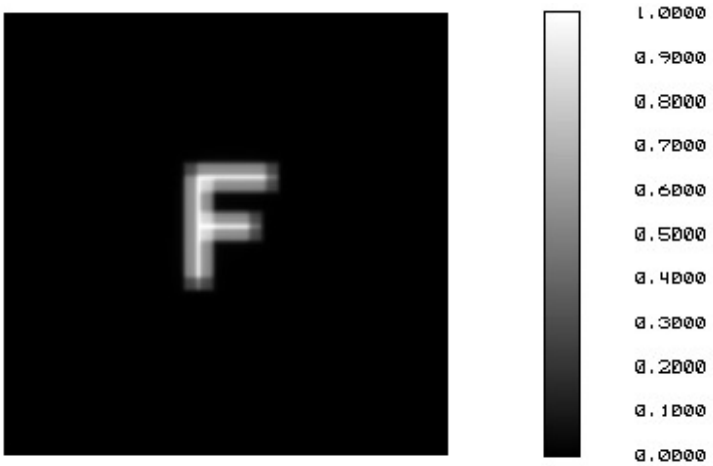

Figure 3.6. Image of a single letter "F" formed by an optical system with four lenticles and a power dominant standard lens.

The image is slightly blurred[15] due to the small displacement between the four images. Considering an IOL with these characteristics, the displacement obtained by the images must be minimum so individuals would not perceive it. Individuals would not notice the image shift if the displacement is less or close to the resolution limit of the human retina. Individuals with this IOL would be benefited by the extended DOF allowing that objects located at somewhat near distance are viewed without spectacles. However, every strategies used to extended the DOF of optical systems imply in some loss of contrast.

The lenticles features larger DOF than the standard lens because they present smaller diameter, yielding more tolerant to defocus images. Strategies including the use of lens with small apertures have been proposed to extend DOF and are already being used in cameras denominated plenoptic [100,101]. Plenoptic cameras are conventional cameras with a microlens array positioned between the main lens and the camera sensor. These cameras obtain many displaced images on the image sensor as the number of microlens in the array. A rendering algorithm is used to combine the microlens images resulting in only one final image. The main advantage of using these cameras is that the set microlens/lens system are able to capture the set of more light rays of a scene, from different directions, which is defined as lightfield [102], allowing that after taking a picture, the

[15] The image is less sensitive to defocus, because it is obtained by a lenticle with smaller aperture than the main lens. To visually perceive it an observer must focus one eye on the image approaches to it. The image will start to blur and the image displacements disappear giving the impression that the image is still sharp and homogeneous.

photographer may choose which plane will be in focus. A more sophisticated rendering algorithm may estimate the microlens image depth and obtain a final image where all planes are in focus [101]. The main optical difference between the Perifocal IOL proposed and the plenoptic strategy is the power dominance relation. The standard lens is the power-dominant element of the set lens/lenticles in the Perifocal IOL. On the other hand, the microlens consist of the power-dominant element of the set main lens/microlens in the plenoptic cameras. Plenoptic cameras depend on the rendering software to yield an easily interpretable image. The function of the rendering software might be analogous to the processing of electrical signals made by the brain in the process of human vision. From the biological perspective, the optical design of a plenoptic camera can be thought as a human eye (camera) with the retina replaced by an insect eye (microlens/photosensor array), although no animal with such hybrid eyes has been discovered [103]. For this reason, it is difficult to predict if the eye/brain system would be able to neurologically render the image of a scene like the camera algorithm, making it difficult to predict the performance of an IOL featuring the same plenoptic strategy.

3.2.*COMPUTATIONAL MODEL*

A computational model of the Perifocal IOL with proposed extended DOF was developed and its optical characteristics were evaluated. The optical design software Zemax® was used to simulate the lens optical performance, such as MTF, image formation and DOF. The results obtained were compared to four commercial monofocal IOLs. All lenses had 22D, which is the average standard adult IOL power [104] and were tested using a model eye to simulate the condition as if they had been implanted. The model eye used was the Liou & Brennan [105] eye model, which takes into account both the chromatic and the corneal spherical aberration. The crystalline lens was removed and the IOL was placed in its niche. Table 3.1 shows the pseudophakic modified Liou & Brennan eye model used in this work.

Table 3.1. Optical design data for the modified Liou & Brennan eye model used in simulations.

Surface	Radius of curvature[mm]	Conic constant	Thickness [mm]	n at λ = 587.6nm[16]
Anterior cornea	7.77	-0.18	0.50	1.376
Posterior cornea	6.40	-0.60	---	1.336
Aqueous humor	Infinity*	---	---	1.336
Pupil	Infinity*	---	---	1.336
IOL	---	---	---	---
Vitreous humor**	Infinity*	+0.96	---	1.336
Retina	-12.00	0.00	---	1.336

λ = wavelength; n= refractive index; *Infinite radius of curvature means that the surface is flat; **The axial length the model eye, given by the sum of all surfaces thickness is 23.95mm.

[16] The value 587.6nm refers to the Fraunhofer Helium d-line wavelength which is commonly adopted as the standard wavelength to specify any material refractive index for general use in the visible range of the spectrum.

Figure 3.7 shows a schematic diagram of the IOL within the modified Liou & Brennan eye model used in this work. In Figure 3.7, pACD is the postoperative anterior chamber depth (detailed in footnote [21]) and AL is the eye axial length.

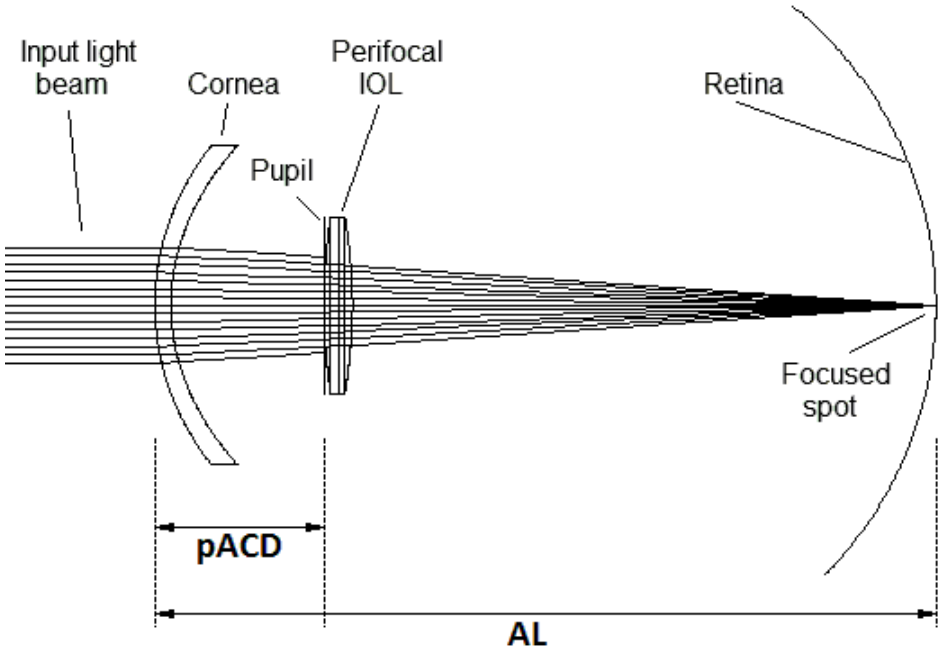

Figure 3.7. Schematic diagram showing the modified Liou & Brennan computational eye model with the IOL.

The schematic design of the Perifocal IOL was already shown in Figure 3.1 and its optical parameters will be described in section 0 in details. The material chosen for the anterior piece and the lenticles is the optical adhesive Norland NOA73 [106], which is flexible and has a high refractive index of 1.56. The posterior piece material is the optical adhesive Norland NOA68 [107] which is flexible and has a high refractive index of 1.54. Both NOA73 and NOA78 materials are flexible, allowing the Perifocal IOL to be foldable, which would require a small incision in case of a cataract surgery.

The lenticles of the Perifocal IOL can be manufactured in two different ways:

- Microfabricated mold by anisotropic etching of silicon [108]: the mold is first filled with NOA73 and after removing the mold, NOA68 is deposited on the lenticles side. The curvatures of the two principal external surfaces are then made with a conventional lathe machine after the material is dry.
- Turning with freeform lathe or using an oscillating tool : the lenticles shape are lathed in a dry NOA73 piece with the freeform lathe or with the oscillating tool. NOA68 is deposited on the lenticles and the curvatures of the two principal external surfaces are then made with a conventional lathe machine after the material is dry.

The chromatic dispersion of NOA73[17] and NOA68[18] are shown in Figure 3.8. The Abbe Number Vd is 42.42 and 40.90 for NOA73 and NOA68, respectively indicating that NOA68 is slightly more sensitive to chromatic dispersion effects.

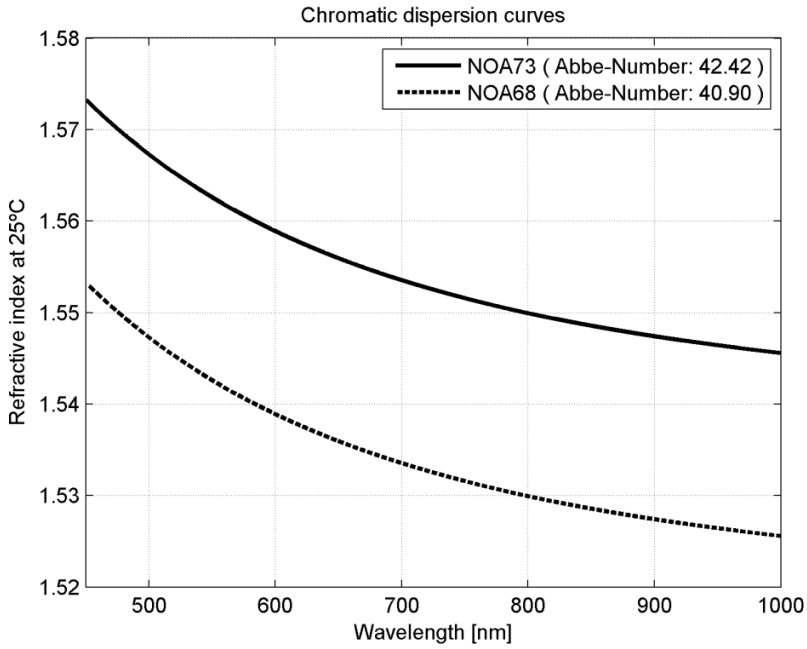

Figure 3.8. Chromatic dispersion of NOA73 and NOA68.

[17] The manufacturer has informed that the chromatic dispersion of the adhesive NOA73 is equal to NOA61 already measured [120] since both materials have the same refractive index.

[18] The manufacturer has informed that the chromatic dispersion of the adhesive NOA68 has not been measured yet, but that it is safe to estimate the curve to be similar to NOA61 already measured [120] with the refractive index offset of 0.02.

4. RESULTS AND DISCUSSION

4.1.*OPTIMIZATION INPUTS*

The Perifocal IOL was developed within a modified Liou&Brennan eye model with the optical system design software Zemax®. It was optimized by a classical multi-objective genetic algorithm entitled "Non-dominated Sorting Genetic Algorithm II" (NSGA-II) written in Matlab. NSGA-II was chosen because it is currently one of the most used multi-objective optimization tool due to its efficiency, simplicity and speed in solving optimization problems with more than one objective. The full description of NSGA-II algorithm is detailed at [109]. NSGA-II as toolbox for Matlab is available at [110]. The IOL anterior and posterior radii of curvature, the diameter of the lenticles and their posterior radius of curvature were optimized to achieve the highest area under the MTF curve when the object was located at infinity and at 80cm. The object was placed at infinity for far vision and at 80cm for intermediate vision, which correspond, in diopters, to +0D and +1.25D, respectively. The NSGA II input parameters used for the Perifocal IOL optimization were:

- number of variables: 7
- number of generations: 250
- population size: 200 (the population consists of a set of individuals, where each individual represents one IOL with different parameters values within the limits defined in Table 4.1)
- crossover fraction: all of the individuals in the population are processed by crossover operator, and only 2/7 of all variables do crossover[19].
- mutation fraction: all of the individuals in the population are processed, and only 2/7 of all variables do mutation[20].
- The design variable lower and upper boundaries are shown in Table 4.1:

Table 4.1. Design variables boundaries used for optimization.

Design variable	Min	Max
Anterior radius of curvature [mm]	12	36
Posterior radius of curvature [mm]	-36	-12
Anterior Conic	-30	-1
Posterior Conic	-30	-1
Lenticle Diameter [mm]	0.8485	2.2627
Lenticle Anterior Radius of Curvature [mm]	-200	-10
pACD[21] [mm]	4.9	5.8

[19] This rate was determined by setting the input parameter 'auto' on the function 'crossoverFraction' which makes NSGA-II to use 2/number of variables as the crossover fraction [110].

[20] This rate was determined by setting the input parameter 'auto' on the function 'mutationFraction' which makes NSGA-II to use 2/number of variables as the mutation fraction [110].

[21] The postoperative anterior chamber depth (pACD) do not correlate with the preoperative ACD. Instead, it correlates with the IOL placement within the eye after surgery, which is uncertain. All IOLs feature one constant (A-constant) which is used in the SRK II and SRK/T formulas [98]. Other formulas specify other constants that can be derived from A-constant [98]. The A-constant is obtained by statistical regression that is used to calculate its dioptric power. The A-constant encompasses multiple variables that include the implant manufacturer, implant style, surgeon's technique, implant placement within the eye and measuring equipment. The pACD in this work refers to the distance between the corneal and IOL anterior surfaces.

The anterior and posterior radii of curvature boundaries were determined to limit the Perifocal IOL dioptric power range, which is within approximately 12D and 36D for a lens compliant to the Perifocal IOL optical design, composed of two materials with different refractive indices: 1.56 on the anterior and 1.54 on the posterior piece. The dioptric power range is adequate to the purpose of this work, since the model eye used calls for a 22D IOL. The conic constants were limited to negative values to ensure that the IOL surface is hyperbolic (conic constant less than -1), which corresponds to the ideal profile for aspheric optical surfaces immersed in a medium of lower refractive index. The lenticle diameter was restricted to within 0.8485mm and 2.2627mm to guarantee that their surfaces together occupy a reasonable area of the Perifocal IOL, which is limited by pupils with diameters within 2 and 4mm. This ensures that the optical effect caused by lenticles does not prevail throughout the IOL surface nor is negligible. Although the lenticles were set to be spherical, aspheric surfaces were also tested. However, the differences observed between aspheric and spherical profiles were insignificant, because as their diameter are very small compared to a usual IOL, the lenticles can be regarded as paraxial lenses, in which the spherical aberration is considerably small.

The optimization problem was defined by the maximization of two distinct objectives:

- Objective 1: Area under the MTF curve with the object placed at infinity with a 5.0 mm diameter pupil
- Objective 2: Area under the MTF curve with the object placed at 80cm with a 3.0mm diameter pupil

In practice, objective 1 simulates night driving condition and objective 2 a situation of working with a computer in an office, for example. In terms of dioptric power, objective 1 regards to +0D and objective 2 to +1.25D, which is compliant to the difference between the two IOLs recommended by specialists for the modest monovision technique [18,20]. The area under the MTF curve was calculated for spatial frequencies between 0 and 100lp/mm at polychromatic light composed of 486, 546 and 633nm wavelengths, which correspond to the lower, the center and upper peaks of blue, green and red cones sensitivity shown in Figure 2.2.

The MTF and CSF were multiplied point by point in order to obtain the highest MTF at the most sensitive spatial frequencies to the human eye. The IOL optics diameter was fixed at 6.0mm and the pupil considered was 5.0mm for objective 1 and 3.0mm for object 2. The Standards ANSI Z80.30 [111], ISO 11979-2 [112] and ISO 11979-9 [113] establish pupil diameters of 3.0 and 5.0mm for IOL testing.

The optimization problem was subjected to five constraints (C_1, C_2, C_3, C_4 and C_5):

- C_1: The lenticle central thickness (lt_{SAG}) must be larger than 2µm and lower than 20µm. It is calculated according to Equation 4.1, where R_{lt} is the lenticle radius of curvature and d_{lt} its diameter. This constraint is compliant to the lenticle fabrication method that limits and avoids the lenticles to be too shallow or too deep.

$$lt_{SAG} = R_{lt} - \sqrt{R_{lt}^2 - \left(\frac{d_{lt}}{2}\right)^2} \qquad 4.1$$

- C_2: The Perifocal IOL dioptric power must be within 21.8D and 22.2D. The ISO and ANSI Standards establish power tolerance for a 22D IOL of ±0.4D. The constraint C_2 determines

power tolerance of ±0.2D which is a half that tolerance established by the Standards. The Perifocal IOL dioptric power $\Phi_{\text{Perifocal}}$ is calculated in diopters by Equation 4.2 [79]:

$$\Phi_{\text{Perifocal}} = \Phi_{\text{A}} + \Phi_{\text{P}} - (0.001.\Phi_{\text{A}}.\Phi_{\text{P}}.\text{t}_{\text{eff}}) \quad 4.2$$

where Φ_{A} and Φ_{P} are the anterior and posterior Perifocal IOL dioptric power in diopters calculated by Equation 2.16 and t_{eff} is the effective lens thickness, given by $(\delta - \delta^*)/1.336$. δ and δ^* are calculated by Equation 2.17, with the parameter t equal to 0.45mm, which is the thickness of the anterior and the posterior pieces of the Perifocal IOL. The factor 0.001 was used to express t_{eff} in millimeters and the dioptric powers Φ in diopters (1/m) in Equation 4.2.

- C_3: The area under the MTF curve with the object at 6m and 5.0mm pupil must be equal or greater than 20.5. The value of 20.5[22] was chosen based on the author experience to ensure good visual acuity at 6m, which is the distance used in the clinical Snellen test.
- C_4: Objective 1 must be greater than 16, in order to prevent the algorithm from reaching biased results favoring the objective 2: a lens with excellent near vision and poor far vision. The value of 16 was chosen based on the author experience[23].
- C_5: Objective 2 must be greater than 16, in order to prevent the algorithm from reaching biased results favoring the objective 1: a lens with excellent far vision and poor near vision. The value of 16 was chosen based on the author experience[23].

4.2.*OPTIMIZATION RESULTS*

The presence of multiple objectives in a problem, in principle, gives rise to a set of optimal solutions (largely known as Pareto-optimal solutions), instead of a single optimal solution. In the absence of any further information, one of these Pareto-optimal solutions cannot be said to be better than the other [109]. The Pareto-optimal solutions found by NSGA-II are shown in Figure 4.1, where the solution on the set considered as the most appropriate to the problem is assigned.

[22] The value of 20.5 was the result of the author subjective evaluation regarding the quality of the image formed by the lens. A psychophysical test was performed with the author where images formed by different lenses in the same condition were analyzed. Optical systems with the area under the MTF curve greater than 20.5, in this condition, formed images with very good quality, which is exactly what the constraint C_3 is ensuring. It is important to observe that if the same test were performed with different people, values other than 20.5 would have been found.

[23] The value of 16 was the result of an author subjective evaluation regarding the quality of the image formed by the lens. A psychophysical test was performed with the author where images formed by different lenses in the same condition were analyzed. Optical systems with the area under the MTF curve lower than 16, in this condition, formed images with poor quality, which were not interesting for the purpose of this work. It is important to observe that if the same test were performed with different people, values other than 16 would have been found.

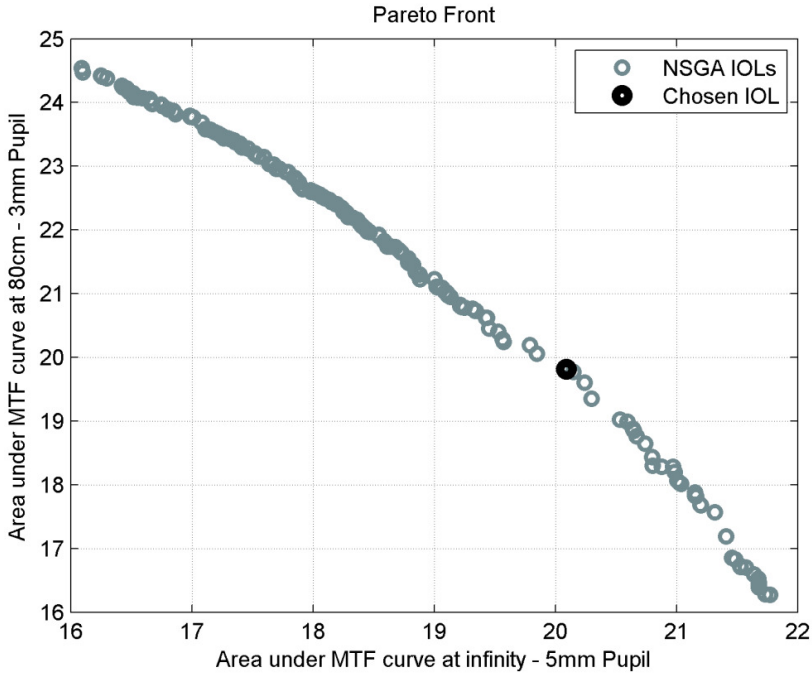

Figure 4.1. Pareto-front: Optimal solutions obtained by NSGA-II.

The indicator used to decide which is the best lens on the set of solutions was based on the first IOL in which the area under the MTF curve with 5.0mm pupil and the object placed at infinity is greater than the area under the MTF curve with 3.0mm pupil and the object placed at 80cm. It is important to observe that the criterion used favors the far vision with minimum compromise in near vision. Although the Perifocal IOL has a balanced performance between far and near vision, the resolution and, consequently, the contrast are smaller as the depth of focus increases. It is important to observe that the criterion used to choose one IOL on the set of solutions might change if the habits of the patient are studied before the surgery. For example, if a patient performs more tasks that require near vision, then a Perifocal IOL for this specific individual should have slightly higher performance at near vision (objective 2) than at far vision (objective 1). Depending on the patient's habits, even the optimization objectives might alter, based on the results of a daily registration of one's activities. This would lead to the concept of developing personalized IOLs, where patients are given options to suit their lifestyle.

The pACD obtained for the Perifocal IOL was 4.99mm and its design parameters obtained by the NSGA-II optimization are shown in Table 4.2:

Table 4.2. Perifocal IOL parameters obtained by NSGA II optimization.

Surface	Radius of curvature [mm]	Conic constant (K)	Thickness [mm]	Z location* [mm]	Refractive index
Anterior lens surface	19.69	-17.13	0.45	0	1.56
Posterior lens surface	-18.89	-30.00	0.45	0.45	1.54
Lenticles	-159.81	---	$3.8*10^{-3}$	0.45	1.56

* The Z location is the longitudinal position of each component.

The lenticles obtained by optimization have approximately 0.6% of the power dominant element of the Perifocal IOL, which is composed of the anterior and posterior lens surfaces. The lenticle diameter was calculated as a consequence of its position from the center in order to guarantee that the edge of adjacent lenticles intercept at the IOL center point, avoiding unwanted diffraction caused by light passing through a small star-shaped aperture formed by the touching but non-overlapping edges of the lenticles. The schematic diagram of the Perifocal IOL top view presenting in detail the lenticle positions is shown in Figure 4.2.

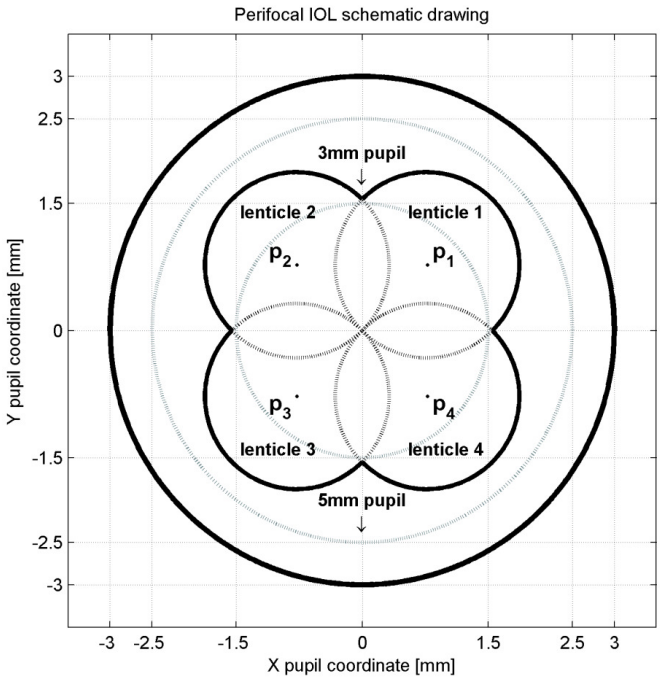

Figure 4.2. Schematic diagram of the lenticles center position and diameter.

The location of the centers (p_1, p_2, p_3 and p_4) of the lenticles obtained by NSGA-II optimization and their diameters are shown in Table 4.3:

Table 4.3. Lenticle center position obtained by NSGA II optimization and diameter.

Surface	Center position		Diameter [mm]
	X position [mm]	Y position [mm]	
Lenticle 1	0.775	0.775	2.191
Lenticle 2	-0.775	0.775	2.191
Lenticle 3	-0.775	-0.775	2.191
Lenticle 4	0.775	-0.775	2.191

The Perifocal IOL was compared to four different commercial 22.0D monofocal IOLs. Two of them are negative aspheric IOLs, one is a neutral aspheric IOL and the other is spherical. The average amplitude of the spherical aberration of the human cornea is +0.27µm over a 6mm diameter optical zone. Spherical IOLs contribute to increase the spherical aberration of the eye because, like the cornea, they also introduce a certain degree of positive spherical aberration, the amplitude of which depends on the magnitude of its refractive power. Negative IOL models are designed with a

modified surface to have negative spherical aberration values to compensate for the positive corneal spherical aberration. Neutral IOL models are designed to have null spherical aberration. These IOLs neither introduce nor compensate corneal spherical aberration. These commercial IOLs represent the main variations of monofocal lenses implanted currently. The commercial IOL models are:

- Negative aspheric IOL with -0.27µm of spherical aberration correction: (Tecnis Z9002 Advanced Medical Optics) ;
- Negative aspheric IOL with -0.20µm of spherical aberration correction: (AcrySof® IQ SN60WF Alcon);
- Neutral aspheric IOL: (Miniflex Mediphacos);
- Spherical IOL: (OP-72 Mediphacos).

The final position (pACD) was optimized for each IOL model in order to achieve the maximum area under the MTF curve with 5.0mm diameter pupil. Different IOL positions were obtained because the location of the lens posterior principal planes is different from model to model since it depends on the design parameters like radii of curvature, refractive index and central thickness. It is observed that the pACD is larger for the spherical IOL, because in this case, the optimization routine directs the lens slightly toward the retina in an attempt to reduce the spherical aberration of the optical system composed of the eye and the IOL. By moving the IOL toward the retina, the eye's dioptric power is somewhat decreased and consequently, spherical aberration is reduced. On the other hand, it may introduce some defocus. The design data of the four IOL models tested are presented in Table 4.4:

Table 4.4. Optical design data of the tested IOLs.

Parameters	IOL Model			
	Tecnis Z9002	SN60WF	Miniflex	OP-72
Design Concept	Negative aspheric	Negative aspheric	Neutral aspheric	Spherical
Power [D]	22.0	22.0	22.0	22.0
Anterior Surface	6th order asphere	Sphere	Sphere	Sphere
Radius [mm]	11.043	19.583	11.31	10.32
Conic Constant (K)	-1.03613	0	0	0
2nd order coefficient ρ_2^*	0	0	0	0
4th order coefficient ρ_4^*	$-9.44*10^{-4}$	0	0	0
6th order coefficient ρ_6^*	$-1.37*10^{-5}$	0	0	0
Posterior Surface	Sphere	6th order asphere	Conic asphere	Sphere
Radius [mm]	-11.043	-20.000	-11.39	-22.41
Conic Constant	0	-33.227	-5.8	0
2nd order coefficient ρ_2^*	0	$-2.5*10^{-4}$	0	0
4th order coefficient ρ_4^*	0	$-1.7*10^{-5}$	0	0
6th order coefficient ρ_6^*	0	$8.7*10^{-7}$	0	0
Optical diameter [mm]	6.0	6.0	6.0	7.0
Center Thickness	1.164	0.633	0.97	1.08
Refractive index	1.458	1.554	1.4613	1.492
Abbe number	42	37	58	57.44
pACD	5.42	5.84	5.83	5.98

* The coefficients are high order aspheric-terms (see Equation 4.3)

4.3.*SIMULATION RESULTS*

Polychromatic MTF curves obtained for the Perifocal, Tecnis, SN60WF, Miniflex, OP-72 IOLs are shown in Figure 4.3 for 3.0 and 5.0mm pupils. The MTF curve was calculated considering the object placed at infinity (+0D), 6m (+0.17D), 2m (+0.5D), 1m (+1D) and 80cm, (+1.25D). All MTF curves were calculated with the IOLs on the same condition, within the modified eye model presented in Figure 3.7. The combined wavelengths considered to calculate the polychromatic MTFs were 486, 546, and 633nm with equal weights.

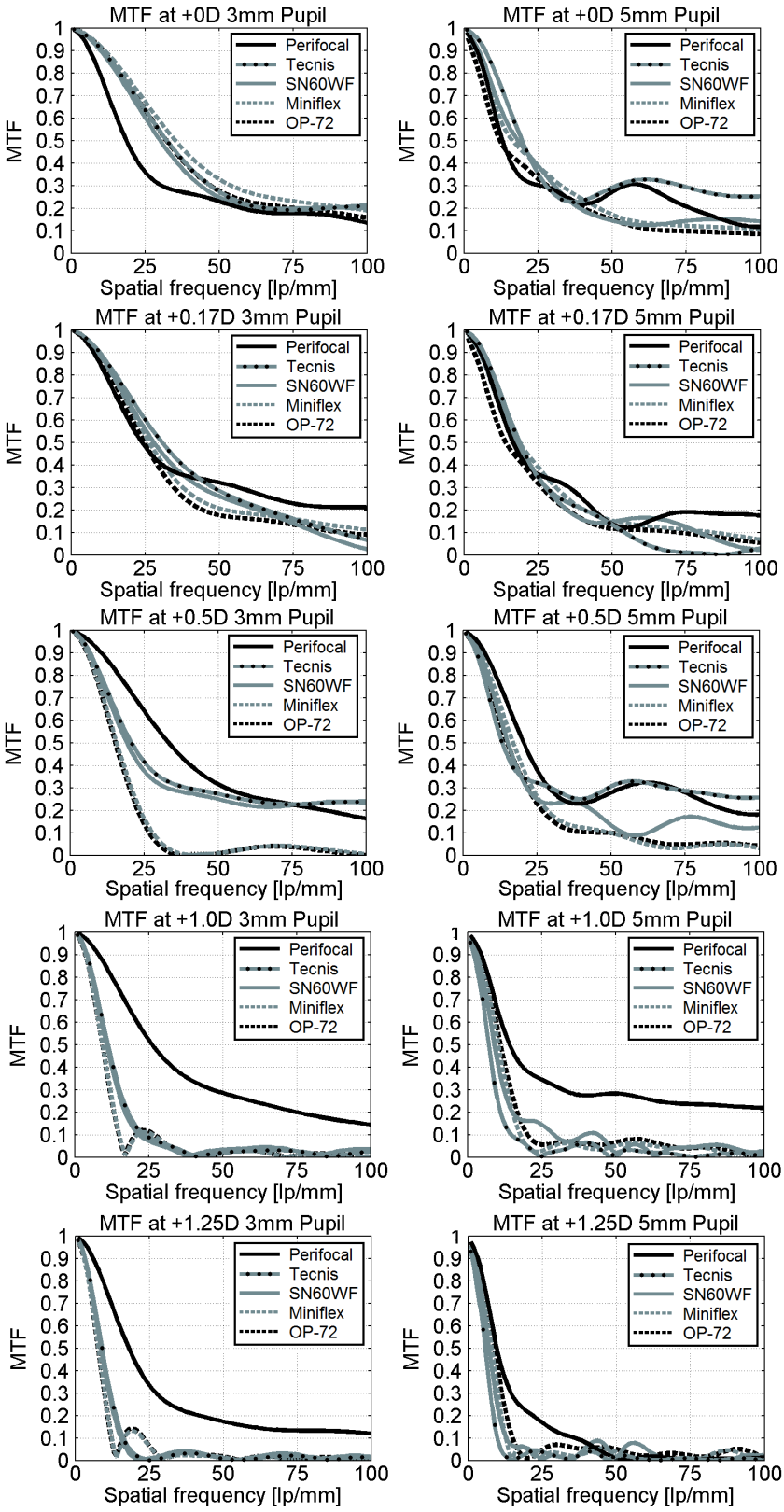

Figure 4.3. Polychromatic MTF curves. From above: object at infinity (+0D), 6m (+0.17D), 2m (+0.5D), 1m (+1D) and 80cm (+1.25D), for 3.0mm [left] and 5.0mm [right] diameter pupils.

The Perifocal IOL features the lowest polychromatic MTF at 3mm for the object at infinity (+0D), while the other lenses have very similar MTF values with slightly higher values for the Miniflex IOL. Considering the object at infinity and 5mm diameter pupil, the Tecnis IOL features the highest MTF. The performance of the Perifocal IOL increases in frequencies above 40lp/mm, while for the lower frequencies it has slightly lower values than the other models. The spherical IOL showed smaller MTF values than both negative and neutral aspheric IOLs, due to spherical aberration impact. When the object is located at 6m (+0.17D) the Perifocal IOL obtained the highest MTF values for high spatial frequencies for both 3mm and 5mm diameter pupil, indicating that an individual with this IOL would perform better in a visual acuity test during an ophthalmologic consultation. Both negative and neutral aspheric IOLs showed higher MTF values than the neutral and spherical IOLs. The Perifocal IOL features the highest MTF for 3mm diameter pupil in frequencies below 75lp/mm with the object at 2m (+0.5D). At this condition, the negative aspheric IOLs feature higher MTF than the neutral and spherical IOLs. The Perifocal IOL is the most advantageous IOL for a +1D defocus (object at 1m). All other IOLs showed similar lower MTF behavior, while the Perifocal IOL features superior MTF values for all spatial frequencies and 3mm and 5mm diameter pupils. At +1.25D (object at 80cm), the Perifocal IOL still features the highest MTF for 3mm diameter pupil and for 5mm pupil it is superior on the lower spatial frequencies. Neutral aspheric and spherical IOLs showed very similar MTF curves, which suggests an individual might not notice differences in contrast sensitivity between these two IOLs.

The polychromatic MTF through focus curve was obtained for the IOL models and is presented in Figure 4.4 for a 3mm diameter pupil. The defocus range is 0D when the object is located at infinity to 1.5D when the object is placed at 67cm.

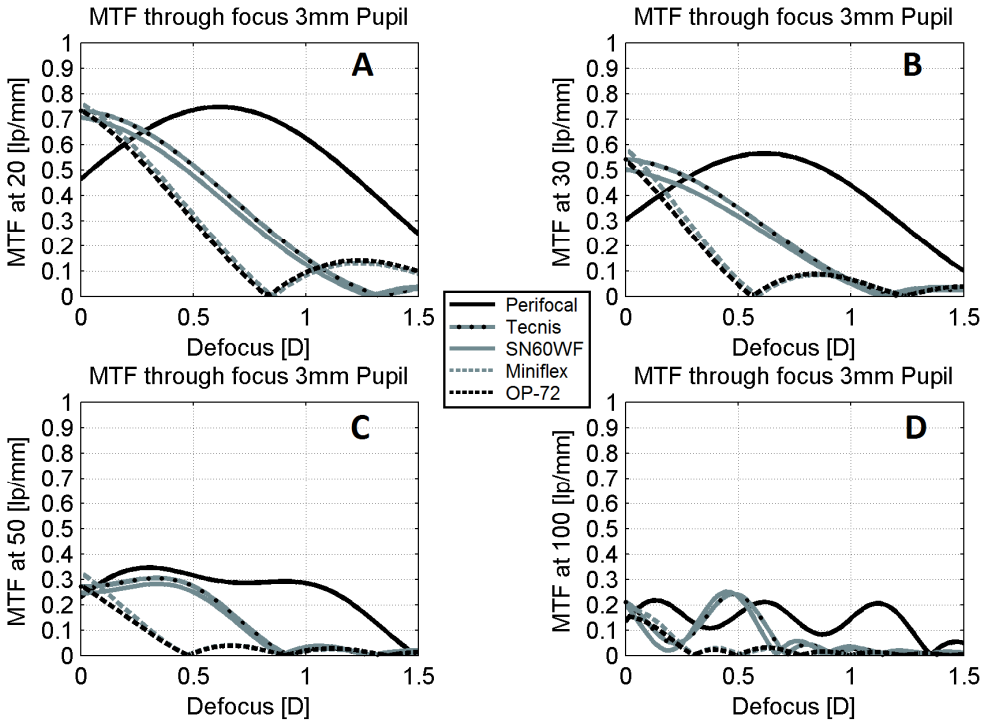

Figure 4.4. Polychromatic MTF through focus curves obtained for each IOL model for 3mm diameter pupil at spatial frequencies in lp/mm equal to 20 (A), 30 (B), 50 (C), 100 (D).

Figure 4.4 shows that the Perifocal IOL features larger DOF than the commercial IOLs for 3mm diameter pupil. The MTF through focus curves of the Perifocal IOL reaches the zero for larger defocus (object closer to the eye) than the other IOLs. However, when the object is far (defocus next to 0), the commercial IOLs present higher MTF value, indicating that these lenses will provide sharper images for far vision. The aberration correcting IOLs feature higher DOF than the spherical and neutral aspheric IOLs for 3mm diameter pupil. The neutral aspheric IOL has the highest contrast for far vision. There are no significant differences between the DOF of the spherical and neutral aspheric IOLs, with small advantage for the second model. The higher the spatial frequency, the lower the MTF for all models. When the object lies around 1m (+1D) or closer, all commercial models have MTF through focus next to 0, indicating that an individual with any of these IOLs would not be capable of seeing clearly without additional spectacles, whereas the Perifocal IOL allows higher contrast levels.

The MTF through focus was analyzed for a 5mm diameter pupil and it is presented in Figure 4.5:

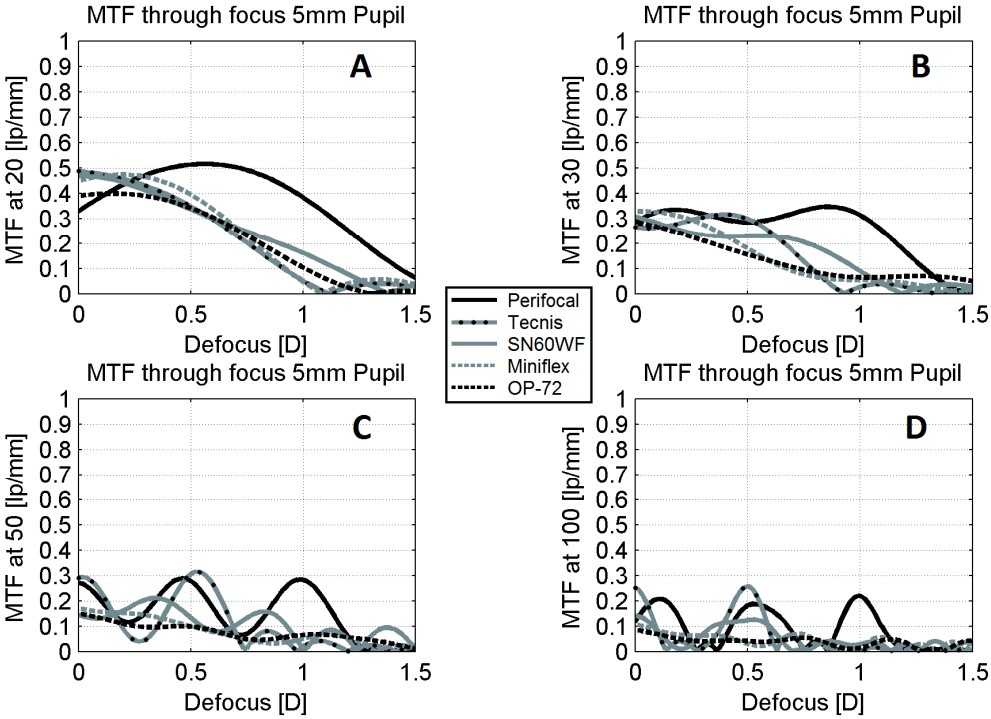

Figure 4.5. Polychromatic MTF through focus curves obtained for each IOL model for 5mm diameter pupil at spatial frequencies in lp/mm equal to 20 (A), 30 (B), 50 (C), 100 (D).

Figure 4.5 shows that for 5mm diameter pupil, the Perifocal IOL features larger DOF than the commercial IOLs at lower spatial frequencies, which consist of the peak of the human contrast sensitivity (CSF, shown in Figure 2.6). It is observed that at lower frequencies the curves for the MTF through focus of the Perifocal IOL are maintained at higher levels than the other IOLs as defocus increases. However, when the object is far (defocus next to 0), the commercial IOLs present higher MTF value, indicating that these lenses provide sharper images for far vision at lower frequencies. At 50 and 100lp/mm, the Perifocal and the negative aspheric IOLs present, in general, higher MTF through focus curves than the neutral aspheric and spherical IOLs. The MTF

through focus oscillations at 50 and 100lp/mm indicates that some longitudinal planes will have preferential foci in comparison to others along the optical axis, which are more evident at higher spatial frequencies. The neutral aspheric and spherical showed similar and narrow DOF at 5mm diameter pupil.

The Perifocal IOL was designed to provide an extended DOF in comparison to commercial monofocal aspheric IOL. This IOL would allow an individual to perform some tasks that require far vision and intermediate-to-near vision without using spectacles. However, the decrease in contrast level in far vision consists of a loss that is inherent to the process of extending the DOF. The loss of contrast and the DOF are evidenced in the peak and in the area under the MTF through focus curve, respectively. The MTF through focus curves were obtained and are shown in Figure 4.4 and Figure 4.5, however in each figure, the analysis were restricted to only four specific spatial frequencies in lp/mm: 20 (A), 30 (B), 50 (C) and 100 (D). In order to assess a complementary analysis containing MTF through focus at spatial frequencies ranging from 1 to 100lp/mm, a hundred curves were obtained. Each curve was evaluated at one specific spatial frequency. These curves were arranged together to form a surface where the y axis regards the spatial frequency (ranging from 1 to 100lp/mm), the x axis regards defocus (ranging from 0 to 1.5D) and the z axis regards the MTF values. To calculate the MTF of the optical system considering the human sensitivity to contrast, the Equation 2.9 must be used so that each MTF curve is weighted by the CSF function. Figure 4.6 shows the MTF through focus surface contour for pupil diameters of 3mm (left) and 5mm (right). Intermediate spatial frequencies correspond to the peak of the CSF function of the human eye as it was shown earlier in shown in Figure 2.6).

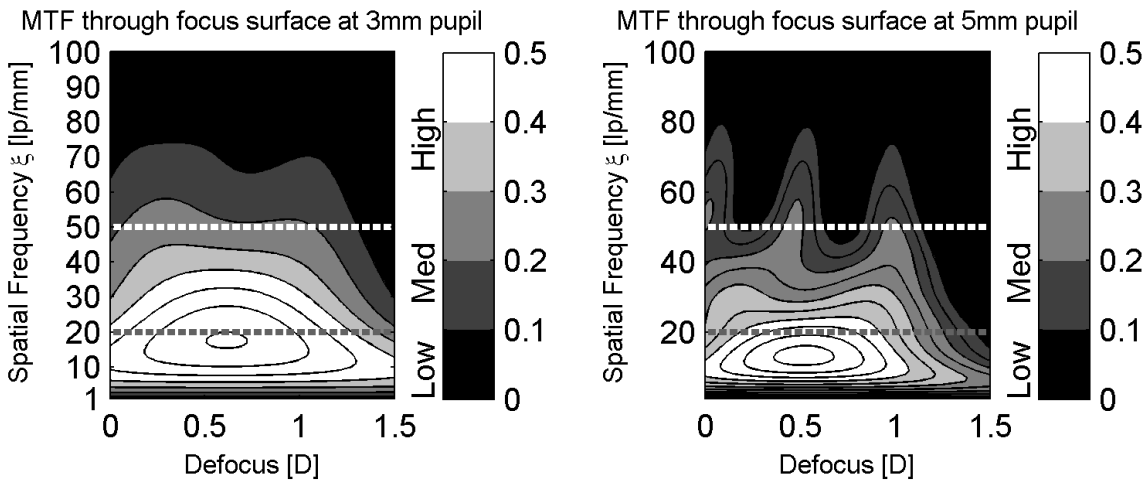

Figure 4.6. Perifocal IOL MTF through focus surface contour for 3mm [left] and 5mm [right] diameter pupils.

Figure 4.6 shows that the highest performance of the Perifocal IOL is obtained at low and intermediate spatial frequencies, as indicated in the graphs lighter region. The Periocal IOL features higher DOF at 3mm diameter pupil than at 5mm. The MTF at higher spatial frequencies are close to zero because it has been weighted by the CSF function, which has the highest values at low and intermediate spatial frequencies according to the human eye contrast sensitivity function, shown in Figure 2.6.

In order to assess the performance of the Perifocal IOL in comparison to the commercial IOL models, the residual MTF through focus surface was calculated and it is shown in Figure 4.7.The residual MTF through focus surface is calculated by the difference between the Perifocal and the commercial IOLs MTF values weighted by the CSF function. Figure 4.7 shows the residual MTF through focus surface contour for 3 and 5mm diameter pupil.

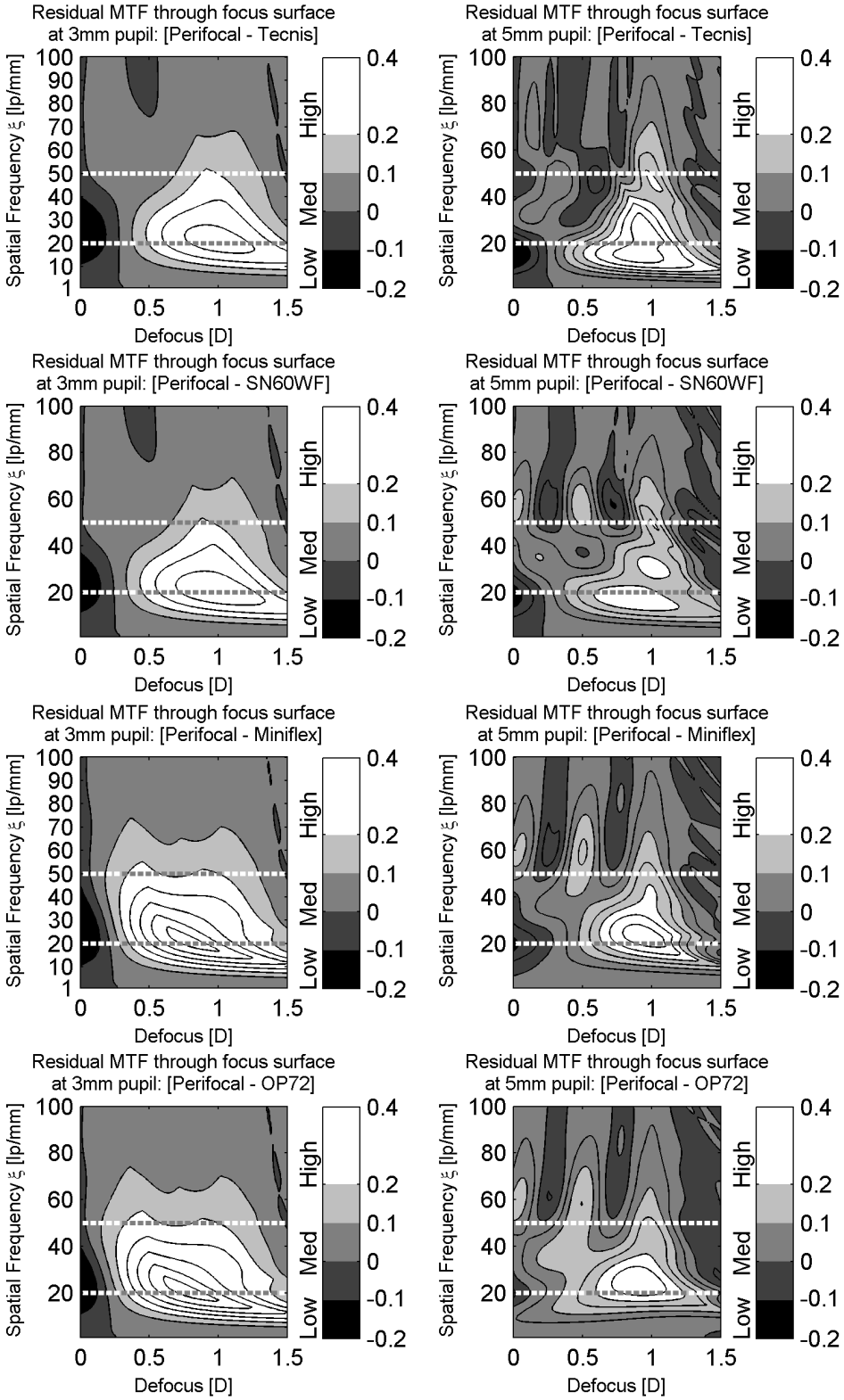

Figure 4.7. Residual MTF through focus surface for 3mm [left] and 5mm [right] diameter pupils. Negative values regard to situations in which the MTF of the commercial IOL model is higher and positive values regard to situations in which the MTF of the Perifocal IOL is higher.

By the analysis of Figure 4.7 it is concluded that for lower spatial frequencies (between 10 and 50lp/mm) and defocus ranging from 0.5 to 1.5D, the Perifocal IOL features higher MTF values with the major difference being approximately 0.4 for a 3mm diameter pupil. Considering lower frequencies and smaller defocus values, the commercial IOLs feature higher MTF values with the major difference being approximately 0.2 for a 3mm diameter pupil. Although the commercial models have higher MTF at small defocus at 3mm diameter pupil, it is observed that the area of the graphs with positive values (where the Perifocal IOL has higher MTF than the commercial models) is larger than the area with negative values (where the Perifocal IOL has smaller MTF than the commercial models). This indicates that the trade-off between reducing contrast at infinity (0D) and extending DOF was beneficial to the Perifocal IOL, since the benefits are larger than the losses as indicated by the graphs shown in Figure 4.7. At 5mm diameter pupil, the Perifocal IOL has higher MTF from approximately 0.5 to 1.5D at low and intermediate spatial frequencies. At smaller defocus values, the Perifocal IOL and the commercial IOL had similar performance, but it was observed a small region of MTF loss in comparison to Tecnis, SN60WF and Miniflex on frequencies close to 20lp/mm.

In order to provide a general analysis of DOF, the concept of focal range is introduced herein, which consists of calculating the area under the MTF curve at each object position. The focal range provides a complementary analysis of the optical system which is composed of all spatial frequencies from 0 to 100lp/mm at each object position. However, the focal range does not allow individual spatial frequency analysis of the MTF through focus, which are important to determine precisely the visual acuity (i.e. 50lp/mm and 100lp/mm which regard 20/40 and 20/20 visual acuities, respectively). The MTF through focus curves and the focal range together provides a more complete analysis of the optical system performance because the first provides information of MTF variation on individual spatial frequencies related to defocus and the second brings information of the whole set of spatial frequencies related to defocus. The focal range was calculated for 3mm and 5mm diameter pupil for the Perifocal and all commercial IOLs and is presented in Figure 4.8. In this work it was considered, to calculate the focal range, spatial frequencies within 0 and 100 lp/mm and object positions from infinity (0D) to 67cm (+1.5D).

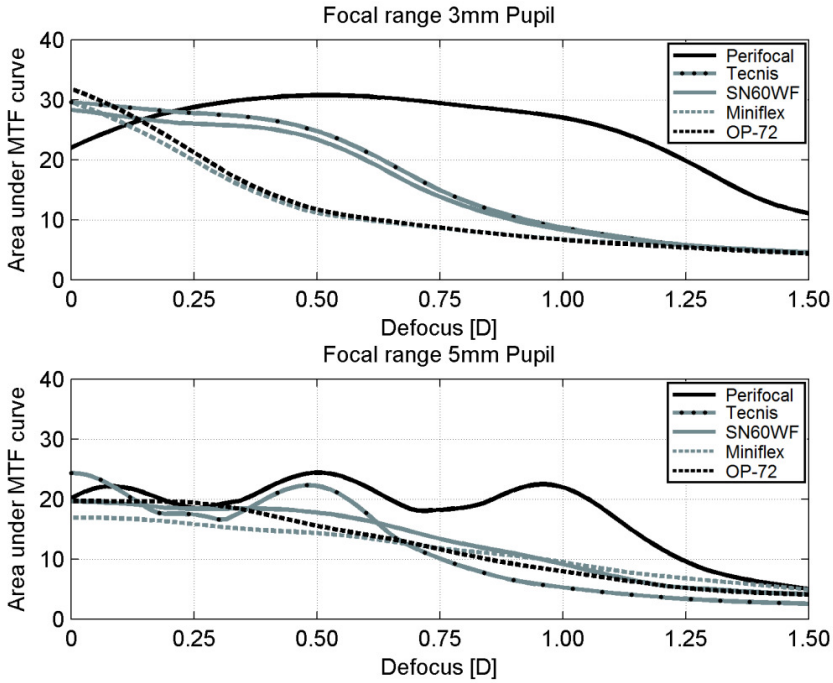

Figure 4.8. Polychromatic focal range calculated for each IOL model for 3mm [up] and 5mm [down] pupils.

By analyzing Figure 4.8, it is concluded that the Perifocal IOL provides larger focal range starting from the object at 4m (+0.25D) for both 3mm and 5mm diameter pupil, with little compromise in distant vision. The Perifocal IOL features the narrowest focal range between 0 and approximately 0.125D at 3mm diameter pupil. Tecnis and SN60WF showed better performance than Miniflex and OP-72 at 3mm diameter pupil. At 5mm diameter pupil all commercial IOLs are similar, while the Perifocal IOL showed to have approximately equal or superior performance.

The MTF as a function of pupil size was calculated at 50lp/mm and 100lp/mm at five object positions related to the viewer: infinity (+0D), 6m (+0.17D), 2m (+0.5D), 1m (+1.0D) and 80cm (+1.25D).

Figure 4.9 shows the MTF response as a function of pupil size:

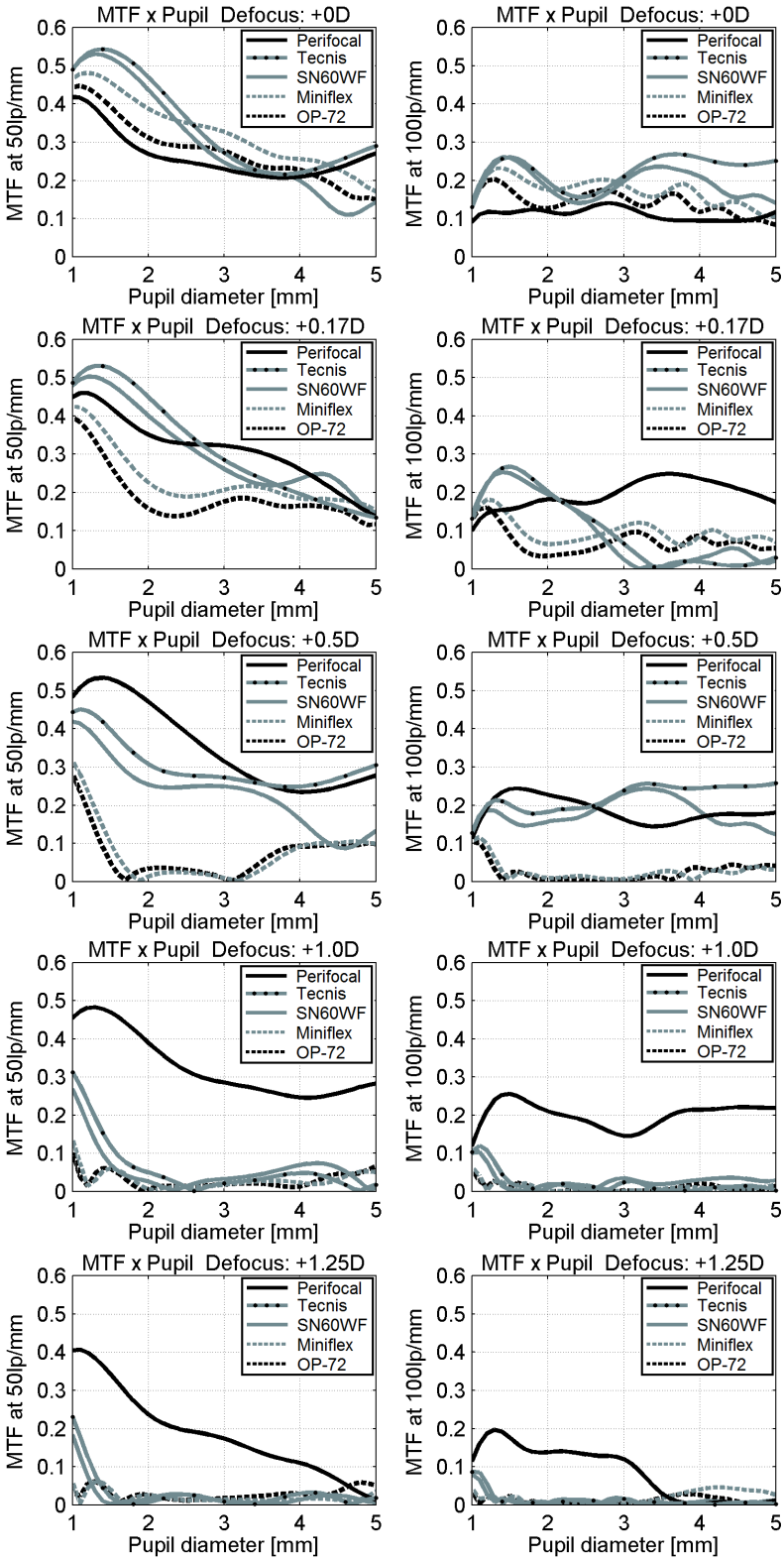

Figure 4.9. Polychromatic MTF curves versus pupil diameter variation. From above: object at infinity (+0D), 6m (+0.17D), 2m (+0.5D), 1m (+1D) and 80cm (+1.25D), for 50lp/mm [left] and 100lp/mm [right].

With the object at infinity, the Perifocal IOL showed the lowest MTF for pupil diameter smaller than 3mm at 50lp/mm. On this condition, the aberration correcting IOLs showed the highest MTF followed by the neutral and spherical IOLs, respectively. For pupil diameter between 3 and 4mm, Miniflex showed the highest MTF at 50lp/mm followed by OP-72. At 100lp/mm and the object at infinity, the aberration correcting IOLs performed better in general and the Perifocal IOL showed the smallest MTF, although with less variation with pupil size. When the object is at 6m, the Perifocal IOL showed the best MTF for pupils larger than 2mm at 100lp/mm. The aberration correcting IOLs still performed better than the neutral and spherical IOLs, with advantage to the Tecnis IOL, which has larger spherical aberration correction of 0.27µm against 0.20µm from SN60WF. With the object at 2m the Perifocal IOL stands out on smaller pupils, followed by Tecnis and SN60WF, while Miniflex and OP-72 showed smaller MTFs on this condition. For larger pupil, Tecnis had the best performance for both 50 and 100lp/mm. At 1m and 80cm the Perifocal IOL had the largest MTF. Tecnis and SN60WF had better performance than Miniflex and OP-72 for small pupils.

All IOLs are pupil dependent and Tecnis and SN60WF showed to be superior than the neutral and spherical IOLs, indicating that the correction of spherical aberration plays an important role in increasing contrast sensitivity. In general, the neutral and the spherical IOLs showed lower MTF, which suggests that there is no significant improvement between designing an aberration-free or a spherical IOL.

Although the Perifocal IOL presented the highest DOF, it has the smallest MTF for the object at infinity and small pupils, but its optical performance presented improvements when the pupil is larger. From these observations it is concluded that besides attempting to minimize the contrast loss for far objects, there is a tradeoff between extending DOF and distant vision quality.

A simulation of images formed by each optical system composed of the eye model and the IOLs was carried out. The simulation considered images formed under defocus conditions of 0D, 0.17D, 0.5D, 1.0D, and 1.25D, consisting of situations where the object is placed at infinity[24], 6m, 2m, 1m and 80cm from the optical system, respectively. The target images were simulated for polychromatic light (λ =546nm, 486nm and 633nm) considering pupil sizes of 3 and 5mm. The images shown in Figure 4.10 and Figure 4.11 are representations of a target image with three rows of three letters, where the contrast level is different in each row. This image is known as the Pelli-Robson Contrast Sensitivity Chart. The letters in the upper, middle and lower rows have high, average and low contrast, respectively. The size of each letter at 6m is 8.73mm, in order to be compliant to the dimensions of the letters on the 20/20 row of the Snellen Chart used in clinical visual acuity test. The size of the letters at infinity, 2m, 1m and 80cm are proportional to that simulated at 6m, being 145mm, 2.91mm, 1.46mm and 1.16mm, respectively. Figure 4.10 and Figure 4.11 show simulations of the Pelli-Robson Contrast Sensitivity Chart for 3mm and 5mm diameter pupil, respectively.

[24] The simulations of the images in this work considered infinity as 100m.

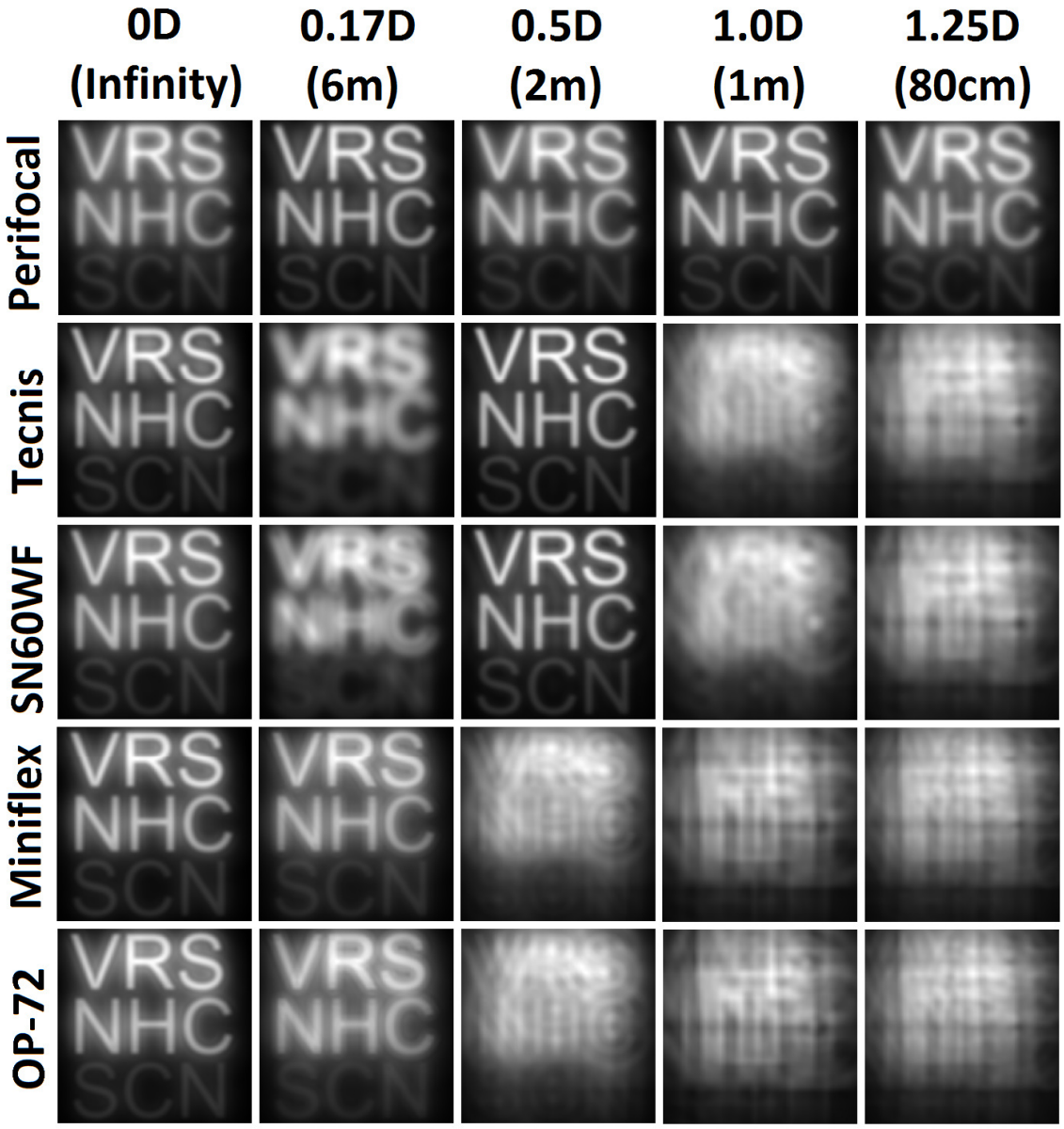

Figure 4.10. Image simulation result for 3mm diameter pupil: Pelli-Robson Contrast Sensitivity Chart.

By analyzing Figure 4.10 it is concluded that the Perifocal IOL had the best performance at 3mm diameter pupil, because it obtained sharp images for the object at all simulated distances. It was the only IOL capable of forming sharp images for the object at 1m and 80cm. Miniflex and OP-72 obtained similar recognizable images only at infinity and 6m. Tecnis and SN60WF had similar performances with sharp images at infinity and 2m. It is also possible to conclude that the depth of focus is more critical to the letters on the third row, since it features the lowest contrast level condition that was simulated. As the object approaches the viewer, the letters on the third row tend to become unrecognizable earlier than the letters on the second row, which is followed by the first row.

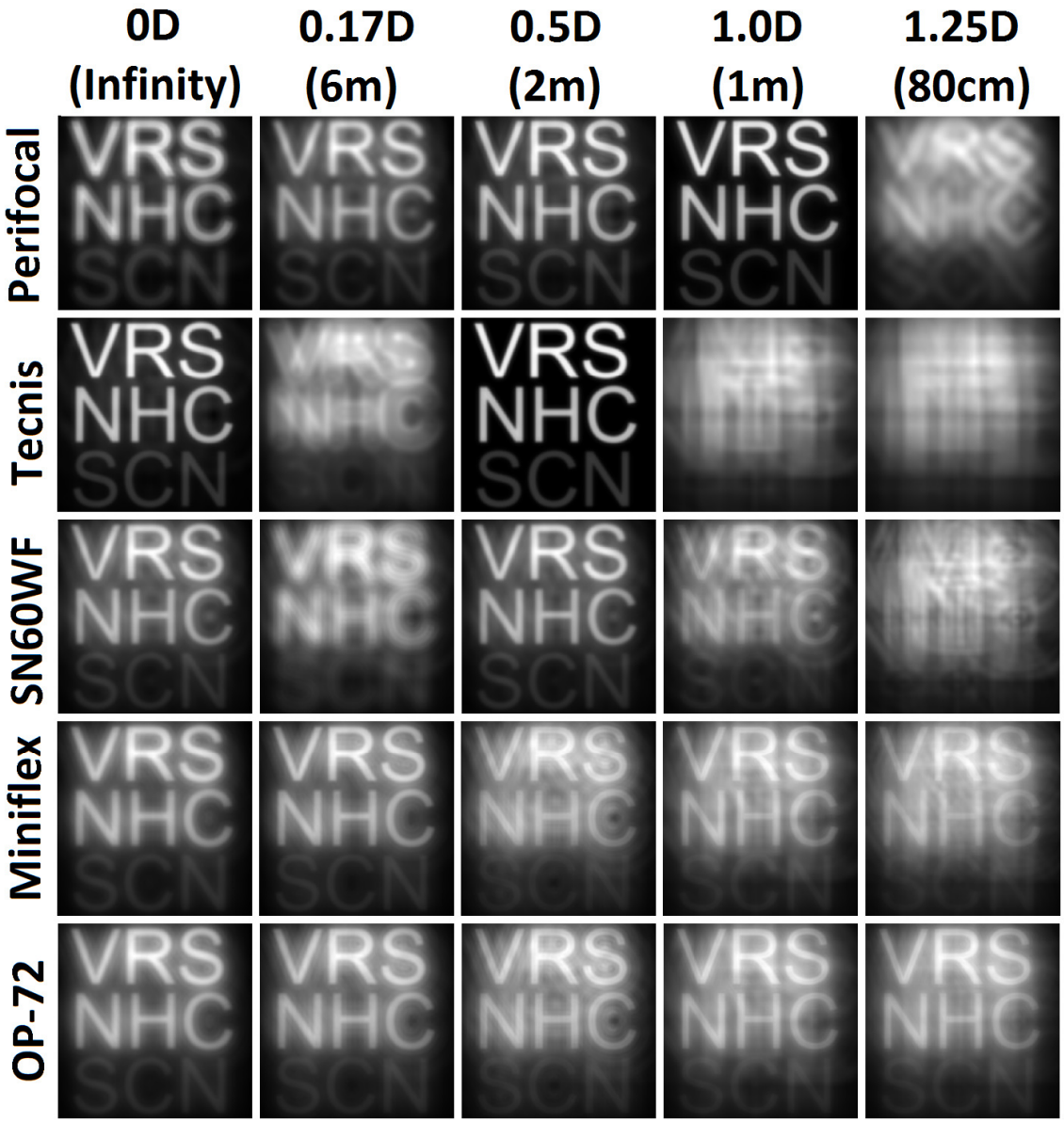

Figure 4.11. Image simulation result for 5mm diameter pupil: Pelli-Robson Contrast Sensitivity Chart.

The simulation results on Figure 4.11 showed that Tecnis IOL had the sharpest image for the object at infinity, followed by the Perifocal IOL. Tecnis and SN60WF obtained sharp images for the object at infinity and at 2m. However, these lenses provided images more blurred at 5mm pupil for closer objects, which indicates that an individual with these IOL models would be compromised in situations like reading at night and doing the makeup, for example. The Perifocal IOL obtained sharp images at infinity, 6m, 2m and 1m, although at 80cm, it yielded a blurred image. Miniflex and OP-72 obtained recognizable images in all distances tested, but with significant blur and scatter at 2m, 1m and 80cm, which prevents the perception of fine details in a scene. The blur effect in distorting the image is more evident where the letters have low contrast (third row).

In order to analyze a scene with more details, more contrast levels and a larger range of spatial frequencies than single letters, a simulation of the Mona Lisa painting was performed for each IOL model at 3mm, shown in Figure 4.12 and at 5mm diameter pupil, shown on Figure 4.13. The simulations were performed with polychromatic light (λ =546nm, 486nm and 633nm). The object distances considered on the simulations were: infinity, 6m, 2m, 1m and 80cm. The raw size of the image of the Mona Lisa is 113.7mm, which is about thirteen times the size of each letter shown in Figure 4.11 on the 0.17D (6m) column. However, the size of these images should not be the only limiting factor to analyze contrast sensitivity. According to Holladay [114], "not being able to see things at low contrast can be debilitating , causing patients to miss steps, increasing the risk of falls and severely affecting nighttime driving ability. A patient who is able to see a high-contrast street sign in broad daylight may not be able to detect a gray truck on a highway in the fog". In Figure 4.12 and Figure 4.13 it is important to observe the details and the difference in contrast throughout the scene.

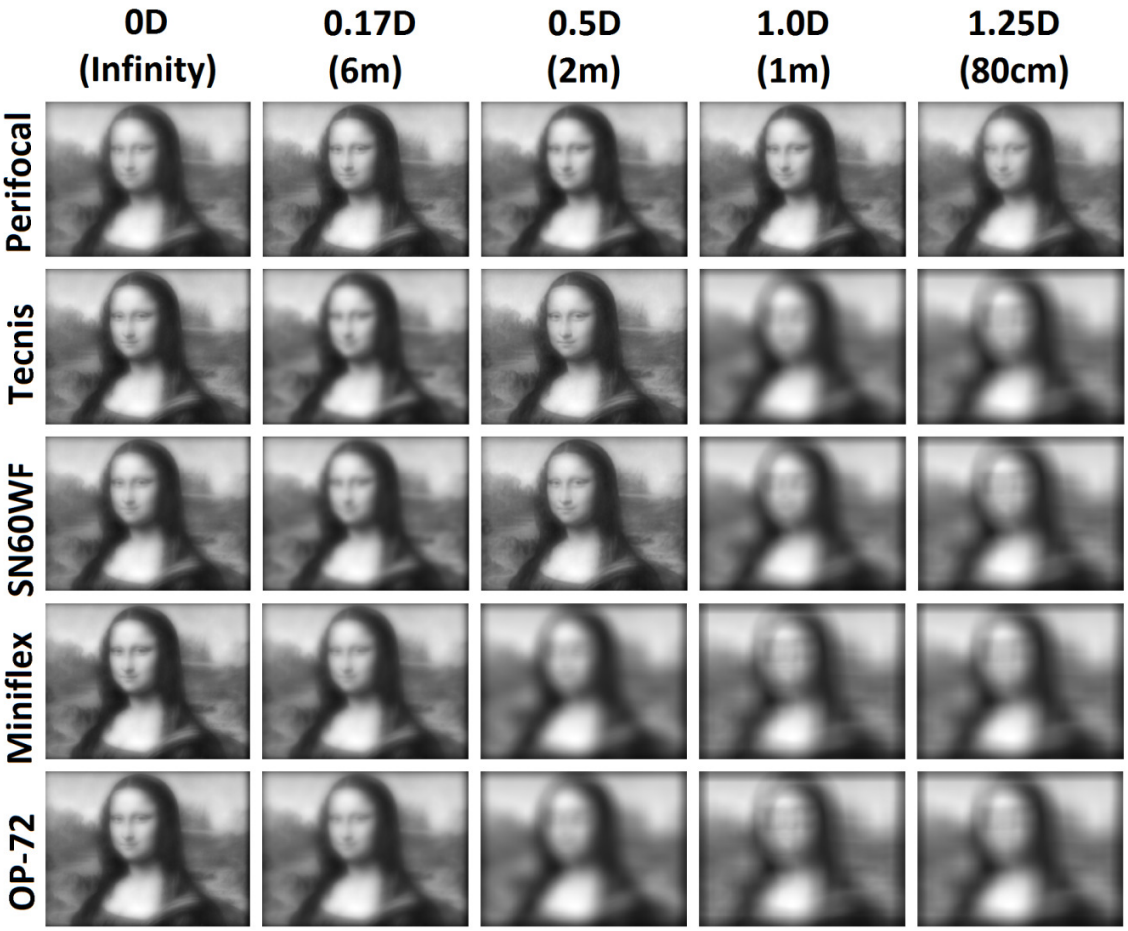

Figure 4.12. Image simulation result for 3mm diameter pupil: Mona Lisa.

By analyzing Figure 4.12, it is observed that the Perifocal IOL is the only model that allows Mona Lisa face recognition at all simulated distances at 3mm diameter pupil. Tecnis and SN60WF obtained similar images with good quality at infinity, 6m and 2m. At 1m and 80cm both models

obtained blurred images, which allows the detection of the contours only. Miniflex and OP-72 obtained sharp images only at infinity and 6m. At 2m, 1m and 80cm these models obtained blurred and distorted images which allows the detection of the contours only.

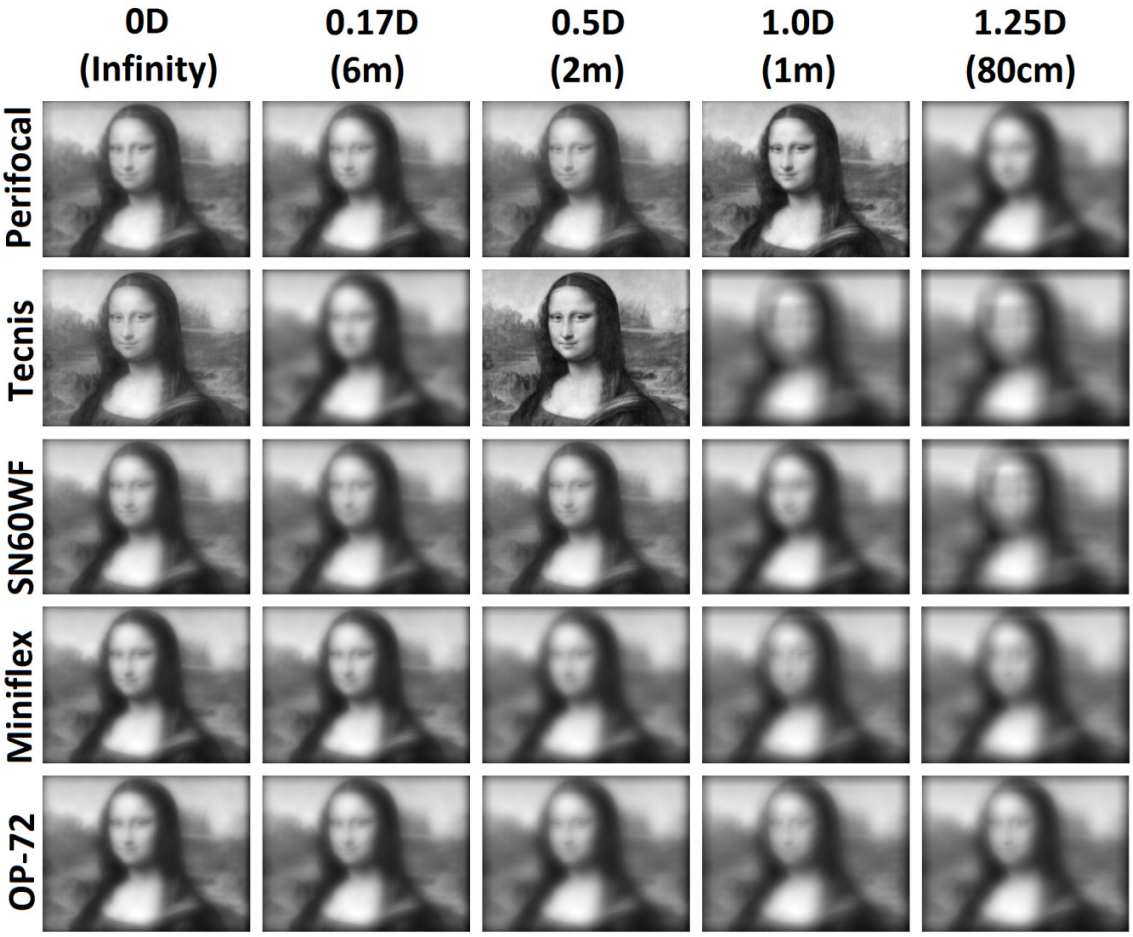

Figure 4.13. Image simulation result for 5mm diameter pupil: Mona Lisa.

By analyzing Figure 4.13, it is observed that the Perifocal IOL obtained sharp images at infinity, 6m, 2m, 1m. At 1m it obtained the sharpest image among all models. Like all models, it obtained blurred image at 80cm, allowing the detection of the contours only. Considering solely the images at 80cm, the Perifocal and OP-72 obtained slightly better images, while still blurred. Tecnis and SN60WF obtained similar images with good quality at infinity, 6m and 2m. At 2m, Tecnis yielded the sharpest image among the models and at 1m and 80cm both models obtained blurred images, which allows the detection of the contours only. At 1m, SN60WF obtained a slightly less distorted image than Tecnis. Miniflex and OP-72 had the worst performance at 5mm diameter pupil, allowing Mona Lisa face recognition only at infinity and 6m. At 2m, 1m and 80cm these models obtained blurred and distorted images which allows the detection of the contours only. It is evidenced that the image scatter associated with these two last models that was observed in Figure 4.11 compromises the perception of details in an image. Although blurred, Miniflex and OP-72 allowed identification of the single letters in Figure 4.11, but these models obtained more

compromised and distorted images for one scene or a part of it having more details, like the face of Mona Lisa, shown in Figure 4.13 that could not be recognized with these two IOL models at 2m, 1m and 80cm.

By analyzing Figure 2.14, the luminances associated with 3 and 5mm diameter pupil are approximately within the interval from 10^0 to 10^6 cdm^{-2}. Considering solely 3mm diameter pupil, the associated luminance is within the interval of 10^2 to 10^6 cdm^{-2}. The Perifocal IOL might be advantageous in relation to the commercial IOLs considering contrast at 3mm diameter pupil and intermediate-to-near vision. By analyzing the data provided in Table 2.2, it is possible to conclude that this IOL would be preferable to perform some daily activities such as:

- work in an office;
- use a tablet under 50% to 100% white color brightness;
- use a computer (LCD monitor);
- watch TV;
- handle a mobile phone (smart phone).

4.4.*TOLERANCE ANALYSIS*

The typical manufacturing tolerances shown on Table 2.1 were used as a starting point to determine each Perifocal IOL parameter variation limit. However, the values shown on Table 2.1 regard to a 50mm diameter lens while the Perifocal IOL features 6mm diameter. In order to make the tolerance analysis compliant to a component with the Perifocal IOL dimensions, the values shown on Table 2.1 must be proportionally converted to a 6mm diameter lens, because higher sized components are more sensitive to parameter change (i.e. supposing a plano-convex lens with 20mm radius of curvature and conic constant equal to -15: the sag deviation caused by 1 unit change on its conic constant is about 150 times larger on a 50mm than in a 6mm diameter lens). The aspheric profile tolerance is related in this work to the sag variation caused only by a conic constant departure from its nominal value. The exact conversion of the conic constant from 50mm to 6mm is not straightforward because it is not directly proportional to the lens diameter only: it depends on the other parameters that are being tolerated at the same time like the diameter, the radius of curvature and the conic constant itself. A satisfactory, but not exact conversion factor for aspheric profile is obtained by the ratio of the square of the diameters ($6^2/50^2$). This conversion factor is obtained from the approximate sag equation: $D^2/8R_L$. By maintaining the radius of curvature R_L constant, the sag ratio between lenses with different diameter (D_1 and D_2) is equal to the ratio of the square of the diameters (D_1^2/D_2^2). The conversion factor was tested on the Perifocal IOL and the differences obtained from an exact conversion were significantly small. A linear factor defined by the ratio of the diameters (6/50) was used to convert the lens wedge and diameter tolerance values from 50mm to 6mm diameter lens. The edge thickness absolute difference and the diameter variation are directly proportional to the lens size: the higher the diameter, the higher the edge thickness and diameter deviation from their nominal values. The conversion factor for the radius of curvature is equal to 1 because it depends only on the manufacturing process precision with no relationship to the component size.

Table 4.6 shows the typical commercial manufacturing tolerances presented on Table 2.1, the conversion factor used to adequate the component size from 50mm to 6mm diameter and the resulted tolerance values after being converted to 6mm diameter. The analysis of tolerance performed in this work considered only commercial quality attribution because it has the widest error range yielding more conservative results, besides being easier to fabricate.

Table 4.5. Manufacturing tolerances for 50mm and 6mm diameter lenses

Parameter	Tolerance at 50mm	Conversion factor	Tolerance at 6mm
Radius of curvature [%]	±0.2	1	±0.2
Diameter [mm]	±0.1	6/50	±0.012
Wedge lens [mm]	0.05	6/50	0.006
Aspheric profile [µm]	±25	36/2500	±0.36

In order to obtain the conic constant boundaries as a function of the sag variation determined by the aspheric profile tolerance, Equation 4.3 is used as a starting point [83]. Equation 4.3 describes a rotationally symmetric aspheric surface,

$$Z(r) = \frac{\left({}^{1}/_{R}\right).r^2}{1+\sqrt{1-(K+1).\left({}^{1}/_{R}\right)^2.r^2}} + \sum_{i=1} A_i.\rho^{2i} \qquad 4.3$$

where Z is the aspheric profile (sag), R is the radius of curvature, r is the radial distance from the vertex of the surface, K is the conic constant, and A_i are the higher order aspheric terms[83]. However, the standard aspheric surface, defined by a simple conicoid, where the terms A_i are null (the case of Perifocal IOL) has been successfully used to correct aberrations in a wide variety of systems [115,116].

Solving Equation 4.3 in terms of the conic constant K, where D is the lens diameter, given by two times the maximum radial distance[25] (r in Equation 4.3) from the vertex of the surface yields:

$$K(Z) = \frac{-D^2}{4.Z^2} + \frac{2.R}{Z} - 1 \qquad 4.4$$

Differentiating Equation 4.4 with respect to Z results in:

$$\frac{\partial K}{\partial Z} = \frac{D^2}{2.Z^3} - \frac{2.R}{Z^2} \qquad 4.5$$

The parameter ∂Z regards the sag deviation of ±0.36µm, shown on Table 4.5 and ∂K is the conic constant variation needed to produce changes equal to ∂Z on the lens aspheric profile. The conic constant variation is calculated by Equation 4.5 if ∂Z is known.

The radius of curvature of the lenticles are subjected to the process of microfabrication tolerances on the designed sag (σ_r), defined by Equation 4.6 [108], where σ_i represents the intrinsic roughness due to the nature of the etching process and σ_s the structural approximation error:

$$\sigma_r = \sqrt{{\sigma_i}^2 + {\sigma_s}^2} \qquad 4.6$$

[25] Twice the maximum radial distance (lens diameter) is used because it relates to the worst case for the tolerance analysis, where the maximum variation of the sag is achieved due to conic constant variation.

The tolerance of the radius of curvature calculated by sag variation is given by calculating Equation 4.1 in terms of the radius of curvature shown in Equation 4.7 and differentiating it with respect to $\mathrm{lt_{SAG}}$ as it is shown in Equation 4.8:

$$\mathrm{R_{lt}(lt_{SAG})} = \frac{\mathrm{d_{lt}}^2}{8.\,\mathrm{lt_{SAG}}} + \frac{\mathrm{lt_{SAG}}}{2} \qquad 4.7$$

$$\frac{\partial \mathrm{R_{lt}}}{\partial \mathrm{lt_{SAG}}} = -\frac{\mathrm{d_{lt}}^2}{8.\,\mathrm{lt_{SAG}}^2} + \frac{1}{2} \qquad 4.8$$

The parameter $\partial \mathrm{lt_{SAG}}$ regards the sag deviation, defined by σ_r in Equation 4.6, and $\partial \mathrm{R_{lt}}$ is the lenticle radius of curvature variation needed to produce changes equal to $\partial \mathrm{lt_{SAG}}$ on the lenticle sag. The lenticle radius of curvature variation is calculated by Equation 4.8 if $\partial \mathrm{lt_{SAG}}$ is known. The literature reports values of 17.5nm for σ_s and 25nm for σ_i to be used in Equation 4.6. To conduct a more conservative analysis, the values used in this work for σ_s and σ_i were twice those reported in the literature. Because Equation 4.6 is related to the microfabrication tolerance in a laboratory, the value found for σ_r doubled, in order to arbitrarily take into account uncertainties concerning an industrial environment for batch production, as the temperature accuracy of the etch solution; the concentration and ageing of the solution; and the reuse of the solution with increasing concentration of silicon.

The Perifocal IOL parameter boundaries are shown on Table 4.6:

Table 4.6. Perifocal IOL manufacturing parameter variation range

Parameter	Theoretical design values	Lower boundary	Upper boundary
Anterior radius of curvature [mm]	19.69	19.65	19.73
Posterior radius of curvature [mm]	-18.89	-18.93	-18.85
Lenticle radius of curvature [mm]	-159.81	-165.26	-154.36
Diameter [mm]	6.00	5.99	6.01
Anterior conic constant	-17.13	-17.50	-16.75
Posterior conic constant	-30.00	-30.42	-29.58
Lens Wedge [mm]	0.00	0.00	0.006

The center thickness variation was determined by the changes on the lens diameter, radii of curvature ant conic constants on anterior and posterior side, according to Equation 4.3. The center thickness variation boundaries as a function of parameters change is approximately ±2.9µm.

The tolerances proposed in this work were compared to available precision of two of the major commercial CNC lathes currently available, in order to assure that they are consistent to the IOL manufacturing in practice:

- Lathe 1 [117]: ±2µm radius of curvature, ±2.5µm center thickness, ±5µm diameter.
- Lathe 2 [118]: ±5µm radius of curvature, ±2.5µm center thickness, ±5µm diameter.

Both lathes are capable of manufacturing optical components with smaller tolerances than those proposed in this work, indicating that the analysis are being more conservative because they consider a wider parameter variation range.

The refractive index was not included in the tolerance analysis, but it may vary between material batches. A common practice in industry is to measure it before fabricating the IOL and then

perform small adjustments on the lens parameters in order to compensate for the material refractive index variation. However, the refractive index variation should be included in a tolerance analysis in future work.

After determining parameters interval of variation, a set of 500 lenses was created with the combination of different random disturbances on each parameter, in order to simulate the manufacturing errors. Each lens was created with parameter variation within its previously assigned tolerance range. MTF curves were obtained for each lens with the object at infinity and at 80cm , with 3mm and 5mm diameter pupils. In order to analyze the clinical impacts of these manufacturing errors, myopia and hyperopia were introduced on the theoretical Perifocal IOL design, as a basis of comparison. Because myopia compromises distant vision, it was introduced when the object was placed at infinity, and hyperopia when the object was placed at 80cm as it impairs near vision. Two degrees of those refractive errors were introduced: 0.25D and 0.5D. The main goal of the refractive errors analysis is to evaluate if the manufacturing errors would lead to spectacle correction for a patient after being submitted to cataract surgery and IOL implantation. Spectacle correction would be necessary only if the MTF had decayed to levels equal to or lower than the curves that include refractive error.

Figure 4.14 shows the MTF variation caused by manufacturing errors (gray shaded area), the MTF of the Perifocal IOL theoretical design (black solid line), 0.25D and 0.5D of introduced myopia (dotted and dashed black lines) for the object placed at infinity with 3mm (up) and 5mm (down) diameter pupil.

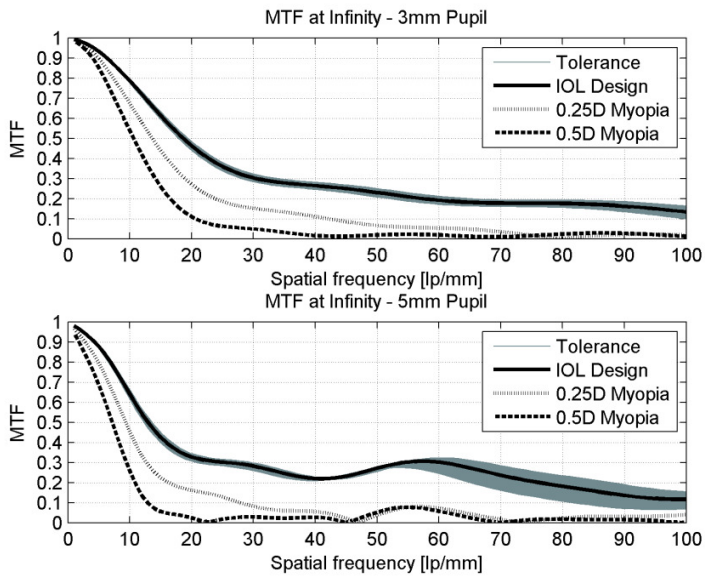

Figure 4.14. MTF variation caused by manufacturing errors for 3mm [up] and 5mm [down] diameter pupil with the object placed at infinity. The dotted and dashed curves represents 0.25D and 0.5D of myopia, respectively.

By analyzing Figure 4.14 it is concluded that although the manufacturing errors cause MTF changes, they might yield lenses with slightly higher MTF than the theoretical design for the object at infinity. The lens project is considered robust, because the theoretical design results in MTF

curves (black lines) sufficiently close to the maximum MTF curve obtained by the tolerated lenses (gray lines). The MTF is more sensitive to manufacturing errors in spatial frequencies above 50lp/mm for 5mm diameter pupil, while the variation maintain approximately constant for 3mm diameter pupil. It is important to observe that the manufacturing errors affect contrast more in higher frequencies. However, these errors have less impact on a patient vision because the contrast in higher frequencies is already lower in comparison to lower and intermediate frequencies, which are closer to the peak of the CSF function. The higher the myopia amplitude, the larger the MTF degradation for both 3mm and 5mm diameter pupil, showing that this refractive error impairs contrast sensitivity at distant vision. It is evident that MTF changes with the introduction of manufacturing errors. However, the variations are not sufficient to result in spectacle correction needs for distant vision, because the MTF curve does not decrease the contrast to levels of 0.5D even 0.25D of myopia.

Figure 4.15 shows the MTF variation caused by manufacturing errors (gray shaded area), the MTF of the Perifocal IOL theoretical design (black solid line), 0.25D and 0.5D of introduced hyperopia (dotted and dashed black lines) for the object placed at 80cm with 3mm (up) and 5mm (down) diameter pupil.

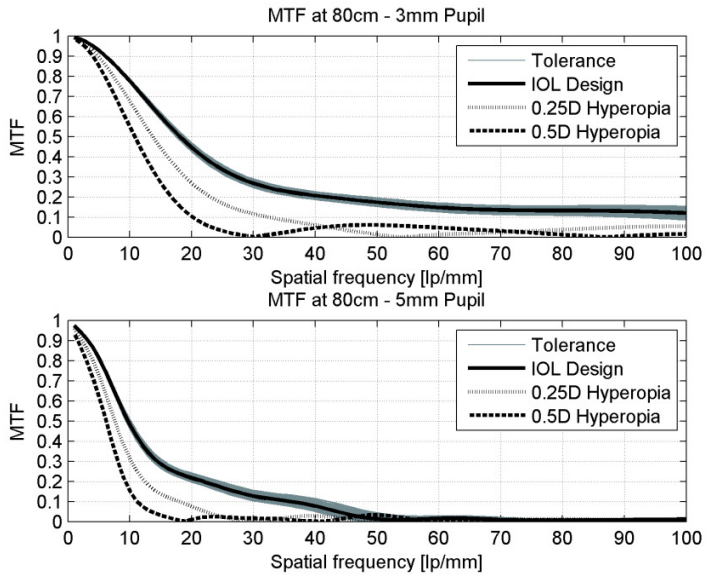

Figure 4.15. MTF variation caused manufacturing errors for 3mm [up] and 5mm [down] diameter pupil with the object placed at 80cm. The dotted and dashed curves represents 0.25D and 0.5D of hyperopia, respectively.

Figure 4.15 shows that the curves vary in function of manufacturing deviations, yielding higher or smaller MTF in comparison to the theoretical design. The lens project is considered robust, because the theoretical design results in MTF curves (black lines) are sufficiently close to the maximum MTF curve obtained by the tolerated lenses (gray lines). The higher the hyperopia amplitude, the larger the MTF degradation for both 3mm and 5mm diameter pupil, showing that this refractive error impairs contrast sensitivity at intermediate-to-near vision. Considering the object at 80cm, the MTF variation as a function of manufacturing errors are sufficiently small and would not result in spectacle correction needs for intermediate-to-near vision, because the MTF

curve does not decrease the contrast to levels of 0.5D or even 0.25D of hyperopia. The MTF is more sensitive to manufacturing errors in distant vision with 5mm diameter pupil, suggesting that night driving condition would be the most affected situation. However, the impact would not be clinically noticed by an individual, because 0.25D is the smallest spectacle correction prescription currently available and the MTF variation is not high enough to reduce the contrast sensitivity to levels compared to 0.25D of myopia.

Figure 4.16 shows the area under the MTF curve obtained by the 500 analyzed lenses considering the object at infinity and at 80cm for 3mm and 5mm diameter pupils. The area under the MTF curve of 0.25D and 0.5D of myopia and hyperopia is plotted to allow comparison.

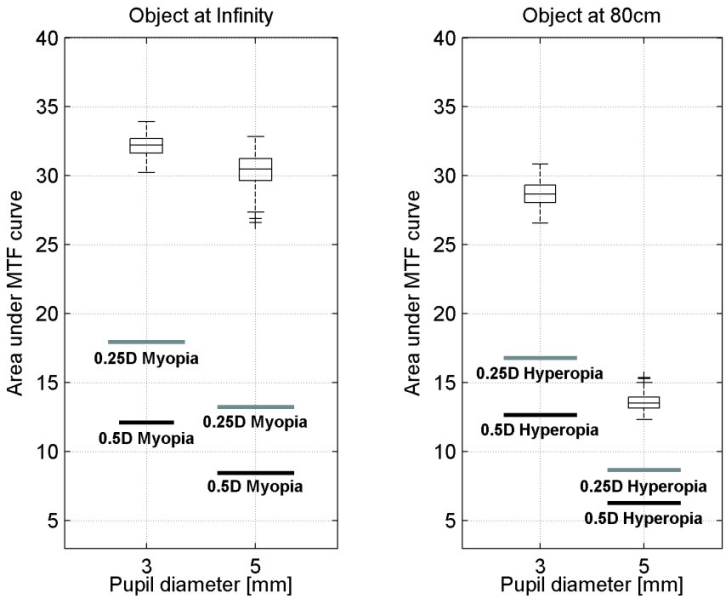

Figure 4.16. Comparison between the areas under MTF curve for the tolerated lens for 3 and 5mm diameter pupil: object placed at infinity versus 0.25D and 0.5D of myopia [left] and object placed at 80cm [right] versus 0.25D and 0.5D of hyperopia.

By analyzing Figure 4.16 it is concluded that none of the tolerance randomized lenses (shown on the boxplots) obtained contrast levels with the area under the MTF curve below 0.25D or 0.5D of refractive errors. The deviations would not demand the use of spectacles, since the fabrication errors cause much less variation on the area under the MTF curve than the smallest correction prescription practiced (0.25D). Neither distant vision nor intermediate-to-near vision would be compromised by the manufacturing errors, confirming that the Perifocal IOL is clinically feasible. The tolerance analysis and the comparison with commercial lathes allowed us to conclude that besides being clinically feasible, the Perifocal IOL can also be manufactured.

5. CONCLUSIONS

This study describes the design of an IOL with extended depth of focus, herein denominated perifocal. The Perifocal IOL was tested and compared to four commercial monofocal IOLs, where three lenses are aspheric and one is spherical. Two aspheric IOLs have negative spherical aberration of -0.27µm and -0.2 µm and one is neutral. The IOLs were tested in a modified computational eye model to render the results closer to an actual IOL implantation.

Commercial aspheric IOLs are usually designed for far vision and compensate for the total or partial spherical-aberration component or do not introduce any, yielding sharper images, but featuring narrow depth of focus, and consequently depth of field. Therefore, individuals with these lenses require the use of additional spectacles to perform activities demanding near focus. The Perifocal IOL was optimized to yield both high contrast and extended depth of focus in order to reduce the spectacle dependence, inherent to the conventional monofocal IOLs, without sacrificing the contrast.

Computer simulations were performed with the optical design software Zemax®. Blue, green and red wavelengths were considered in the tests in order to include chromatic dispersion in the analysis. All IOLs were designed for the same dioptric power (22D). The metric used to evaluate contrast was the MTF through focus. Although the Perifocal IOL presented a lower MTF curve for far objects than some of the commercial IOLs, the depth of focus was larger. The extended depth of focus produced a considerable additional power of approximately 1D for intermediate spatial frequencies that correspond to the peak of the human contrast sensitivity function.

The Perifocal IOL has also been shown to be an alternative to be deployed in the monovision implant technique. Ophthalmologists have reported that the dioptric power difference between the two IOLs, implanted in different eyes, should be approximately 1.25D in order to avoid asthenopia and reduction of stereoacuity. The dioptric power difference of 1.25D is compliant to the range of additional power provided by the Perifocal IOL. It is concluded that with the Perifocal IOL, the dioptric power difference in monovision could be higher, so individuals would be able to see closer without spectacles and not experiencing the discomfort caused by the IOL power imbalance.

By analyzing the pupil diameter as a function of the luminance for different light sources, the Perifocal IOL might be advantageous to perform some intermediate-to-near tasks in comparison to the commercial IOLs. In addition, it yields just a slight loss of contrast compared to the commercial IOLs for far vision.

Bifocal IOLs provide additional near power between 3 and 4 diopters allowing individuals to read without spectacles. However, due to the high additional power, individuals may experience halos, glare and reduced contrast, which might be uncomfortable. Due to the lower additional power, the Perifocal IOL does not present these drawbacks inherent to bifocal IOLs and, when implanted with the monovision technique, individuals might be able to read without near glasses.

The fabrication process of the Perifocal IOL requires an additional step to that of the conventional monofocal IOLs, because it needs two separate bonded pieces, which may be very sensitive to misalignments that could compromise its optical performance. However, all commercial IOLs are subjected to the same manufacturing errors analyzed in this work, except for the microfabrication

process step of the Perifocal IOL lenticles. Because of the foldable consistency of the Perifocal IOL material, it would require a smaller incision than rigid PMMA IOLs, like OP-72, for the implant.

This study also evaluated the mathematical derivation of the complete equations of the depth of field, depth of focus and hyperfocal distance for thick lenses. All of the equations were validated with Zemax® simulations. These equations present analytical functions where it is possible to evaluate the contribution of each lens design parameter. These equations can also be incorporated into any code or algorithm to analyze the optical performance of lenses providing a more comprehensive understanding of lens design.

Considering the state-of-the-art intraocular lenses, there is no such IOL that is able to perform perfectly all the functions of the crystalline lens of the natural eye. This would require the development of a smart lens in order to reproduce the crystalline lens accommodation mechanism. Although there are some pseudo-accommodative lenses available on the market, monofocal and bifocal lenses are still the most implanted lenses. Since these lenses are static (do not present any accommodation), there will always be some inherent disadvantage in comparison to the crystalline lens. It is concluded that increasing the depth of focus of a static lens will always cause loss of contrast.

It is expected that this study will strengthen the knowledge between the areas of ophthalmology and engineering. This study may also favor the collaboration between professionals of distinct areas due to its multidisciplinary nature. The approximation of ophthalmologists and engineers has an enormous potential for the development of more effective solutions and products with higher aggregated value.

6. PROPOSED NEXT STEPS

This section discusses some proposed next steps for the continuity of this study:

- Fabrication of the Perifocal IOL. This action will require the investigation of the most appropriate manufacturing method which can be performed by either a CNC lathe or microfabrication techniques based on etched silicon molds.
- Design an optical setup to characterize the Perifocal IOL and the commercial IOLs using a proper optical bench, optomechanical and optical components. This action will require the development of a physical model eye with the optical characteristics of the computational eye model used in this study. The optical setup should evaluate aberrations, effect of misalignment of the lenticles, impact of fabrication errors on the optical performance, depth of focus and the resulting images of the IOLs in order to compare to the results presented so far in this study. The results of the polychromatic analysis depend on the spectrum of the light source used.
- Simulation analysis of the IOL performance considering its placement and alignment in the eye. This simulation would help to evaluate the impacts of IOL tilt and vertical/horizontal and longitudinal displacements within a model eye.
- Tolerance analysis considering refractive index variation.
- Investigate and calculate practical examples associated to spatial frequency intervals. The relationship between the low, intermediate and high spatial frequencies to practical activities like using computers, smartphones, reading newspapper and traffic signs, playing chess and checkers might be helpful information to lens design optimization.

7. REFERENCES

1. MANN, S. Steve Mann: My "Augmediated" Life. IEEE Spectrum, 1 March 2013.
2. GUPTA, A.; AMIRPARVIZ, B.; SHARMA, S. Lightweight eyepiece for head mounted display. US 2013/0070338 A1, 21 March 2013.
3. ROBERTS, T. V. et al. Femtosecond laser cataract surgery: technology and clinical practice. Clinical and Experimental Ophthalmology, v. 41, n. 2, p. 180-186, March 2013.
4. WORLD HEALTH ORGANIZATION. Vision 2020 - Developing an action plan to prevent blindness at national, provincial and district level, 2005.
5. FATTORE, G.; TORBICA, A. Cost and reimbursement of cataract surgery in Europe: a cross-country comparison. Health Economics, v. 17, n. Suppl, p. S71-S82, 2008.
6. CHARALAMPIDOU, S. et al. Effect on refractive outcomes after cataract surgery of intraocular lens constant personalization using the Haigis formula. Journal of Cataract & Refractive Surgery, v. 36, n. 7, p. 1081-1089, July 2010.
7. MANCIL, G. L. et al. Care of the patient with presbyopia, 2011.
8. GATINEL, D. et al. Design and qualification of a diffractive trifocal optical profile for intraocular lenses. Journal of Cataract & Refractive Surgery, v. 37, n. 11, p. 2060-2067, November 2001.
9. WOODWARD, M. A.; RANDLEMAN, B.; STULTING, D. Dissatisfaction after multifocal intraocular lens implantation. Journal of Cataract & Refractive Surgery, v. 35, n. 6, p. 992-997, June 2009.
10. VRIES, N. E. D. et al. Dissatisfaction after implantation of multifocal intraocular lenses. Journal of Cataract & Refractive Surgery, v. 37, n. 5, p. 859-865, May 2011.
11. MARCOS, S. et al. Three-dimensional evaluation of accommodating intraocular lens shift and alignment in vivo. Ophthalmology - Article in Press, p. 1-11, 2013.
12. PALLIKARIS, I. G.; KONTADAKIS, G. A.; PORTALIOU, D. M. Real and pseudoaccommodation in accommodative lenses. Journal of Ophthalmology, v. 2011, September 2001.
13. KOHNEN, T. Accommodating IOL: Is the name already justified? Journal of Cataract & Refractive Surgery, v. 36, n. 4, p. 537-538, April 2010.
14. DHITAL, A.; SPALTON, D. J.; GALA, K. B. Comparison of near vision, intraocular lens movement, and depth of focus with accommodating and monofocal intraocular lenses. Journal of Cataract & Refractive Surgery - Article in Press, p. 1-7, 2013.
15. KOEPPL, C. et al. Pilocarpine-induced shift of an accommodating intraocular lens: AT-45 Crystalens. Journal of Cataract & Refractive Surgery, v. 31, n. 7, p. 1290-1297, July 2005.
16. FINDL, O. et al. Intraocular lens movement caused by ciliary muscle contraction. Journal of Cataract & Refractive Surgery, v. 29, n. 4, p. 669-676, April 2003.
17. HANCOX, J. et al. Objective measurement of intraocular lens movement and dioptric change with a focus shift accommodating intraocular lens. Journal of Cataract & Refractive Surgery, v. 32, n. 7, p. 1098-1103, July 2006.
18. O'HEINEACHAIN, R. Modest Monovision - Presbyopic approach with sight defocus in nondominant eye achieves high patient satisfaction. Eurotimes - ESCRS, v. 17, n. 5, p. 22.
19. BOYLE, E. L. Presbyopia - Monovision revised. EyeWorld, 18, n. 6, June 2013.
20. BARRETT, G. D. My standpoint on monovision as a cataract surgeon. Cataract & Refractive Surgery

Today Europe, 4, n. 9, October 2009. 58-60.

21. BARBERO, S.; MARCOS, S.; JIMENEZ-ALFARO, I. Optical aberrations of intraocular lenses measured in vivo and in vitro. Journal of the Optical Society of America A, v. 20, n. 10, p. 1841-1851, October 2003.
22. HOLLADAY, J. T. et al. A new intraocular lens design to reduce spherical aberration of pseudophakic eyes. Journal of Refractive Surgery, v. 18, n. 6, p. 683-691, 2002.
23. MESTE, U.; DILLINGER, P.; ANTERIST, N. Impact of a modified optic design on visual function: Clinical comparative study. Journal of Cataract & Refractive Surgery, v. 29, n. 4, p. 652-660, April 2003.
24. KERSHNER, R. M. Retinal image contrast and functional visual performance with aspheric, silicone, and acrylic intraocular lenses. Journal of Cataract & Refractive Surgery, v. 29, n. 9, p. 1684-1694, September 2003.
25. ROCHA, K. M. et al. Spherical aberration and depth of focus in eyes implanted with aspheric and spherical intraocular lenses: a prospective randomized study. American Academy of Ophthalmology, v. 114, n. 11, p. 2050-2054, November 2007.
26. MARCOS, S.; BARBERO, S.; JIMENEZ-ALFARO, I. Optical quality and depth-of-field of eyes implanted with spherical and aspheric intraocular lenses. Journal of Refractive Surgery, v. 21, May/June 2005.
27. HECHT, E. Optics. 4. ed. [S.l.]: India Pearson Education, 2003.
28. J.K., J.; TSENG, S. S. Simple method for accurate alignment in toric phakic and aphakic intraocular lens implantation. Journal of Cataract & Refractive Surgery, v. 34, n. 10, p. 1631–36, October 2008.
29. FELIPE, A. et al. Residual astigmatism produced by toric intraocular lens rotation. Journal of Cataract & Refractive Surgery, v. 37, n. 10, p. 1895-901, October 2011.
30. WALTZ, K. L. et al. Clinical outcomes of Tecnis toric intraocular lens implantation after cataract removal in patients with corneal astigmatism. American Academy of Ophthalmology, v. 122, n. 1, p. 39-47, January 2015.
31. SUN, X.-Y. et al. Toric intraocular lenses for correcting astigmatism in 130 eyes. Ophthalmology, v. 107, n. 9, p. 1776-81, September 2000.
32. AHMED, I. I. K. et al. Visual function and patient experience after bilateral implantation of toric intraocular lenses. Journal of Cataract & Refractive Surgery, v. 36, n. 4, p. 609-16, April 2010.
33. FELIPE, A. et al. Modulation transfer function of a toric intraocular lens: evaluation of the changes produced by rotation and tilt. Journal of Refractive Surgery, v. 28, n. 5, May 2012.
34. HOLLICK, E. J. Intraocular lens implantation. The Official Journal of the Association of Optometrists, v. 3 , n. 11, p. 27-33, November 2001.
35. ASBELL, P.; PRASAD, S.; AUGUSTIN, A. J. Blue- and violet-light? Filtering IOLs. Cataract & Refractive Surgery Today Europe, p. 18-21, July 2008.
36. MONTEIRO, D. W. D. L. CMOS-based integrated wavefront sensor. [S.l.]: Delft University Press, 2002.
37. GOODMAN, J. W. Introduction to Fourier Optics. 2. ed. [S.l.]: McGraw-Hill, 1996.
38. TRIPOLI, N. The Zernike polynomials. University of North Carolina. [S.l.], p. 1-15. 2003.
39. KRUEGER, R. R.; APPLEGATE, R. A.; MACRAE, S. M. Wavefront customized visual corrections: the quest for super vision II. Thorofare: SLACK Incorporated, 2004.
40. PELI, E. Contrast in complex images. Journal of the Optical Society of America A, v. 7, n. 10, p. 2032-2040, October 1990.
41. GROSS, H. et al. (Eds.). Handbook of Optical Systems: Aberration Theory and Correction of Optical

Systems. [S.l.]: Wiley, v. 3, 2007.

42. MCALINDEN, C.; MCCARTNEY, M.; MOORE, J. Mathematics of Zernike polynomials: a review. Clinical and Experimental Ophthalmology, v. 39, n. 8, p. 820-827, November 2011.
43. COLLINS-UNRUH, J. Understanding Rasters. Université de Montréal. Available at: <www.iro.unmontreal.ca/~mignotte/IFT6150/ComplementCours/UnderstandingRasters.pdf>. Accessed in: November 2013.
44. PRESS, W. H. et al. Numerical recipes in C. 2. ed. [S.l.]: Cambridge University Press, 1992.
45. RAVIKUMAR, S.; THIBOS, L. N.; BRADLEY, A. Calculation of retinal image quality for polychromatic light. Journal of the Optical Society of America A, v. 25, n. 10, p. 2395-2407, October 2008.
46. BESCOS, J.; GLASER, I.; SAWCHUK, A. A. Restoration of color images degraded by chromatic aberrations. Applied Optics, v. 19, n. 22, p. 3869-3876, November 1980.
47. COLOR and Vision. The Physics Classroom. Available at: <www.physicsclassroom.com/class/light/u12l2b.cfm>. Accessed in: November 2013.
48. THIBOS, L. N.; BRADLEY, A.; ZHANG, X. Effect of ocular chromatic aberration on monocular visual performance. Optometry and Vision Science, v. 68, n. 8, p. 599-607, August 1991.
49. SALEH, B. E. A.; TEICH, . C. Fundamentals of Photonics. 2. ed. [S.l.]: Wiley, 2007.
50. RAO, F. et al. Achromatic customized intraocular lens based on an individual pseudophakic eye model. Optik - International Journal for Light and Electron Optics, v. 121, n. 4, p. 366-372, February 2010.
51. LÓPEZ-GIL, N.; MONTÉS-MICÓ, R. New intraocular lens for achromatizing the human eye. Journal of Cataract & Refractive Surgery, v. 33, n. 7, p. 1296-1302, July 2007.
52. FERNÁNDEZ, E. J. et al. Chromatic aberration correction of the human eye for retinal imaging in the near infrared. Optics Express, v. 14, n. 13, p. 6213-6225, June 2006.
53. AKROMALENS™ SeeLens AC. Hanita Lenses. Available at: <http://www.hanitalenses.com/wp-content/uploads/2011/09/aKromalens_Seelens_AC.pdf>. Accessed in: November 2013.
54. ASWAD, A. E. et al. Outcomes of New Monofocal Achromatic Presbyopic Pseudophakic IOL: Pilot Study. ASCRS. [S.l.]: [s.n.]. 2012.
55. BORN, M.; WOLF, E. Principles of optics. 7th expanded. ed. [S.l.]: Cambridge University Press, 2002.
56. IWAI, H. Roadmap for 22 nm and beyond. Microelectronic Engineering, v. 86, n. 7-9, p. 1520-1528, July-September 2009.
57. BOREMAN, G. D. Modulation Transfer Function in Optical and Electro-optical Systems. [S.l.]: SPIE Press, 2001.
58. MASALEHDAN, H. et al. Modeling of Zernike optical aberrations by MTF and PSF. Biomedical Optics. [S.l.]: [s.n.]. August 2010.
59. OISC.NET. Vision Optics. Available at: <http://oisc.net/Vision%20Optics.pdf>. Accessed in: November 2013.
60. CAMBRIDGE in Colour. Lens Diffraction & Photography. Available at: <www.cambridgeincolour.com/tutorials/diffraction-photography.htm>. Accessed in: November 2013.
61. FACTS and Figures concerning the human retina. In: KOLB, H., et al. Webvision: The Organization of the Retina and Visual System- Facts and Figures Concerning the Human Retina. [S.l.]: [s.n.], 2013. Cap. XIII.
62. PURVES, D. (Ed.). Neuroscience. 3. ed. [S.l.]: Sinauer Associates, 2004.
63. HIRISH, J.; CURCIO, C. A. The spatial resolution capacity of human foveal retina. Vision Research, v. 29,

n. 9, p. 1095-1101, 1989.

64. DALSA TECHNOLOGY WITH VISION. CourierTronics. Pixel Pitch versus Lenses: The Effect of Modulation Transfer Function (MTF). Available at: <http://www.couriertronics.com/docs/notes/sensor_application_notes/_Modulation_Transfer_Function.pdf>. Accessed in: November 2013.
65. THIBOS, L. N.; CHENEY, F. E.; WALSH, D. J. Retinal limits to the detection and resolution of gratings. Journal of the Optical Society of America A, v. 4, n. 8, p. 1524-1529, August 1987.
66. RUSS, J. C. The Image Processing Handbook. 5. ed. [S.l.]: Taylor & Francis Group, 2007.
67. WATSON, A. B. A formula for the mean human optical modulation transfer function as a function of pupil size. Journal of Vision (2013) 13(6):18, 1–11, v. 13, n. 6, p. 1-11, January 2013.
68. MANNOS, J. L.; SAKRISON, D. J. The Effects of a Visual Fidelity Criterion on the Encoding of Images. IEEE Transactions on Information Theory, v. 20, n. 4, p. 525-536, July 1974.
69. SMITH, W. J. Modern Optical Engineering. 4. ed. [S.l.]: McGraw-Hill, 2008.
70. ATCHISON, D. A. et al. Blur limits for defocus, astigmatism and trefoil. Vision Research, v. 49, n. 19, p. 2393-2403, September 2009.
71. BAKARAJU, R. C. et al. Depth-of-focus and its association with the spherical aberration sign. A ray-tracing analysis. Journal of Optometry, v. 3, n. 1, p. 51-59, 2010.
72. CHENG, X. et al. The visual impact of Zernike and Seidel forms of monochromatic aberrations. Optometry and Vision Science , v. 87, n. 5, p. 300-312, May 2010.
73. ROCHA, K. M. et al. Expanding depth of focus by modifying higher-order aberrations induced by an adaptive optics visual simulator. Journal of Cataract & Refractive Surgery, v. 35, n. 11, p. 1885–1892, November 2009.
74. LERAY, B. et al. Relationship between induced spherical aberration and depth of focus after hyperopic LASIK in presbyopic patients. Ophthalmology, v. 122, n. 2, p. 233-243, February 2015.
75. VILLEGAS, E. A. et al. Extended depth of focus with induced spherical aberration in light-adjustable intraocular lenses. American Journal of Ophthalmology, v. 157, n. 1, p. 142–149, January 2014.
76. BELBACHIR, A. N. (Ed.). Smart Cameras. [S.l.]: Springer, 2010.
77. CASTREJÓN-PITA, J. R.; CASTREJÓN-GARCÍA, R.; HUTCHINGS, I. M. High Speed Shadowgraphy for the Study of Liquid Drops. In: KLAPP, J., et al. Fluid Dynamics in Physics, Engineering and Environmental Applications. [S.l.]: [s.n.], 2013.
78. HIGHTON, S. Virtual Reality Photography: Creating Panoramic and Object Images. [S.l.]: [s.n.], 2010.
79. DERENIAK, E. L.; DERENIAK, T. D. Geometrical and Trigonometric Optics. [S.l.]: Cambridge University Press, 2008.
80. KATZ, M. Introduction to Geometrical Optics. [S.l.]: World Scientific Publishing, 2002.
81. MIROTZNIK, M. S. et al. Design of cubic-phase optical elements using subwavelength microstructures. Optics Express, v. 16, n. 2, p. 1250-1259, 2008.
82. FÖRSTER, S. et al. Extended depth of focus as a process of pupil manipulation. SPIE Proceedings - Optical Design and Engineering II. [S.l.]: [s.n.]. 2005.
83. FISCHER, R. E.; TADIC-GALEB, B.; YODER, P. R. Optical system design. 2nd. ed. [S.l.]: McGraw Hill, 2008.
84. OSA (Ed.). Handbook of optics. 3rd. ed. [S.l.]: McGraw Hill, v. II, 2010.
85. HOLLADAY, L. L. The fundamentals of glare and visibility. Journal of the Optical Society of America and

Review of Scientific Instruments, v. 12, n. 4, p. 271-319, April 1926.

86. CRAWFORD, B. H. The dependence of pupil size upon external light stimulus under static and variable conditions. Proceedings of the Royal Society of London - Series B, Biological Sciences. [S.l.]: Jstor. 1936. p. 376-395.
87. MOON, P.; SPENCER, D. E. On the Stiles-Crawford Effect. Journal of the Optical Society of America, v. 34, n. 6, p. 319-329, June 1944.
88. GROOT, S. G. D.; GEBHARD, J. W. Pupil Size as Determined by Adapting Luminance. Journal of the Optical Society of America, v. 42, n. 7, p. 492-495, July 1952.
89. BLACKIE, C. A.; HOWLAND, H. C. An extension of an accommodation and convergence model of emmetropization to include the effects of illumination intensity. Ophthalmic and Physiological Optics, v. 19, n. 2, p. 112-125, March 1999.
90. STANLEY, P. A.; DAVIES, A. K. The effect of field of view size on steady-state pupil diameter. Ophthalmic and Physiological Optics, 1995, v. 15, n. 6, p. 601-603.
91. ATCHISON, D. A. et al. Influence of field size on pupil diameter under photopic and mesopic light levels. Clinical & Experimental Optometry, v. 94, n. 6, p. 545–548, 2001.
92. WINN, B. et al. Factors affecting light-adapted pupil size in normal human subjects. Investigative Ophthalmology & Visual Science, v. 35, n. 3, p. 1132-1137, March 1994.
93. GREIVENKAMP, J. E. Field Guide to Geometrical Optics. [S.l.]: SPIE Press, v. FG01, 2004.
94. DOESSCHATE, J. T.; ALPERN, M. Effect of photoexcitation of the two retinas on pupil size. Journal of Neurophysiology, v. 30, n. 3, p. 562-576, May 1967.
95. WATSON, A. B.; YELLOTT, J. I. A unified formula for light-adapted pupil size. Journal of Vision, v. 12, n. 10, p. 1-16, 2012.
96. MACEVOY, B. Handprint. Available at: <http://www.handprint.com/HP/WCL/color4.html#lightrange>. Accessed in: November 2013.
97. APPLE iPad 3 review. GSMARENA. Available at: <http://www.gsmarena.com/apple_ipad_3-review-739p3.php>. Accessed in: November 2013.
98. SHAMMAS, H. J. Intraocular lens power calculation. [S.l.]: [s.n.], 2003.
99. HAIGIS, W. Challenges and approaches in modern biometry and IOL calculation. Saudi Journal of Ophthalmology, v. 26, n. 1, p. 7-12, January 2012.
100. LYTRO. Available at: <www.lytro.com>. Accessed in: November 2013.
101. GEORGIEV, T.; LUMSDAINE, A. tgeorgiev.net. Focused Plenoptic Camera and Rendering. Available at: <www.tgeorgiev.net/rendering.pdf>.
102. NG, R. Lytro. Digital Light Field Photography, 2006. Available at: <www.lytro.com/downloads/resources/renng-thesis.pdf>. Accessed in: November 2013.
103. NG, R. et al. Light Field Photography with a Hand-held Plenoptic Camera. Stanford University. [S.l.]. 2005.
104. OLSEN, T. Calculation of intraocular lens power: a review. Acta Ophthalmologica Scandinavica, v. 85, n. 5, p. 472-485, 2007.
105. LIOU, H.-L.; BRENNAN, N. A. Anatomically accurate, finite model eye for optical modeling. Journal of the Optical Society of America A, v. 14, n. 8, p. 1684-1695, August 1997.
106. NORLAND Optical Adhesive 73. Norland Products. Available at:

<https://www.norlandprod.com/adhesives/NOA%2073.html>. Accessed in: April 2015.

107. NORLAND Optical Adhesive 68. Norland Products. Available at: <www.norlandprod.com/adhesives/NOA%2068.html>. Accessed in: November 2013.
108. MONTEIRO, D. W. D. L. et al. Single-mask microfabrication of aspherical optics using KOH anisotropic etching of Si. Optics Express, v. 11, n. 18, p. 2244-2252, September 2003.
109. DEB, K. et al. A Fast and Elitist Multiobjective Genetic Algorithm: NSGA-II. Evolutionary Computation, v. 6, n. 2, 2002.
110. SONG, L. NGPM - A NSGA-II Program in Matlab. Mathworks, 2011. Available at: <http://www.mathworks.com/matlabcentral/fileexchange/31166-ngpm-a-nsga-ii-program-in-matlab-v1-4>. Accessed in: March 2015.
111. THE ACCREDITED COMMITTEE Z80 FOR OPHTHALMIC STANDARDS. American National Standard for Ophthalmics – Toric Intraocular Lenses Z80.30, 2010.
112. INTERNATIONAL STANDARD. Ophthalmic implants - Intraocular Lenses - Part 2: Optical properties and test methods - ISO 11979-2, 1999.
113. INTERNATIONAL STANDARD. Ophthalmic implants - Intraocular Lenses - Part 9: Multifocal intraocular lenses - ISO11979-9, v. 2006.
114. HOLLADAY, J. T. Quality of vision - Essential optics for the catarct and refractive surgeon. [S.l.]: Slack incorporated, 2007.
115. LERNER, S. A.; SASIAN, J. M. Optical design with parametrically defined aspheric surfaces. Applied Optics, v. 39, n. 28, p. 5205-5213, October 2000.
116. LERNER, S. A.; SASIAN, J. M. Novel Aspheric Surfaces For Optical Design. Proceedings of SPIE. [S.l.]: SPIE. 2000. p. 17-25.
117. DAC International. DAC ALM Lens Lathe. Available at: <http://www.dac-intl.com/products/diamond-turning-equipment/2-axis-alm-lens-lathe-series-iv/>. Accessed in: April 2015.
118. OPTOFORM 80. Sterling Ultra Precision. Available at: <http://www.sterlingint.com/docs/Opto80EngSpec.pdf>. Accessed in: April 2015.
119. TRATTLER, W. B.; KAISER, P. K.; FRIEDMAN, N. J. Review of Ophthalmology: Expert Consult. 2. ed. [S.l.]: Elsevier, 2012.
120. NORLAND Optical Adhesive 61. Norland Products. Available at: <www.norlandprod.com/adhesives/noa61pg2.html>. Accessed in: November 2013.
121. NAVARRO, R.; SANTAMARIA, J.; BESCÓS, J. Accommodation-dependent model of the human eye with aspherics. Journal of the Optical Society of Amarica A, v. 2, n. 8, p. 1273-1280, August 1985.

APPENDIX

In this section, it is presented the mathematical deduction of some equations used in this work. The equations presented here were compared with computational simulation in Zemax®. The deduction and validation of this set of equations are part of this work.

Depth of focus and magnification:

Figure 0.1 shows a schematic diagram of a thin lens, where D is the lens diameter, DOF is the depth of focus, s_o and s_i are the object and the image distances. D, DOF, s_o and s_i are given in millimeters.

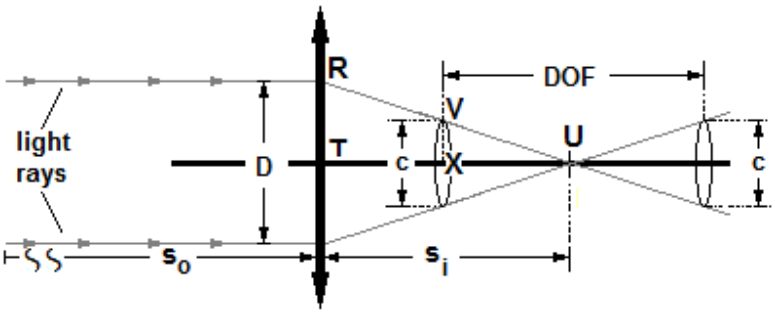

Figure 0.1. Schematic diagram of a thin lens.

From similar triangles (RTU and VXU) it is known that:

$$\frac{D}{s_i} = \frac{c}{\frac{DOF}{2}} \qquad 0.1$$

$$DOF = \frac{2.s_i.c}{D} \qquad 0.2$$

Starting with the thin lens equation, where f is the lens focal length:

$$\frac{1}{f} = \frac{1}{s_o} + \frac{1}{s_i} \qquad 0.3$$

s_i and f can be given as:

$$s_i = \frac{s_o.f}{s_o - f} \quad \text{and} \quad f = \frac{s_o.s_i}{s_o + s_i} \qquad 0.4$$

Replacing s_i from Equation 0.4 in Equation 0.2 yields:

$$DOF = 2.c.\frac{f}{D}.\frac{s_o}{s_o - f} \qquad 0.5$$

The F-number ($F_\#$) is defined as the ratio f/D. Replacing the ratio f/D in Equation 5 by the $F_\#$ yields:

$$\mathrm{DOF} = 2.\mathrm{c}.\mathrm{F}_{\#}.\frac{\mathrm{s_o}}{\mathrm{s_o} - \mathrm{f}} \qquad 0.6$$

Replacing f from Equation 0.4 in Equation 0.6 yields:

$$\mathrm{DOF} = 2.\mathrm{c}.\mathrm{F}\#.\frac{\mathrm{s_o}}{\mathrm{s_o} - \frac{\mathrm{s_o}.\mathrm{s_i}}{\mathrm{s_o} + \mathrm{s_i}}} \qquad 0.7$$

$$\mathrm{DOF} = 2.\mathrm{c}.\mathrm{F}_{\#}.\frac{\mathrm{s_o}}{\frac{{\mathrm{s_o}}^2 + \mathrm{s_o}.\mathrm{s_i} - \mathrm{s_o}.\mathrm{s_i}}{\mathrm{s_o} + \mathrm{s_i}}} \qquad 0.8$$

$$\mathrm{DOF} = 2.\mathrm{c}.\mathrm{F}_{\#}.\frac{\mathrm{s_o}.(\mathrm{s_o} + \mathrm{s_i})}{{\mathrm{s_o}}^2} \qquad 0.9$$

$$\mathrm{DOF} = 2.\mathrm{c}.\mathrm{F}_{\#}.\left(1 + \frac{\mathrm{s_i}}{\mathrm{s_o}}\right) \qquad 0.10$$

<u>Thick lens s_i as a function of the object vergence OBj:</u>

The vergence of any object varies with its distance from the optical system. The larger the distance, the smaller the object vergence. An object located at 1m from a single lens will yield a vergence of -1D at the lens plane. A vergence of -1D can also be obtained by adding a -1D paraxial lens right before the lens, since the object is maintained at infinity (vergence 0D). The effect of shifting the object or varying the power of a paraxial lens added in front of the optical system is exactly the same. It is known that when the object is located at infinity, than the distance between the image and the lens is exactly equal to the lens back focal length (BFL), which in this case is equal to f+ $\delta^*{}_{\mathrm{lens}}$. If the object is not located at infinity, than BFL of the optical system composed of the combination of a paraxial lens and a single lens will be given by [27]:

$$\mathrm{BFL} = \mathrm{f_{lens}}.\frac{(\delta_{\mathrm{lens}} - \mathrm{f_{paraxial}})}{\delta_{\mathrm{lens}} - (\mathrm{f_{lens}} + \mathrm{f_{paraxial}})} + \delta^*{}_{\mathrm{lens}} \qquad 0.11$$

where f_{lens} and $f_{paraxial}$ are the focal length of the lens and the paraxial lens that represents the object, respectively and δ_{lens} and $\delta^*{}_{\mathrm{lens}}$ are the location of the anterior and posterior lens principal planes. δ_{lens}, $\delta^*{}_{\mathrm{lens}}$, f_{lens} and $f_{paraxial}$ must be given in the same unit. When the object is at infinity, s_i is equal to f+ $\delta^*{}_{\mathrm{lens}}$. Otherwise, $f_{paraxial}$ is equal -s_o and s_i is given by Equation 0.12:

$$\mathrm{s_i} = \mathrm{f_{lens}}.\frac{(\delta_{\mathrm{lens}} + \mathrm{s_o})}{\delta_{\mathrm{lens}} - \mathrm{f_{lens}} + \mathrm{s_o}} + \delta^*{}_{\mathrm{lens}} \qquad 0.12$$

In order to extend the calculation of s_i for any object distance s_o, including infinity, a conversion of focal distance to dioptric power must be performed. The dioptric optical power is given in diopters by Φ=1000/f with f given in millimeters. OBJ is the object vergence in diopters given by -1000/s_o, with s_o in millimeters. Replacing the focal distances in Equation 0.12 by optical power yields:

$$s_i = \frac{1000}{\Phi_{lens}} . \frac{\left(\delta_{lens} - \frac{1000}{OBJ}\right)}{\delta_{lens} - \frac{1000}{\Phi_{lens}} - \frac{1000}{OBJ}} + \delta^*{}_{lens} \qquad 0.13$$

$$s_i = \frac{1000}{\Phi_{lens}} . \frac{\left(\frac{OBJ.\delta_{lens} - 1000}{OBJ}\right)}{\frac{\Phi_{lens}.OBJ.\delta_{lens} - 1000.OBJ - 1000.\Phi_{lens}}{\Phi_{lens}.OBJ}} + \delta^*{}_{lens} \qquad 0.14$$

$$s_i = 1000. \frac{(-1000 + \delta_{lens}.OBJ)}{\Phi_{lens}.OBJ.\delta_{lens} - 1000.OBJ - 1000.\Phi_{lens}} + \delta^*{}_{lens} \qquad 0.15$$

$$s_i = \frac{1000 - \delta_{lens}.OBJ}{\Phi_{lens} + OBJ - 0.001.\Phi_{lens}.OBJ.\delta_{lens}} + \delta^*{}_{lens} \qquad 0.16$$

If the object is at infinity than OBJ is equal to 0 and s_i is given by $f_{lens}+\delta^*{}_{lens}$.

<u>Depth of field:</u>

Considering the situation shown in Figure 0.2, where s_o is the distance between the object that is in focus and the lens and s_i represents the distance between the lens and the image plane.

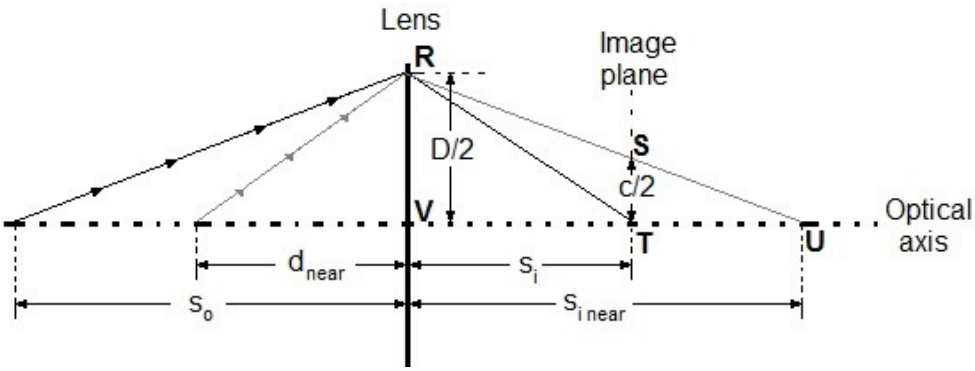

Figure 0.2. Schematic diagram used to calculate d_{near}.

d_{near} is the object position that yields a spot on the image plane with diameter equal to the permissible circle of confusion c and D is the lens diameter (only a half of the light cone is represented in Figure 0.2). Figure 0.2 shows that triangles RVU and STU are similar. From similar triangles it is known that:

$$\frac{D}{s_{i_{near}}} = \frac{c}{s_{i_{near}} - s_i} \qquad 0.17$$

$$\frac{D.s_i}{D - c} = s_{i_{near}} \qquad 0.18$$

$s_{i_{near}}$ is calculated by Equation 0.16 where Φ and OB_{near} are lens dioptric power and the vergence of the near object, both given in diopters. δ and δ^* are the location of the anterior and posterior lens principal planes in millimeters.

$$s_{i_{near}} = \left[\frac{1000 - \delta.OB_{near}}{\Phi + OB_{near} - 0.001\delta.\Phi.OB_{near}}\right] + \delta^* \qquad 0.19$$

Combining Equations 0.18 and 0.19:

$$\frac{D.s_i}{D-c} = \left[\frac{1000 - \delta.OB_{near}}{\Phi + OB_{near} - 0.001.\delta.\Phi.OB_{near}}\right] + \delta^* \qquad 0.20$$

$$\frac{D.s_i - \delta^*.D + \delta^*.c}{D-c} = \left[\frac{1000 - \delta.OB_{near}}{\Phi + OB_{near} - 0.001.\delta.\Phi.OB_{near}}\right] \qquad 0.21$$

$$\begin{aligned}\Phi.(D.s_i - \delta^*.D + \delta^*.c) + OB_{near}.(D.s_i - \delta^*.D + \delta^*.c)\\ - 0.001.\delta.\Phi.OB_{near}.(D.s_i - \delta^*.D + \delta^*.c)\\ = 1000.(D-c) - \delta.OB_{near}.(D-c)\end{aligned} \qquad 0.22$$

$$\begin{aligned}OB_{near}.(D.s_i - \delta^*.D + \delta^*.c) - 0.001.\delta.\Phi.OB_{near}.(D.s_i - \delta^*.D + \delta^*.c)\\ + \delta.OB_{near}.(D-c) = 1000.(D-c) - \Phi.(D.s_i - \delta^*.D + \delta^*.c)\end{aligned} \qquad 0.23$$

$$\begin{aligned}OB_{near}.[(D.s_i - \delta^*.D + \delta^*.c).(1 - 0.001.\delta.\Phi) + \delta.(D-c)]\\ = 1000.(D-c) - \Phi.(D.s_i - \delta^*.D + \delta^*.c)\end{aligned} \qquad 0.24$$

$$OB_{near} = \frac{1000.(D-c) - \Phi.(D.s_i - \delta^*.D + \delta^*.c)}{(D.s_i - \delta^*.D + \delta^*.c).(1 - 0.001.\delta.\Phi) + \delta(D-c)} \qquad 0.25$$

A conversion from the object negative vergence in diopters to object distance in millimeters must be performed to calculate d_{near} in millimeters:

$$d_{near} = -\frac{1000}{OB_{near}} = 1000.\left[\frac{(D.s_i - \delta^*.D + \delta^*.c).(0.001.\delta.\Phi - 1) - \delta.(D-c)}{1000.(D-c) - \Phi.(D.s_i - \delta^*.D + \delta^*.c)}\right] \qquad 0.26$$

Considering the situation shown in Figure 0.3, where s_o is the distance between the object that is in focus and the lens and s_i represents the distance between the lens and the image plane.

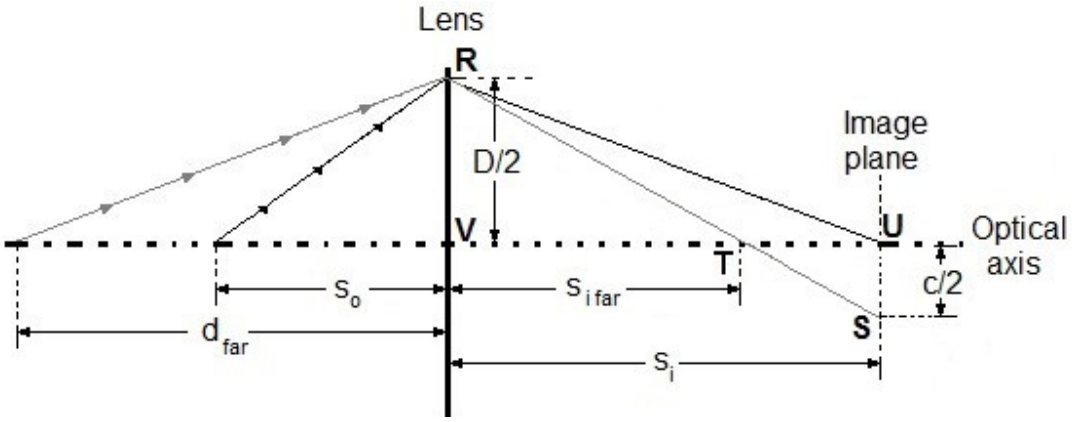

Figure 0.3. Schematic diagram used to calculate d_{far}.

d_{far} is the object position that yields a spot on the image plane with diameter equal to the permissible circle of confusion c and D is the lens diameter (only a half of the light cone is represented in Figure 0.3). Figure 0.3 shows that triangles RVT and UTS are similar. From similar triangles it is known that:

$$\frac{D}{s_{i_{far}}} = \frac{c}{s_i - s_{i_{far}}} \qquad 0.27$$

$$\frac{D.s_i}{D+c} = s_{i_{far}} \qquad 0.28$$

$s_{i_{far}}$ is calculated by Equation 0.16, where Φ and OB_{far} are lens dioptric power and the vergence of the far object, both given in diopters. δ and δ^* are the location of the anterior and posterior lens principal planes in millimeters.

$$s_{i_{far}} = \left[\frac{1000 - \delta.OB_{far}}{\Phi + OB_{far} - 0.001.\delta.\Phi.OB_{far}}\right] + \delta^* \qquad 0.29$$

Combining Equations 0.28 and 0.29:

$$\frac{D}{D+c}.s_i = \left[\frac{1000 - \delta.OB_{far}}{\Phi + OB_{far} - 0.001.\delta.\Phi.OB_{far}}\right] + \delta^* \qquad 0.30$$

$$\frac{D.s_i - \delta^*.D - \delta^*.c}{D+c} = \left[\frac{1000 - \delta.OB_{far}}{\Phi + OB_{far} - 0.001.\delta.\Phi.OB_{far}}\right] \qquad 0.31$$

$$\begin{aligned}\Phi.(D.s_i - \delta^*.D - \delta^*.c) + OB_{far}.(D.s_i - \delta^*.D - \delta^*.c) \\ - 0.001.\delta.\Phi.OB_{far}.(D.s_i - \delta^*.D - \delta^*.c) \\ = 1000.(D+c) - \delta.OB_{far}.(D+c)\end{aligned} \qquad 0.32$$

$$\begin{aligned}OB_{far}.(D.s_i - \delta^*.D - \delta^*.c) - 0.001.\delta.\Phi.OB_{far}.(D.s_i - \delta^*.D - \delta^*.c) \\ + \delta.OB_{far}.(D+c) = 1000.(D+c) - \Phi.(D.s_i - \delta^*.D - \delta^*.c)\end{aligned} \qquad 0.33$$

$$\begin{aligned}OB_{far}.[(D.s_i - \delta^*.D - \delta^*.c).(1 - 0.001.\delta.\Phi) + \delta.(D+c)] \\ = 1000.(D+c) - \Phi.(D.s_i - \delta^*.D - \delta^*.c)\end{aligned} \qquad 0.34$$

$$OB_{far} = \frac{1000.(D+c) - \Phi.(D.s_i - \delta^*.D - \delta^*.c)}{(D.s_i - \delta^*.D - \delta^*.c).(1 - 0.001.\delta.\Phi) + \delta.(D+c)} \qquad 0.35$$

A conversion from the object negative vergence in diopters to object distance in millimeters must be performed to calculate d_{far} in millimeters:

$$d_{far} = -\frac{1000}{OB_{far}} = 1000.\left[\frac{(D.s_i - \delta^*.D - \delta^*.c).(0.001.\delta.\Phi - 1) - \delta.(D+c)}{1000.(D+c) - \Phi.(D.s_i - \delta^*.D - \delta^*.c)}\right] \qquad 0.36$$

The depth of field extends from d_{far} to d_{near}.

<u>Hyperfocal distance:</u>

The optical system is focused at the hyperfocal distance when d_{far} is equal to infinity. By analyzing Equation 0.36, it is concluded that d_{far} is equal to infinity when the denominator is equal to zero. Φ and OBJ are the lens power and object vergence, respectively, both given in diopters.

$$d_{far} = \infty \rightarrow 1000.(D+c) - (D.s_i - D.\delta^* - c.\delta^*).\Phi = 0 \qquad 0.37$$

Thus s_i in this situation is given by:

$$s_i = \frac{(1000 + \delta^*.\Phi).(D+c)}{\Phi.D} \qquad 0.38$$

The combination of Equations 0.16 and 0.38 results in:

$$\left[\frac{1000 - \delta.OBJ}{\Phi + OBJ - 0.001.\delta.\Phi.OBJ}\right] + \delta^* = \frac{(1000 + \delta^*.\Phi).(D+c)}{\Phi.D} \qquad 0.39$$

The object vergence OBJ that satisfies Equation 0.39 is the vergence related to the hyperfocal distance:

$$\left[\frac{1000-\delta.\mathrm{OBJ}}{\Phi+\mathrm{OBJ}-0.001.\delta.\Phi.\mathrm{OBJ}}\right]=\frac{(1000+\delta^{*}.\Phi).(\mathrm{D}+\mathrm{c})-\delta^{*}.\Phi.\mathrm{D}}{\Phi.\mathrm{D}} \quad 0.40$$

$$1000.\Phi.\mathrm{D}-\Phi.\mathrm{D}.\delta.\mathrm{OBJ} = [\Phi+\mathrm{OBJ}-0.001.\delta.\Phi.\mathrm{OBJ}].[(1000+\delta^{*}.\Phi).(\mathrm{D}+\mathrm{c})-\delta^{*}.\Phi.\mathrm{D}] \quad 0.41$$

$$1000.\Phi.\mathrm{D}-\Phi.\mathrm{D}.\delta.\mathrm{OBJ} = (\Phi+\mathrm{OBJ}-0.001.\delta.\Phi.\mathrm{OBJ}).(1000.\mathrm{D}+1000.\mathrm{c}+\delta^{*}.\Phi.\mathrm{D}+\delta^{*}.\Phi.\mathrm{c}-\delta^{*}.\Phi.\mathrm{D}) \quad 0.42$$

$$1000.\Phi.\mathrm{D}-\Phi.\mathrm{D}.\delta.\mathrm{OBJ}=(\Phi+\mathrm{OBJ}-0.001.\delta.\Phi.\mathrm{OBJ}).(1000.\mathrm{D}+1000.\mathrm{c}+\delta^{*}.\Phi.\mathrm{c}) \quad 0.43$$

$$1000.\Phi.\mathrm{D}-\Phi.\mathrm{D}.\delta.\mathrm{OBJ} = 1000.\Phi.\mathrm{D}+1000'.\Phi.\mathrm{c}+\delta^{*}.\Phi^{2}.\mathrm{c}+1000.\mathrm{OBJ}.\mathrm{D}+1000.\mathrm{OBJ}.\mathrm{c}+\delta^{*}.\Phi.\mathrm{c}.\mathrm{OBJ}-\Phi.\mathrm{D}.\delta.\mathrm{OBJ}-\delta.\Phi.\mathrm{OBJ}.\mathrm{c}-0.001.\delta.\delta^{*}.\Phi^{2}.\mathrm{OBJ}.\mathrm{c} \quad 0.44$$

$$0=1000.\Phi.\mathrm{c}+\delta^{*}.\Phi^{2}.\mathrm{c}+1000.\mathrm{OBJ}.\mathrm{D}+1000.\mathrm{OBJ}.\mathrm{c}+\delta^{*}.\Phi.\mathrm{c}.\mathrm{OBJ}-\delta.\Phi.\mathrm{OBJ}.\mathrm{c}-0.001.\delta.\delta^{*}.\Phi^{2}.\mathrm{OBJ}.\mathrm{c} \quad 0.45$$

$$\mathrm{OBJ}.(1000.\mathrm{D}+1000.\mathrm{c}+\delta^{*}.\Phi.\mathrm{c}-\delta.\Phi.\mathrm{c}-0.001.\delta.\delta^{*}.\Phi^{2}.\mathrm{c}) = \Phi.\mathrm{c}.(-1000-\delta^{*}.\Phi) \quad 0.46$$

$$\mathrm{OBJ}=\frac{\Phi.\mathrm{c}.(-1000-\delta^{*}.\Phi)}{1000.(\mathrm{D}+\mathrm{c})+\Phi.\mathrm{c}.(\delta^{*}-\delta-0.001.\delta.\delta^{*}.\Phi)} \quad 0.47$$

A conversion from the negative object vergence in diopters to millimeters must be performed to calculate the hyperfocal distance H:

$$\mathrm{H}=-\frac{1000}{\mathrm{OBJ}}=-1000.\left[\frac{1000.(\mathrm{D}+\mathrm{c})+\Phi.\mathrm{c}.(\delta^{*}-\delta-0.001.\delta.\delta^{*}.\Phi)}{\Phi.\mathrm{c}.(-1000-\delta^{*}.\Phi)}\right] \quad 0.48$$

$$\mathrm{H}=1000.\left[\frac{1000.(\mathrm{D}+\mathrm{c})+\Phi.\mathrm{c}.(\delta^{*}-\delta-0.001.\delta.\delta^{*}.\Phi)}{\Phi.\mathrm{c}.(1000+\delta^{*}.\Phi)}\right] \quad 0.49$$

<u>Proof that the near distance between object and lens when it is focused at the hyperfocal distance H is approximate H/2:</u>

The near distance dH_{near} is obtained by replacing s_i from Equation 0.38 in Equation 0.26:

$$\mathrm{dH_{near}}=1000.\left[\frac{(\mathrm{D}.\mathrm{s_i}-\delta^{*}.\mathrm{D}+\delta^{*}.\mathrm{c}).(0.001.\delta.\Phi-1)-\delta.(\mathrm{D}-\mathrm{c})}{1000.(\mathrm{D}-\mathrm{c})-\Phi.(\mathrm{D}.\mathrm{s_i}-\delta^{*}.\mathrm{D}+\delta^{*}.\mathrm{c})}\right] \quad 0.50$$

$$dH_{near} = \frac{D.s_i.\delta.\Phi - 1000.D.s_i - D.\Phi.\delta.\delta^* + 1000.D.\delta^* + c.\Phi.\delta.\delta^* - 1000.c.\delta^* - 1000.\delta.D + 1000.\delta.c}{1000.D - 1000.c - \Phi.D.s_i + \Phi.D.\delta^* - \Phi.c.\delta^*} \quad 0.51$$

$$dH_{near} = \frac{D.\left[\frac{(1000+\delta^*.\Phi).(D+c)}{\Phi.D}\right].\delta.\Phi - 1000.D.\left[\frac{(1000+\delta^*.\Phi).(D+c)}{\Phi.D}\right] - D.\Phi.\delta.\delta^* + 1000.(D.\delta^* - c.\delta^* - \delta.D + \delta.c) + c.\Phi.\delta.\delta^*}{1000.D - 1000.c - \Phi.D.\left[\frac{(1000+\delta^*.\Phi).(D+c)}{\Phi.D}\right] + \Phi.D.\delta^* - \Phi.c.\delta^*} \quad 0.52$$

$$A_1 = D.\Phi.\delta.\left[\frac{(1000+\delta^*.\Phi).(D+c)}{\Phi.D}\right]; B_1 = -1000.D.\left[\frac{(1000+\delta^*.\Phi).(D+c)}{\Phi.D}\right]; C_1 = \frac{\Phi.D.[-D.\Phi.\delta.\delta^* + 1000.(D.\delta^* - c.\delta^* - \delta.D + \delta.c) + c.\Phi.\delta.\delta^*]}{\Phi.D} \quad 0.53$$

$$dH_{near} = \frac{A_1 + B_1 + C_1}{\frac{1000.\Phi.D^2 - 1000.c.\Phi.D - 1000.D^2.\Phi - 1000.c.\Phi.D - \Phi^2.D^2.\delta^* - \Phi^2.D.c.\delta^* + \Phi^2.D^2.\delta^* - \Phi^2.D.c.\delta^*}{\Phi.D}} \quad 0.54$$

$$A_1 = \frac{1000.D^2.\Phi.\delta + 1000.D.\Phi.\delta.c + \Phi^2.D^2.\delta.\delta^* + \Phi^2.D.c.\delta.\delta^*}{\Phi.D} \quad 0.55$$

$$B_1 = \frac{-10^6.D^2 - 10^6.D.c - 1000.D^2.\Phi.\delta - 1000.\Phi.D.c.\delta^*}{\Phi.D} \quad 0.56$$

$$C_1 = \frac{-D^2.\Phi^2.\delta.\delta^* + 1000.\Phi.D^2.\delta^* + c.\Phi^2.D.\delta.\delta^* - 1000.\Phi.D.c.\delta^* - 1000.D^2.\Phi.\delta + 1000.D.\Phi.\delta.c}{\Phi.D} \quad 0.57$$

$$A_1 + B_1 + C_1 = \frac{2000.D.\Phi.\delta.c + 2.\Phi^2.D.c.\delta.\delta^* - 10^6.D^2 - 10^6.c.D - 2000.\Phi.D.c.\delta^*}{\Phi.D} \quad 0.58$$

$$dH_{near} = \frac{2000.\Phi.\delta.c + 2.\Phi^2.c.\delta.\delta^* - 10^6.D - 10^6.c - 2000.\Phi.c.\delta^*}{-2000.\Phi.c - 2.\Phi^2.D.c.\delta^*} \quad 0.59$$

$$dH_{near} = 1000.\left[\frac{2.\Phi.\delta.c + 0.002.\Phi^2.c.\delta.\delta^* - 1000.D - 1000.c - 2.\Phi.c.\delta^*}{2.\Phi.c.(-1000 - \delta^*.\Phi)}\right] \quad 0.60$$

$$dH_{near} = \frac{1000}{2}.\left[\frac{1000.(D+c) + \Phi.c.(2.\delta^* - 2.\delta - 0.002.\Phi.\delta.\delta^*)}{\Phi.c.(1000 + \delta^*.\Phi)}\right] \quad 0.61$$

Since the term $\Phi.c.(2.\delta^* - 2.\delta - 0.002.\Phi.\delta.\delta^*)$ is much smaller than $1000.(D + c)$, dH_{near} can be approximated to H/2. It is concluded that when the optical system is focused on the hyperfocal distance, the depth of field extends from infinity to approximately H/2.